PHYSICAL REVIEW A VOLUME 47, NUMBER 4 APRIL 1993

Application of Hilbert-space coupled-cluster theory to simple $(H_2)_2$ model systems: Planar models

J. Paldus
Department of Applied Mathematics, University of Waterloo, Waterloo, Ontario, Canada N2L 3G1 and Department of Chemistry and Guelph-Waterloo Center for Graduate Work in Chemistry, Waterloo Campus, University of Waterloo, Waterloo, Ontario, Canada N2L 3G1

P. Piecuch
Department of Applied Mathematics, University of Waterloo, Waterloo, Ontario, Canada N2L 3G1 and Institute of Chemistry, University of Wrocław, F. Joliot-Curie 14, 50-383 Wrocław, Poland

L. Pylypow
Department of Chemistry and Guelph-Waterloo Center for Graduate Work in Chemistry, Waterloo Campus, University of Waterloo, Waterloo, Ontario, Canada N2L 3G1

B. Jeziorski
Department of Applied Mathematics, University of Waterloo, Waterloo, Ontario, Canada N2L 3G1 and Department of Chemistry, University of Warsaw, Pasteura 1, 02-093 Warsaw, Poland
(Received 12 August 1992)

The recently developed explicit formalism of orthogonally-spin-adapted, Hilbert-space (or state-universal), multireference (MR), coupled-cluster (CC) theory, exploiting the model space spanned by two closed-shell-type reference configurations, is applied to a simple four-electron model system consisting of two interacting hydrogen molecules. Four planar minimum-basis-set H_4 models are examined, each characterized by a single parameter that fully determines its geometry, assuming the trapezoidal (H4 model), rectangular (P4 model), linear (D4 model), and square (S4 model) nuclear configuration. Varying this geometry-determining parameter, in each case we obtain different cross sections of the H_4 potential-energy hypersurface, involving the dissociation of one, two, or all four H—H "bonds." Comparing the resulting CC energies with exact values that are easily obtained for this model using the full configuration-interaction method, we can assess the performance of various MRCC Hilbert-space approaches at both the linear and nonlinear levels of approximation, while a continuous transition is being made between the degenerate and nondegenerate regimes. This enables us to elucidate the sources and the type of singular behavior in both linear and nonlinear versions of MRCC theory, to examine the role played by various intruder states, the existence and types of multiple solutions and their ability to describe various excited states, and, by performing a cluster analysis of the exact solutions, to assess the quality of the MRCC wave functions as well as the energies.

PACS number(s): 31.15.+q, 31.20.Tz, 31.50.+w, 03.65.Ge

I. INTRODUCTION

An extension of standard, single-reference (SR) coupled-cluster (CC) theory (see, e.g., Refs. [1–10]) that is capable of describing many-electron correlation effects in closed-shell (CS) nondegenerate ground states, to the general open-shell (OS) case, proved to be extremely challenging though highly desirable in view of the reliability and size-extensive property of CC results. All genuine OSCC approaches employ a general multireference (MR) formalism and are based on an effective Hamiltonian, acting in some relatively small model space, that is in turn determined by the solutions of the generalized Bloch equation (for a general account, see, e.g., Refs. [10–12]). The existing MRCC approaches of this kind are basically of two types, constituting the so-called *Fock-space* or *valence-universal* (VU) methods [10–20] and *Hilbert-space* or *state-universal* (SU) methods [7,10,12,21–30]. While the former ones employ a single—valence universal—cluster operator, similarly, as in the SR case, the latter ones represent the wave operator as a superposition of exponential Ansätze, one for each reference configuration spanning the model space. In either case, however, there is no "natural vacuum" that one can employ as a reference, so that in contrast to SR theory, when the cluster operator involves only creation operators of the hole-particle formalism, operators of both types appear for the so-called active or valence orbitals in the MR case.

The VU approach resolves the above-indicated problem by simultaneously considering the studied system as well as all possible ions, up to and including the one in which all electrons occupying valence orbitals are removed. So far this approach found its greatest use in the computation of various "differential" properties, such as excitation or ionization energies, rather than in the deter-

mination of potential-energy hypersurfaces of a number of strongly interacting states over a wide range of nuclear framework geometries. In fact, all such attempts required the use of incomplete model spaces or even the use of different model spaces for different geometries (cf., e.g., Ref. [31]). Nonetheless, a great deal of progress was made during the past decade in the implementation and use of these theories (see, e.g., Refs. [32,33] and references therein), which was not the case for the SU methods. Recently, the so-called *cluster conditions* that ascertain the negligibility of higher excited cluster components in VUCC approaches, and thus the appropriateness of truncation at the pair-cluster or higher excitation level, were derived [20] and examined for two simple models [34] as was the VUCC method itself in the approximation restricted to pair clusters [35].

In the SU or Hilbert-space approach [21], the "vacuum" ambiguity is resolved by considering each reference configuration separately and by introducing for each the corresponding cluster operator. In general, this will obviously lead to a large multitude of cluster amplitudes, assuming that there are many reference configurations spanning the model space. On the other hand, there is no need to consider the whole hierarchy of ionized species, which may also be very demanding when many electrons occupy valence orbitals. So far, there have only been a few applications of this method [22,24,26–28], including preliminary studies of the model systems considered in this paper.

Here and in subsequent work [36], we wish to explore the basic properties and potential of Hilbert-space-type MRCC approaches, using a simple four-electron model [37] consisting of two interacting, slightly stretched hydrogen molecules. This model system was successfully employed to explore the performance of various SRCC methods [37–39], both SR [40] and MR [41,42] perturbation theory as well as other approaches [43]. Preliminary studies of the so-called H4 model were also carried out using both Hilbert-space [26,27,30], and, lately, Fock-space [34,35] MRCC formalisms. In this paper we examine four planar models, while the nonplanar models will be the subject of future work [36]. For the sake of simplicity and easy insight we employ minimum-basis-set (MBS) models [37], each of which is uniquely specified by a single geometric parameter α that enables us to vary continuously the degree of degeneracy between the two configurations spanning the model space employed. The nuclear framework then assumes the trapezoidal (H4 model), rectangular (P4 model), linear (D4 model), and square (S4 model) conformation, so that when varying the geometry-determining parameter α we obtain various cross sections of the H_4 potential-energy hypersurface. When $\alpha \rightarrow \infty$ (or $\alpha \rightarrow 0.5$ in the H4 model), we examine the fragmentation of the system, thus modeling the dissociation of one, two, or all four simple H—H "bonds."

We first present a brief outline of the Hilbert-space MRCC approach in Sec. II and its specialized orthogonally-spin-adapted two-reference version, pertinent to our model problems, in Sec. III. The detailed description of the studied models, as well as other computational and methodological details (choice of reference orbitals and configurations, their degeneracy characteristics, the model spaces, and numerical procedures employed) are given in Sec. IV, while Sec. V presents the main results for all four planar models examined in this paper. The singular behavior of linear approximation is then examined in Sec. VI and the cluster analysis of the MRCC wave functions for both ground and excited states is described in Sec. VII. The possibility to handle the higher excited states is examined in Sec. VIII while the last Sec. IX summarizes and discusses the results obtained.

II. MULTIREFERENCE HILBERT-SPACE COUPLED-CLUSTER APPROACH

While for nondegenerate CS states, an SR description [1–10,44] is generally adequate, an entirely different situation arises when the OS or highly (quasi)degenerate CS systems are considered. In this case, the group of states that emerges through a strong interaction of two or more configurations must be simultaneously considered. Thus a suitable set of configurations $|\Phi_p\rangle$, $p=1,\ldots,M$, must be found that is capable of providing a reasonable zeroth-order description of these states over a sufficiently wide range of relevant nuclear geometries. In other words, we have to choose an appropriate multidimensional model space $\mathcal{M}_0$, spanned by configurations $|\Phi_p\rangle$, that may serve as a reasonable zeroth-order approximation to the exact manifold $\mathcal{M}$ spanned by M exact solutions $|\Psi_\mu\rangle$, $\mu=1,\ldots,M$, of the Schrödinger equation

$$(H-E_\mu)|\Psi_\mu\rangle=0 \ . \tag{1}$$

This is achieved by partitioning the spin-orbital or molecular-orbital (MO) set, defining the one-electron space employed, into three disjoint subsets of core, valence (or active), and virtual (or excited) (spin) orbitals. The reference configurations $|\Phi_p\rangle$, $p=1,\ldots,M$, differ in the occupancies of valence (spin) orbitals, while having core and virtual (spin) orbitals completely occupied and unoccupied, respectively. Thus, considering all possible distributions of valence electrons [electrons occupying valence (spin) orbitals] among valence (spin) orbitals we obtain a *complete model space* [21] $\mathcal{M}_0$ that is invariant under unitary transformations of valence (spin) orbitals. Although this complete space may be unnecessarily large for the description of states that are of interest to us, and its use may lead to the appearance of intruder state problems [26,45], the requirement of the completeness of $\mathcal{M}_0$ is essential for the theoretical developments that follow. Indeed, completeness of the model space implies the connectivity of cluster operators and of the effective Hamiltonian, and the resulting MRCC theory leads to a size-extensive description of many-body systems (for a rigorous formulation, see Ref. [21]). When the completeness of $\mathcal{M}_0$ is not required, disconnected terms appear [21]. For special types of incomplete model spaces, connectivity of cluster operators and of the effective Hamiltonian can be restored by relaxing the so-called intermediate normalization conditions [12,25]. General incomplete model-space MRCC methods that employ only

connected cluster amplitudes and the connected effective Hamiltonian have been successfully formulated (both within the Fock- [46] and Hilbert-space [25,47] frameworks), thus providing size-extensive results. In the following, however, we restrict ourselves to the case of a complete reference space. The use of an incomplete model space is essential when the dimension of the corresponding complete space is large. Clearly, the larger the model space is, the more costly the practical implementation of the formalism becomes, and the more likely we encounter intruder states. In the present paper, however, we deal with a small two-dimensional model space that is complete for the symmetry species considered [23,26,29] (cf. Sec. III).

As mentioned in the Introduction, the aim of this series is to apply the SUCC approach [21] to simple four-electron models. Assuming that the reference configurations $|\Phi_p\rangle$ have been selected, we define projection operators onto $\mathcal{M}_0$ and its orthogonal complement $\mathcal{M}_0^{\perp}$ (in the N-electron Hilbert space $\mathcal{H}_N$), which we designate by P and Q, respectively. We obviously have

$$P=\sum_{q=1}^{M} P_q \equiv \sum_{q} P_q, \quad P_q=|\Phi_q\rangle\langle\Phi_q| \ , \tag{2}$$

$$Q=1-P \ . \tag{3}$$

Since $\mathcal{M}_0$ represents a reasonable zeroth-order approximation to the exact manifold $\mathcal{M}$, we further assume that no function from $\mathcal{M}$ is orthogonal to all of $|\Phi_p\rangle$, so that the model-space projections of the exact states $|\Psi_\mu\rangle$,

$$|\tilde{\Phi}_\mu\rangle=P|\Psi_\mu\rangle \ , \tag{4}$$

are linearly independent and span $\mathcal{M}_0$. This in turn implies that P generates a bijective mapping $\tilde{P}=P\downarrow\mathcal{M}$ from $\mathcal{M}$ onto $\mathcal{M}_0$. The inverse of this bijection

$$\tilde{U}\equiv\tilde{P}^{-1}\colon \mathcal{M}_0\rightarrow\mathcal{M} \ , \tag{5}$$

can be extended to the whole N-electron Hilbert space $\mathcal{H}_N$ by defining it as the zero operator on $\mathcal{M}_0^{\perp}$. The resulting wave operator U, referred to as the Bloch wave operator [48], transforms model states $|\tilde{\Phi}_\mu\rangle$ into exact solutions $|\Psi_\mu\rangle$,

$$|\Psi_\mu\rangle=U|\tilde{\Phi}_\mu\rangle \ , \tag{6}$$

and annihilates any state from the subspace $\mathcal{M}_0^{\perp}$, so that

$$UQ=U(1-P)=0 \ . \tag{7}$$

Equation (6) implies that PU acts as the identity on $\mathcal{M}_0$, which is equivalent to the relationship

$$PU=P \ . \tag{8}$$

From Eq. (7) we have that

$$UP=U \ , \tag{9}$$

so that U is idempotent,

$$U^2=(UP)^2=U(PU)P=UP^2=UP=U \ , \tag{10}$$

and leaves the exact states $|\Psi_\mu\rangle$ invariant,

$$U|\Psi_\mu\rangle=U^2|\tilde{\Phi}_\mu\rangle=U|\tilde{\Phi}_\mu\rangle=|\Psi_\mu\rangle \ . \tag{11}$$

Bloch wave operator U may thus be regarded as a projector onto $\mathcal{M}$. In contrast to Kato's [49] projectors that are always Hermitian or orthogonal, U is a nonorthogonal projector. Relationship (8) is equivalent to the condition of the intermediate normalization, which in the MR case requires that

$$\langle\Phi_p|U\Psi_q\rangle=\delta_{pq}, \quad (p,q=1,\ldots,M) \ , \tag{12}$$

or, equivalently,

$$\langle\Phi_p|\tilde{\Psi}_q\rangle=\delta_{pq}, \quad (p,q=1,\ldots,M) \ , \tag{13}$$

where the ket states

$$|\tilde{\Psi}_p\rangle=U|\Phi_p\rangle \tag{14}$$

form another set of functions spanning $\mathcal{M}$. In view of Eq. (13) and analogously as in the SR case, every state $|\tilde{\Psi}_p\rangle$ has the form

$$|\tilde{\Psi}_p\rangle=(1+C^{(p)})|\Phi_p\rangle \ , \tag{15}$$

where $C^{(p)}$ designates an excitation operator into $\mathcal{M}_0^{\perp}$ relative to the reference determinant $|\Phi_p\rangle$ regarded as a corresponding Fermi vacuum. Equivalently, every exact wave function $|\Psi_\mu\rangle$ can be written as

$$|\Psi_\mu\rangle=\sum_{q} c_{q\mu}|\Phi_q\rangle+|\Xi\rangle \ , \tag{16}$$

where the remainder $|\Xi\rangle$ belongs to $\mathcal{M}_0^{\perp}$ and

$$c_{q\mu}=\langle\Phi_q|\Psi_\mu\rangle=\langle\Phi_q|\tilde{\Phi}_\mu\rangle \tag{17}$$

are the linear-expansion coefficients of functions $|\tilde{\Phi}_\mu\rangle$ with respect to model states $|\Phi_p\rangle$, $p=1,\ldots,M$. Clearly, the functions $|\tilde{\Phi}_\mu\rangle=\sum_q c_{q\mu}|\Phi_q\rangle$ represent the zeroth-order approximation to the exact states $|\Psi_\mu\rangle$. The question now arises how to determine the wave operator U and the unknown coefficients $c_{q\mu}$.

As in SRCC theory [1–10], we are looking for an energy-independent equation (or equations) determining U. Such an equation can easily be obtained by combining the original Schrödinger equation, Eq. (1), and the property of U described by Eq. (11). In this way, we find that the wave operator U must satisfy the relation

$$UHU=HU \ , \tag{18}$$

which represents the basic equation of the MR formalism and is usually referred to as the generalized Bloch equation [10,11,16,21,48,50,51]. Once this equation is solved and the wave operator U is known, the unknown coefficients $c_{p\mu}$ and the corresponding energies E_μ are determined by diagonalizing the effective Hamiltonian

$$H^{\text{eff}}=PHU=PHUP \tag{19}$$

within the model space $\mathcal{M}_0$. Indeed, by projecting the Schrödinger equation (1) onto $\mathcal{M}_0$ we get

$$PH|\Psi_\mu\rangle=E_\mu P|\Psi_\mu\rangle \ , \tag{20}$$

so that the unknown model states $|\tilde{\Phi}_\mu\rangle$ can be found by solving the equation

$$H^{\text{eff}}|\tilde{\Phi}_\mu\rangle = E_\mu|\tilde{\Phi}_\mu\rangle \ , \tag{21}$$

which is equivalent to the following $M\times M$ secular problem

$$\sum_q (H^{\text{eff}}_{pq}-\delta_{pq}E_\mu)c_{q\mu}=0 \ , \tag{22}$$

with

$$H^{\text{eff}}_{pq}=\langle\Phi_p|H^{\text{eff}}|\Phi_q\rangle=\langle\Phi_p|HU|\Phi_q\rangle \ . \tag{23}$$

The idea of diagonalizing the effective Hamiltonian within the model space is the key concept of all MR theories. It enables us to translate the exact problem, Eq. (1), for a finite number of eigenstates into a simple secular problem, Eq. (22), formulated entirely within a conveniently chosen reference space $\mathcal{M}_0$.

Different Ansätze for the wave operator U lead to distinct MRCC methods [10,20,21]. The Hilbert-space approach [21] is based on a simple observation that the wave operator U can be uniquely represented in the form

$$U=UP=\sum_q |\tilde{\Psi}_q\rangle\langle\Phi_q| \ , \tag{24}$$

so that we can write [cf. Eq. (15)]

$$U=\sum_q (1+C^{(q)})P_q \ . \tag{25}$$

Assuming a separate cluster Ansatz for *every* reference configuration $|\Phi_p\rangle$ by defining cluster operators $T^{(p)}$ in exactly the same way as in SRCC theory, namely,

$$T^{(p)}=\ln(1+C^{(p)}) \ , \tag{26}$$

we obtain that

$$U=\sum_q e^{T^{(p)}}P_q \ . \tag{27}$$

Thus, the exact states $|\Psi_\mu\rangle$, $\mu=1,\ldots,M$, can be expressed in the form

$$|\Psi_\mu\rangle=\sum_q c_{q\mu}e^{T^{(p)}}|\Phi_q\rangle \ , \tag{28}$$

where $\mathbf{c}_\mu=(c_{1\mu},\ldots,c_{M\mu})$ are the eigenvectors of the effective Hamiltonian (19), whose matrix elements now become [21,29] [cf. Eq. (23)]

$$\begin{aligned} H^{\text{eff}}_{pq}&=\langle\Phi_p|e^{-T^{(q)}}He^{T^{(q)}}|\Phi_q\rangle \\ &=\delta_{pq}H_{pp}+\langle\Phi_p|(H_{N_q}e^{T^{(q)}})_C|\Phi_q\rangle \ . \end{aligned} \tag{29}$$

Here $H_{pp}=\langle\Phi_p|H|\Phi_p\rangle$, while H_{N_p} designates the normal product form of H (cf. Refs. [6] and [44]) relative to $|\Phi_p\rangle$. The subscript C indicates the connected part of a given expression [6,44], so that it is sufficient to ascertain the connectedness of $T^{(p)}$ to prove that the effective Hamiltonian contains only connected terms [21].

The MR character of the Hilbert-space formalism [21] requires that all states $|\Psi_\mu\rangle$ from $\mathcal{M}$ are considered simultaneously. We thus have to find as many equations for the cluster operators $T^{(p)}$ as required to determine the entire family $\{T^{(p)}\}_{p=1}^{M}$. Just as in the SR CS case, we expand cluster operators in terms of a conveniently chosen set of excitation operators ${}^{(p)}G_i$,

$$T^{(p)}=\sum_i {}^{(p)}t_i\,{}^{(p)}G_i \ , \tag{30}$$

and then derive the equations for the unknown cluster amplitudes ${}^{(p)}t_i$. The superscript (p) in ${}^{(p)}G_i$ indicates that the excitation operator is defined with respect to the reference $|\Phi_p\rangle$, so that for every model state $|\Phi_p\rangle$ we have a distinct family of operators ${}^{(p)}G_i$ and a distinct family of cluster amplitudes ${}^{(p)}t_i$. Of course, a given excited configuration may originate from different reference states, so that

$${}^{(p)}G_i|\Phi_p\rangle={}^{(q)}G_j|\Phi_q\rangle \tag{31}$$

for $p\neq q$ and $i\neq j$. Completeness of the model space and the requirement of the intermediate normalization, Eq. (13), imply that

$$PT^{(p)}|\Phi_p\rangle=0 \ . \tag{32}$$

Consequently, the excitation operators ${}^{(p)}G_i$ must be chosen in such a way that ${}^{(p)}G_i|\Phi_p\rangle\in\mathcal{M}_0^\perp$, or, equivalently, the cluster amplitudes ${}^{(p)}t_i$ must carry at least one nonvalence (i.e., core or virtual-type) label [21].

The system of coupled equations for the unknown cluster amplitudes ${}^{(p)}t_i$ is obtained by substituting the Ansatz (27) into the Bloch equation (18) acting on a reference state $|\Phi_p\rangle$. Multiplying then from the left by $e^{-T^{(p)}}$ and projecting the result onto the excited configurations $|{}^{(p)}G_i\Phi_p\rangle\equiv{}^{(p)}G_i|\Phi_p\rangle$, we get [21]

$$\begin{aligned} &\langle{}^{(p)}G_i\Phi_p|(H_{N_p}e^{T^{(p)}})_C|\Phi_p\rangle \\ &\quad=\sum_{q\ (\neq p)}\langle{}^{(p)}G_i\Phi_p|e^{-T^{(p)}}e^{T^{(q)}}|\Phi_q\rangle H^{\text{eff}}_{qp} \ , \\ &\qquad\qquad (p=1,\ldots,M) \ , \end{aligned} \tag{33}$$

since [6] [cf. Eq. (29)]

$$H_{N_p}e^{T^{(p)}}|\Phi_p\rangle=e^{T^{(p)}}(H_{N_p}e^{T^{(p)}})_C|\Phi_p\rangle \ . \tag{34}$$

These equations are the basic equations of the Hilbert-space CC formalism [21]. They represent a system of highly nonlinear coupled algebraic equations for the coefficients ${}^{(p)}t_i$.

It has been proved [21] that the MRCC method given by Eqs. (33) and (22), with the effective Hamiltonian matrix elements calculated using Eq. (29), leads to connected expansions for the cluster operators $T^{(p)}$, so that the resulting energies E_μ, obtained by the diagonalization of the effective Hamiltonian, are size extensive. One can thus consider several approximate variants of Eqs. (33) and (29), obtained by neglecting higher nonlinear terms or higher many-body components in expansion (30) (cf. Refs. [10,21–30]; see also Sec. III), without introducing disconnected terms into H^{eff}, i.e., without losing the size extensivity of the resulting approximate energies. As already mentioned, this feature is closely associated with the assumption of the completeness of $\mathcal{M}_0$. To obtain a connected generalization of the Hilbert-space CC method for incomplete model spaces, the requirement (32) must be relaxed and certain types of cluster amplitudes carrying only valence labels must be admitted [47].

One of the main advantages of the SUCC approach is its close relationship with the MR configuration interaction (CI) method [7,22,23] [cf. Eq. (25)], which is useful in deriving the MR generalizations of the Davidson correction [52] to the CI correlation energy [7,38,53]. Unfortunately, the symmetry adaptation of this formalism is not as easy as in the case of the Fock-space approach [20]. For example, the general orthogonally-spin-adapted [3,54,55] Hilbert-space MRCC method has not yet been formulated. So far, only a special case of two CS-type references (corresponding to two active orbitals of different symmetry) was successfully considered [23,26,29,56].

The left-hand side of Eq. (33), referred to as the *direct term,* is exactly the same as in the SRCC method (with $|\Phi_p\rangle$ as a reference). In fact, when $\mathcal{M}_0$ is one-dimensional ($\mathcal{M}_0=\text{span}\{|\Phi_0\rangle\}$), the right-hand side of Eq. (33) vanishes and the MRCC equations (22), (29), and (33) reduce to the well-known equations of the SRCC theory [1–10], with the wave operator U given by $e^T|\Phi_0\rangle\langle\Phi_0|$. The right-hand side of Eq. (33), referred to as the *coupling term,* is characteristic of the MR formalism and has no counterpart in the SR case. The structure of both direct and coupling terms for the special case of a two-dimensional model space is discussed in the next section.

III. ORTHOGONALLY-SPIN-ADAPTED TWO-REFERENCE CC FORMALISMS INVOLVING SINGLE AND DOUBLE EXCITATIONS

To get a better idea of a general structure of the Hilbert-space MRCC equations, we expand the exponentials in Eq. (33) and neglect cubic and higher-order nonlinear terms. We also restrict ourselves to the simplest possible, though broadly applicable [23], case of a two-dimensional model space spanned by CS-type reference configurations $|\Phi_1\rangle$ and $|\Phi_2\rangle$ involving two active orbitals $|k\rangle$ and $|l\rangle$, that belong to different symmetry species of the spatial symmetry group of the system. Such a model space is complete, assuming that we focus our attention on the totally symmetric singlet states. In general, we would also have to consider other reference states, namely a non-CS singlet configuration

$$|\Phi_3'\rangle = {}^{(1)}\left|\begin{matrix} l \\ k \end{matrix}\right\rangle \equiv {}^{(1)}\left|\begin{matrix} l \\ k \end{matrix};00\right\rangle \equiv {}^{(1)}G_k^l|\Phi_1\rangle \ , \tag{35}$$

and, for a spin-dependent Hamiltonian, its triplet analog

$$|\Phi_3''\rangle = {}^{(1)}\left|\begin{matrix} l \\ k \end{matrix};10\right\rangle \ . \tag{36}$$

Here, ${}^{(p)}G_\alpha^\rho$, $p=1,2$, designates the excitation operator generating the orthogonally-spin-adapted singlet state ${}^{(p)}|{}^\rho_\alpha\rangle \equiv {}^{(p)}|{}^\rho_\alpha;00\rangle$ that is monoexcited with respect to $|\Phi_p\rangle$ (here and in the following, α, β, etc. designate orbitals occupied in $|\Phi_p\rangle$, while ρ, σ, etc. are the orbitals unoccupied in $|\Phi_p\rangle$; for definition of ${}^{(p)}G_\alpha^\rho$ operators, see Eq. (3) of Ref. [29] and for definition of the orthogonally-spin-adapted states $|{}^\rho_\alpha;SM_S\rangle$, see Refs. [54,55]; cf. also Refs. [3,23,26,29,57]). Of course, in the presence of symmetry, this model space reduces to a direct sum of invariant subspaces labeled by the symmetry species of the invariance group(s) involved. Then, each invariant subspace (in our case $\mathcal{M}_0=\text{span}\{|\Phi_1\rangle,|\Phi_2\rangle\}$) may be considered as an independent model space [10]. Thus, neglecting cubic and higher-order terms in Eq. (33) and restricting ourselves to the case of a two-dimensional model space $\mathcal{M}_0$, we obtain [10,23,26,29,30]

$$\begin{aligned}\langle\Phi_p|{}^{(p)}G_i^\dagger\{H_{N_p}[1+T^{(p)}+\tfrac{1}{2}(T^{(p)})^2]\}_C|\Phi_p\rangle \\ =\langle\Phi_p|{}^{(p)}G_i^\dagger(T^{(q)}-T^{(p)})|\Phi_q\rangle H_{qp}^{\text{eff}} \\ +\tfrac{1}{2}\langle\Phi_p|{}^{(p)}G_i^\dagger\{(T^{(q)}-T^{(p)})^2 \\ +[T^{(q)},T^{(p)}]\}|\Phi_q\rangle H_{qp}^{\text{eff}} \ ,\end{aligned} \tag{37}$$

where $p=1,2$ and $q=3-p$ [for larger model spaces, a summation $\sum_{q(\neq p)}$ will appear on the right-hand side of Eq. (37)]. On the left-hand side of Eq. (37) we immediately recognize the absolute, linear, and bilinear terms of SRCC theory (cf. e.g., Ref. [57]), while the right-hand side gives the linear and bilinear coupling terms. Since the reference configurations $|\Phi_1\rangle$ and $|\Phi_2\rangle$ are totally symmetric singlet states, the excitation operators ${}^{(p)}G_i$ entering Eq. (37) represent a linearly independent set of spin-adapted singlet excitation operators that generate totally symmetric excitations into the $\mathcal{M}_0^\perp$. We will restrict ourselves to monoexcitation operators ${}^{(p)}G_\alpha^\rho$, Eq. (35), and biexcitation particle-particle–hole-hole (pp-hh) coupled operators ${}^{(p)}G_{\alpha\beta}^{\rho\sigma}(i)$, $i=0,1$ [for their definition, see Eq. (2) of Ref. [29]]. The latter generate orthogonally-spin-adapted doubly excited singlet states ${}^{(p)}|{}^{\rho\ \sigma}_{\alpha\ \beta}\rangle_i \equiv {}^{(p)}|{}^{\rho\ \sigma}_{\alpha\ \beta};00\rangle_i^i$ when acting on $|\Phi_p\rangle$ (see Refs. [3,23,26, 29,54,55,57,58]). Of course, operators carrying only valence orbital labels $[{}^{(1)}G_k^l, {}^{(2)}G_l^k, {}^{(1)}G_{kk}^{ll}(0), {}^{(2)}G_{ll}^{kk}(0)$, etc.] have to be excluded. In the present paper and subsequently [36] we employ the CCSD (CC with singly and doubly excited cluster components) approximation, so that the cluster operators $T^{(p)}$ are approximated by their one- and two-body components $T_1^{(p)}$ and $T_2^{(p)}$, respectively. In the orthogonally-spin-adapted formalism these take the following form:

$$T_1^{(p)} = \sum_{\alpha\rho}\langle\rho|t_1^{(p)}|\alpha\rangle\,{}^{(p)}G_\alpha^\rho \ , \tag{38}$$

$$T_2^{(p)} = \sum_{\substack{\alpha,\beta,\rho,\sigma \\ (\alpha\leq\beta) \\ (\rho\leq\sigma)}}\sum_{i=0}^{1}\langle\rho\sigma|t_2^{(p)}|\alpha\beta\rangle_i\,{}^{(p)}G_{\alpha\beta}^{\rho\sigma}(i) \ , \tag{39}$$

the coefficients $\langle\rho|t_1^{(p)}|\alpha\rangle$ and $\langle\rho\sigma|t_2^{(p)}|\alpha\beta\rangle_i$ representing the corresponding monoexcited and biexcited cluster amplitudes. Thus setting $T^{(p)}=T_1^{(p)}+T_2^{(p)}$, expanding both sides of Eq. (37), and assuming ${}^{(p)}G_i$ to be at most biexcited operators [so that ${}^{(p)}G_i$ represents either ${}^{(p)}G_\alpha^\rho$ or ${}^{(p)}G_{\alpha\beta}^{\rho\sigma}(i)$], we get [23,26,29,57] (see also Ref. [30])

$$\begin{aligned}\sum_{n=0}^{2}L_n^{(p)}(G_i^\dagger)+\sum_{\substack{n,n'=1 \\ (n\leq n')}}^{2}Q_{nn'}^{(p)}(G_i^\dagger) \\ =\sum_{n=1}^{2}R_n^{(p)}(G_i^\dagger)+\sum_{\substack{n,n'=1 \\ (n\leq n')}}^{2}B_{nn'}^{(p)}(G_i^\dagger)+\tilde{B}_{12}^{(p)}(G_i^\dagger) \ ,\end{aligned} \tag{40}$$

where the absolute, linear, and bilinear direct terms $L_0^{(p)}(G_i^\dagger)$, $L_n^{(p)}(G_i^\dagger)$, $(n=1,2)$, and $Q_{nn'}^{(p)}(G_i^\dagger)$, $(n,n'=1,2,\ n\leq n')$, respectively, are given by the well-known

SR-like expressions

$$L_0^{(p)}(G_i^\dagger)=\langle\Phi_p|^{(p)}G_i^\dagger H_{N_p}|\Phi_p\rangle\ , \tag{41}$$

$$L_n^{(p)}(G_i^\dagger)=\langle\Phi_p|^{(p)}G_i^\dagger(H_{N_p}T_n^{(p)})_C|\Phi_p\rangle\ , \tag{42}$$

$$Q_{nn}^{(p)}(G_i^\dagger)=\tfrac{1}{2}\langle\Phi_p|^{(p)}G_i^\dagger[H_{N_p}(T_n^{(p)})^2]_C|\Phi_p\rangle\ , \tag{43}$$

$$Q_{12}^{(p)}(G_i^\dagger)=\langle\Phi_p|^{(p)}G_i^\dagger(H_{N_p}T_1^{(p)}T_2^{(p)})_C|\Phi_p\rangle\ , \tag{44}$$

and the linear and bilinear coupling terms by the formulas

$$R_n^{(p)}(G_i^\dagger)=\langle\Phi_p|^{(p)}G_i^\dagger T_n^{(q)}|\Phi_q\rangle H_{qp}^{\rm eff}\ , \tag{45}$$

$$B_{nn}^{(p)}(G_i^\dagger)=\tfrac{1}{2}\langle\Phi_p|^{(p)}G_i^\dagger(T_n^{(q)})^2|\Phi_q\rangle H_{qp}^{\rm eff}\ , \tag{46}$$

$$B_{12}^{(p)}(G_i^\dagger)=\langle\Phi_p|^{(p)}G_i^\dagger T_2^{(q)}(T_1^{(q)}-T_1^{(p)})|\Phi_q\rangle H_{qp}^{\rm eff}\ , \tag{47}$$

$$\tilde{B}_{12}^{(p)}(G_i^\dagger)=\langle\Phi_p|^{(p)}G_i^\dagger[T_2^{(q)},T_1^{(p)}]|\Phi_q\rangle H_{qp}^{\rm eff}\ . \tag{48}$$

The off-diagonal elements of the effective Hamiltonian matrix $H_{qp}^{\rm eff}$, $p=1,2$, $q=3-p$, take the form [23,26,29,57]

$$H_{21}^{\rm eff}=\langle\Phi_1|^{(1)}G_{ll}^{kk}(0)(H_{N_1}e^{T_1^{(1)}+T_2^{(1)}})_C|\Phi_1\rangle\ , \tag{49}$$

$$H_{12}^{\rm eff}=\langle\Phi_2|^{(2)}G_{kk}^{ll}(0)(H_{N_2}e^{T_1^{(2)}+T_2^{(2)}})_C|\Phi_2\rangle\ , \tag{50}$$

since

$$|\Phi_2\rangle={}^{(1)}G_{kk}^{ll}(0)|\Phi_1\rangle\ , \tag{51}$$

$$|\Phi_1\rangle={}^{(2)}G_{ll}^{kk}(0)|\Phi_2\rangle\ , \tag{52}$$

and [29,57]

$$G_{ll}^{kk}(0)=[G_{kk}^{ll}(0)]^\dagger\ . \tag{53}$$

They can involve at most quartic terms, namely $(T_1^{(p)})^4$. The diagonal elements $H_{pp}^{\rm eff}$, $p=1,2$, which together with off-diagonal terms $H_{qp}^{\rm eff}$, Eqs. (49) and (50), are needed to solve the 2×2 secular problem [cf. Eq. (22)]

$$\begin{aligned}H_{11}^{\rm eff}c_{1\mu}+H_{12}^{\rm eff}c_{2\mu}&=E_\mu c_{1\mu}\ ,\\ H_{21}^{\rm eff}c_{1\mu}+H_{22}^{\rm eff}c_{2\mu}&=E_\mu c_{2\mu}\ ,\end{aligned} \tag{54}$$

are identical with SRCC expressions for the energy (see Refs. [23] and [57]), i.e.,

$$H_{pp}^{\rm eff}=H_{pp}+\langle\Phi_p|\{H_{N_p}[T_1^{(p)}+T_2^{(p)}+\tfrac{1}{2}(T_1^{(p)})^2]\}_C|\Phi_p\rangle\ , \tag{55}$$

and involve at most quadratic terms $(T_1^{(p)})^2$. Once $H_{pp}^{\rm eff}$ and $H_{qp}^{\rm eff}$, $p=1,2$, $q=3-p$, are known, the energies E_μ, $\mu=1,2$, and the corresponding eigenvectors $\mathbf{c}_\mu$, determining $|\Psi_\mu\rangle$, Eq. (28), are easily found. Equations (40)–(50), (54), and (55), together with expansions (38) and (39), represent the basic equations defining the orthogonally-spin-adapted two-reference fully quadratic CCSD approach.

It remains to work out the explicit expressions for the quantities given by Eqs. (41)–(50) and (55) in terms of one- and two-body cluster amplitudes $\langle\rho|t_1^{(p)}|\alpha\rangle$ and $\langle\rho\sigma|t_2^{(p)}|\alpha\beta\rangle_i$ and one- and two-electron integrals. These may be found in Refs. [23] ($L_n^{(p)}$, $R_n^{(p)}$, $H_{pp}^{\rm eff}$, $H_{qp}^{\rm eff}$), [26] ($Q_{nn'}^{(p)}$, $B_{nn'}^{(p)}$, $\tilde{B}_{12}^{(p)}$), [29] ($H_{qp}^{\rm eff}$ up to linear terms, $R_n^{(p)}$, $B_{nn'}^{(p)}$, $\tilde{B}_{12}^{(p)}$), and [57] ($L_n^{(p)}$, $Q_{nn'}^{(p)}$, $H_{pp}^{\rm eff}$, $H_{qp}^{\rm eff}$), where we employed either the algebraic approach exploiting the replacement-operator technique [59] (see Refs. [23] and [26]) or the diagrammatic procedure based on graphical methods of spin algebras [3,55] (see Refs. [29] and [57]). The resulting expressions are highly symmetric and can be cast into a very compact form. The use of Eq. (33) in its actual form, with the product $e^{-T^{(p)}}e^{T^{(q)}}$ on the right-hand side, is not as cumbersome as stated in Ref. [27], at least at the level of approximation described in this section, since most of the terms vanish and only few survive.

Some terms appearing in Eq. (40) can be grouped together, further simplifying final formulas. For example, we can combine the linear and bilinear terms involving cluster components of the same excitation order, such as $L_2^{(p)}(G_i^\dagger)$ and $Q_{11}^{(p)}(G_i^\dagger)$ (see Ref. [57]) or $R_2^{(p)}(G_i^\dagger)$ and $B_{11}^{(p)}(G_i^\dagger)$ (see Ref. [29]). Since we wish to explore the role of individual contributions given by Eqs. (41)–(48) (in particular, the effect of monoexcited clusters), we avoid such grouping. Combining the coupling terms $R_2^{(p)}(G_i^\dagger)$ and $B_{11}^{(p)}(G_i^\dagger)$ is also inconvenient when we wish to test the role of various approximations for the effective Hamiltonian (cf. Ref. [30]), since we must then use the same approximation for $H_{qp}^{\rm eff}$ in both Eqs. (45) and (46). We could also combine the bilinear coupling terms $B_{12}^{(p)}(G_i^\dagger)$ and $\tilde{B}_{12}^{(p)}(G_i^\dagger)$ by introducing the single term

$$\tilde{\tilde{B}}_{12}^{(p)}(G_i^\dagger)=B_{12}^{(p)}(G_i^\dagger)+\tilde{B}_{12}^{(p)}(G_i^\dagger)\ , \tag{56}$$

since [29]

$$\tilde{\tilde{B}}_{12}^{(p)}(G_i^\dagger)=\langle\Phi_p|^{(p)}G_i^\dagger(T_1^{(q)}-T_1^{(p)})T_2^q|\Phi_q\rangle H_{qp}^{\rm eff}\ . \tag{57}$$

This is particularly natural from the diagrammatic viewpoint [29]. However,

$$\tilde{B}_{12}^{(p)}(G_\rho^\alpha)=0\ , \tag{58}$$

while the two-body components $B_{12}^{(p)}[G_{\rho\sigma}^{\alpha\beta}(i)]$ and $\tilde{B}_{12}^{(p)}[G_{\rho\sigma}^{\alpha\beta}(i)]$ contribute for different types of double excitations [29]. It is thus best to consider them separately. We recall [29] here that $G_\rho^\alpha=(G_\alpha^\rho)^\dagger$ and $G_{\rho\sigma}^{\alpha\beta}(i)=[G_{\alpha\beta}^{\rho\sigma}(i)]^\dagger$.

To examine the role of various contributions (41)–(48) in the MRCCSD formalism, different variants of the MRCCSD method are considered. We start with the linear MRCCSD (L-MRCCSD) theory, which arises by neglecting the nonlinear terms $Q_{nn'}^{(p)}(G_i^\dagger)$, $B_{nn'}^{(p)}(G_i^\dagger)$, and $\tilde{B}_{12}^{(p)}(G_i^\dagger)$ in Eq. (40). In this method the off-diagonal elements of the effective Hamiltonian $H_{qp}^{\rm eff}$ that enter the coupling terms $R_n^{(p)}(G_i^\dagger)$ must be approximated by matrix elements H_{qp}, lest the linearity of $R_n^{(p)}(G_i^\dagger)$ be destroyed. Full expansions of the effective Hamiltonian in terms of cluster amplitudes, Eqs. (49), (50), and (55), are only used when evaluating the energies E_μ and coefficients $\mathbf{c}_\mu$, Eq. (54). Since the linear theory works well only in the highly (quasi)degenerate regimes and is often plagued with singularities in nondegenerate cases [26,30] (see Sec. V), we examine three different nonlinear approximations. First, we test the role of disconnected tetraexcited clus-

ters $\frac{1}{2}(T_2^{(p)})^2$ in the direct term. This approximation, referred to as the MRCCSD-1 method, considers the nonlinear contribution $Q_{22}^{(p)}(G_i^\dagger)$, Eq. (43), in addition to absolute and all linear terms. Thus the MRCCSD-1 equations result from Eq. (40) by setting $Q_{11}^{(p)}(G_i^\dagger)=Q_{12}^{(p)}(G_i^\dagger)=B_{nn}^{(p)}(G_i^\dagger)=\tilde{B}_{12}^{(p)}(G_i^\dagger)=0$. Next, the MRCCSD-2 approximation considers pair-cluster interactions in the direct and coupling terms, so that both $Q_{22}^{(p)}(G_i^\dagger)$ and $B_{22}^{(p)}(G_i^\dagger)$ terms, Eqs. (43) and (46), respectively, are retained while the remaining bilinear terms $Q_{11}^{(p)}(G_i^\dagger)$, $Q_{12}^{(p)}(G_i^\dagger)$, $B_{11}^{(p)}(G_i^\dagger)$, $B_{12}^{(p)}(G_i^\dagger)$, and $\tilde{B}_{12}^{(p)}(G_i^\dagger)$ are neglected. This approach was already employed in Ref. [26]. Finally, the fully quadratic MRCCSD approximation, hereafter referred to as the MRCCSD-3 method, considers all bilinear terms given by Eqs. (43), (44), and (46)–(48). Comparison of MRCCSD-2 and MRCCSD-3 results will enable us to assess the role played by the nonlinear terms involving one-body clusters $T_1^{(p)}$.

In all three nonlinear approximations we employ the full expansion for the effective Hamiltonian, Eqs. (49), (50), and (55). The role of various terms appearing in these expressions was already investigated in Ref. [30], where three different truncation schemes for $H^{\rm eff}$ were analyzed in the MRCCSD-3 approach. In the crudest approximation [30], referred to as MRCCSD-3*a*, we considered at most bilinear contributions to $H^{\rm eff}$ and, in addition, we required that the entire expression for the coupling term (taking into account the dependence of $H^{\rm eff}$ on cluster amplitudes) contains at most bilinear terms, so that the absolute term H_{qp} replaced $H_{qp}^{\rm eff}$ in expressions for $B_{nn}^{(p)}(G_i^\dagger)$ and $\tilde{B}_{12}^{(p)}(G_i^\dagger)$, while in computing the linear terms $R_n^{(p)}(G_i^\dagger)$ we assumed that [29] [cf. Eq. (29)]

$$H_{qp}^{\rm eff}=H_{qp}+\langle\Phi_q|[H_{N_p}(T_1^{(p)}+T_2^{(p)})]_C|\Phi_p\rangle\ . \tag{59}$$

In the MRCCSD-3*b* approximation we neglected cubic and quartic terms in $H_{12}^{\rm eff}$ and $H_{21}^{\rm eff}$, so that the effective Hamiltonian matrix elements entering the right-hand side of Eq. (40) and those appearing in the secular problem (54) contained at most bilinear terms. Finally, in the last approximation [30] MRCCSD-3*c*, we simply considered all nonlinear contributions to the effective Hamiltonian (even the cubic and quartic ones). Comparison of energies obtained with the MRCCSD-3x, $x=a,b,c$, approaches showed that different truncation schemes for the effective Hamiltonian matrix elements lead to almost identical results with differences amounting to at most a few millihartrees (couple of microhartrees when the MRCCSD-3*b* and MRCCSD-3*c* energies are compared [30]). In view of this fact and the simplicity of computing $H^{\rm eff}$ for a two-reference model space, we employed the full effective Hamiltonian in all MRCCSD methods investigated in this paper (except for L-MRCCSD).

To explore the basic characteristics of the SUCC approach, in particular its limitations in determining potential-energy surfaces for various molecular systems, and to get detailed information about the quality of the resulting eigenstates, we apply the above-described MRCCSD schemes to simple four-electron model systems consisting of two interacting hydrogen molecules. A brief description of these models and of computational details associated with the implementation and use of the orthogonally-spin-adapted two-reference formalism are given in the next section.

IV. COMPUTATIONAL DETAILS

A. Model description

In this paper and subsequently [36] we study a prototypical molecular system for which the range of the configurational and orbital quasidegeneracies [60] can be continuously varied by changing a single parameter defining its geometry, and which is simple enough to enable numerous computations using many different methods to be carried out, including the full configuration-interaction (FCI) method providing the exact solution. In this way, we can assess the effectiveness of various MRCC approaches and gain deeper insight into the nature of the resulting solutions.

The model consists of two interacting hydrogen molecules in several geometrical arrangements. In this paper we concentrate on planar models introduced by Jankowski and Paldus [37], namely, H4, D4, and P4 (see Fig. 1). Nonplanar geometries will be the subject of future work [36]. In the H4 model [Fig. 1(a)], the H_2 molecules are arranged in an isosceles trapezoidal configuration with all nearest-neighbor internuclear separations (or H—H "bond lengths") fixed and equal to a, while the angle $\delta=\angle$H(1)-H(2)-H(3)$-\pi/2=\angle$H(2)-H(3)-H(4)$-\pi/2$ varies in the interval $\delta\in[0,\pi/2]$. We define the "degeneracy parameter" $\alpha=\delta/\pi$, $\alpha\in[0,\frac{1}{2}]$. Proceeding from the square conformation ($\alpha=0$) to the linear one ($\alpha=\frac{1}{2}$), we obtain a cross section of the H_4 potential-energy surface involving the dissociation of a single chemical bond.

Once the H(1)—H(4) bond is broken, we can vary the H(2)-H(3) distance. This leads to the linear model D4, whose geometry is determined by the intermolecular separation α, defined as the distance between atoms H(2) and H(3) [Fig. 1(b)]. The parameter α can be varied from 0 to infinity, and we can consider both the short-range region $\alpha\le a$ as well as the dissociation of the second chemical bond when $\alpha\gg a$. By proceeding from the square con-

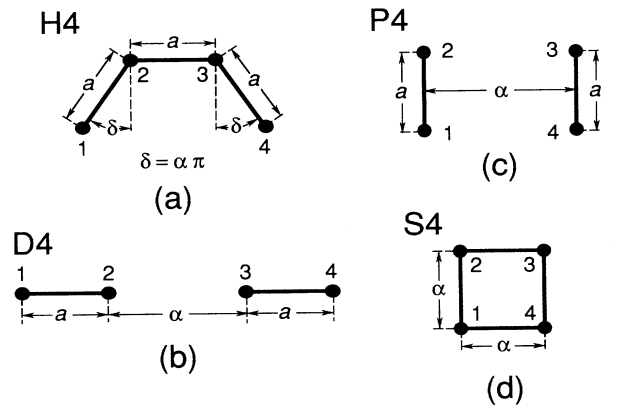

FIG. 1. Nuclear configurations and definition of the parameter α for the H4 (a), D4 (b), P4 (c), and S4 (d) models.

formation to the D4, $\alpha \rightarrow \infty$ limit, we model the consecutive breaking of two chemical bonds.

Another type of dissociation of the H_4 cluster is achieved when two H—H bonds are broken simultaneously. This takes place when we start from the H4, $\alpha=0$ geometry and consider a long-range limit of the P4 model consisting of two parallel hydrogen molecules with nuclei in a rectangular arrangement [Fig. 1(c)]. Geometry of the P4 model is again described by the intermolecular distance α, and the dissociation of the two bonds takes place when $\alpha \gg a$. The highly degenerate compressed case, when $\alpha < a$, is also considered.

The fixed internuclear separation a is usually chosen to be 2.0 a.u., so that the hydrogen molecules involved are slightly stretched (the FCI equilibrium bond length obtained with the MBS used here is approximately 1.667 a.u.; the corresponding restricted Hartree-Fock value is 1.604 a.u.). This enhances the quasidegeneracy effects [26,30] (see later) as illustrated for the trapezoidal geometry (H4 model), for which three different values of a are considered: in addition to the standard stretched bond length $a=2.0$ a.u. we also consider the nearly equilibrium ($a=1.6$ a.u.) and compressed ($a=1.2$ a.u.) geometries.

From this viewpoint it is also interesting to examine the $a \rightarrow \infty$ limit. We thus introduce one additional model, referred to as S4, in which four hydrogen nuclei form a square, and we vary the nearest-neighbor separation from the one corresponding to a compressed geometry to the fully dissociated limit, where all four H—H bonds are broken [Fig. 1(d)]. This is certainly the most demanding model, since our model space cannot describe the simultaneous breaking of all four bonds. It may be compared with a strongly correlated regime in the cyclic polyene model, where most of the many-body methods, including several highly accurate SRCC approaches, encounter serious difficulties (cf., e.g., Refs. [60–63] and references therein).

In this paper and subsequently [36] we restrict ourselves to the MBS models with one $1s$-type atomic orbital [64] (AO) located on each hydrogen nucleus. (The same basis set was employed in Refs. [26–28,30,34,37] and [40–43].) Computations with larger basis sets, including the double zeta plus polarization basis [38] (cf. also Refs. [27] and [39]), clearly indicate the relevance and usefulness of MBS models, which not only display all the qualitative features involved (such as the singular behavior of linear CC (L-CC) approaches [26,30,37,38] and the role of various terms arising in the theory [30,37]), but also give a good quantitative estimate of the performance of various approximate procedures when compared with the corresponding exact FCI results. However, in spite of all these useful features of MBS H_4 models, we must still keep in mind their inherent limitations.

B. Reference configurations and orbitals

To define our model spaces we employ restricted Hartree-Fock (RHF) MO's in the linear combination of atomic orbitals (LCAO) approximation. Since all our models possess at least one symmetry element of order 2, each MO must either be symmetric or antisymmetric with respect to this operation. For example, four RHF MO's for the MBS H4 and D4 models, whose spatial symmetry groups are, respectively, C_{2v} and $D_{\infty h}$, take the following form:

$$\phi_i = a_i[\chi_1 + (-1)^{i+1}\chi_4] + (-1)^{[(i-1)/2]} b_i[\chi_2 + (-1)^{i+1}\chi_3] , \quad (i=1,\ldots,4) , \tag{60}$$

where $[x]$ designates the largest integer not exceeding x (Gauss symbol) and χ_j, $j=1,\ldots,4$ are the $1s$ atomic orbitals centered on nuclei H(j) (cf. Fig. 1). Thus, only four LCAO coefficients (one for each MO) are unknown and must be determined by the RHF iterative procedure. The situation is even simpler for the P4 and S4 models, since corresponding RHF MO's are fully determined by the D_{2h} symmetry group of the P4 model, so that

$$a_i = b_i , \quad (i=1,\ldots,4) . \tag{61}$$

For the S4 model, $a_2=a_3$, so that orbitals ϕ_i, Eqs. (60) and (61), are adapted to the chain $D_{2h} \subset D_{4h}$, the latter group being the symmetry group of S4. Thus, the orbitals (60), (61) for the S4 model can be classified either according to the irreducible representations (irreps) of D_{2h} (symmetry group of the P4 model) or D_{4h}. The symmetry groups of various models and the symmetry species of the corresponding RHF MO's are summarized in Table I. Note that for the S4 model, ϕ_2 and ϕ_3 span two one-dimensional irreps b_{2u} and b_{3u} of D_{2h} or a two-dimensional irrep e_u of D_{4h}, which decomposes into b_{2u} and b_{3u} when subduced to D_{2h},

$$e_u(D_{4h})\downarrow D_{2h} = b_{2u} + b_{3u} . \tag{62}$$

Except for the compressed ($\alpha < a$) P4 model, the orbital labeling ϕ_i, $i=1,2,3,4$, corresponds to the increasing orbital energy and the RHF ground-state configuration is $(\phi_1)^2(\phi_2)^2$. When $\alpha < a$ in the P4 model, the configuration $(\phi_1)^2(\phi_3)^2$ becomes the RHF ground state while $(\phi_1)^2(\phi_2)^2$ represents one of the excited configurations. The orbital energy picture associated with these configurations is shown in Fig. 2. It is evident that both configurations $(\phi_1)^2(\phi_2)^2$ and $(\phi_1)^2(\phi_3)^2$ become degenerate for the square geometry $\alpha=a$, since the orbital energies associated with these two different occupation schemes are equivalent when $\alpha=a$. We could, of course, switch the MO's when passing through the square geometry (when proceeding from large α's toward the $\alpha=0$ limit), but it is more instructive to use $(\phi_1)^2(\phi_2)^2$ as

TABLE I. Symmetry groups of the studied models and symmetry species of the RHF MO's, Eqs. (60) and (61).

Model	Symmetry group	MO symmetry species			
		ϕ_1	ϕ_2	ϕ_3	ϕ_4
H4	C_{2v}	a_1	b_1	a_1	b_1
D4	$D_{\infty h}$	σ_g^+	σ_u^+	σ_g^+	σ_u^+
P4	D_{2h}	a_g	b_{2u}	b_{3u}	b_{1g}
S4	D_{4h}	a_{1g}	e_u	e_u	b_{2g}

a reference even for $\alpha < a$, since the corresponding highest occupied (HOMO) and lowest unoccupied (LUMO) MO's, ϕ_2 and ϕ_3, respectively, become exactly degenerate at some point $\alpha_0 < a$ (for example, for $a = 2.0$ a.u., $\alpha_0 = 1.1428$ a.u.; cf. Fig. 2), which would not happen if we switched to the $(\phi_1)^2(\phi_3)^2$ reference. In this way we can explore the entire range of the orbital quasidegeneracy [60] effects, including nondegenerate cases and vanishing of the HOMO-LUMO gap. With $(\phi_1)^2(\phi_2)^2$ as a reference, the orbital energies ε_2 and ε_3 (ε_i is the energy of ϕ_i) cross one another at α_0, so that for $\alpha < \alpha_0$ we have $\varepsilon_3 < \varepsilon_2$ (cf. Fig. 2). HOMO and LUMO energies associated with the $(\phi_1)^2(\phi_3)^2$ configuration also cross, this time for $\alpha_0' > a$ (for $a = 2.0$ a.u., $\alpha_0' = 3.4611$ a.u.; cf. Fig. 2). The fact that both energy crossings are shifted away from the square geometry, where it should occur according to simple MO theory, was first documented by Fukutome in his study of instabilities of RHF solutions describing chemical reactions [65]. Fukutome proved that crossing of the HOMO and LUMO energy levels of configurations $(\phi_1)^2(\phi_2)^2$ and $(\phi_1)^2(\phi_3)^2$ cannot take place at the square nuclear configuration due to the presence of interelectronic repulsion terms in the Hamiltonian. Consequently, the orbitals ϕ_2 and ϕ_3 for the S4 model are never degenerate, despite the fact that they belong to the same symmetry species e_u of D_{4h}. The size of the HOMO-LUMO gap is measured by the magnitude of the interelectronic repulsion integral $\gamma_{12} = \langle \chi_1\chi_2 | \chi_1\chi_2 \rangle \equiv (\chi_1\chi_1 | \chi_2\chi_2)$ so that the orbitals ϕ_2 and ϕ_3 become degenerate only in the fully dissociated limit of the S4 model, where all the orbital energies are identical and equal to the energy of the $1s$ hydrogenic orbital (see Fig. 3).

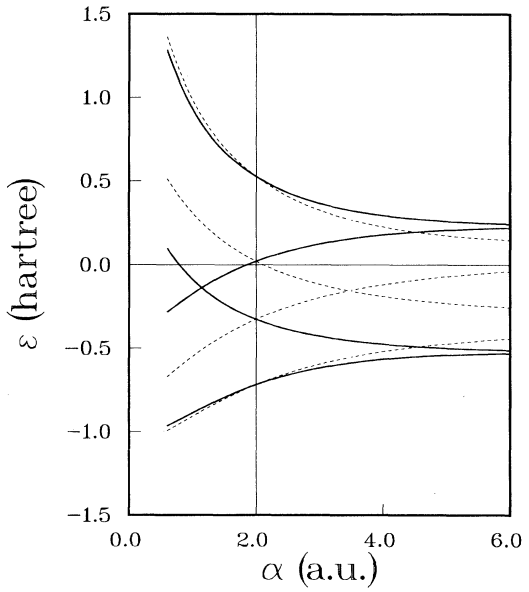

FIG. 2. Dependence of the Hartree-Fock orbital energies ε_i (in hartrees) that are associated with configurations $(\phi_1)^2(\phi_2)^2$ (solid lines) and $(\phi_1)^2(\phi_3)^2$ (short-dashed lines) for the MBS P4 model with $a = 2.0$ a.u. on the parameter α. For both configurations, the energies ε_i of the MO's ϕ_i for $\alpha = 6.0$ a.u. increase in the order: $\varepsilon_1 < \varepsilon_2 < \varepsilon_3 < \varepsilon_4$. Notice that the crossing of HOMO and LUMO energy levels is always shifted away from the square geometry. For the RHF solution $(\phi_1)^2(\phi_2)^2$ it occurs at $\alpha_0 = 1.1428$ a.u., while for the configuration $(\phi_1)^2(\phi_3)^2$ it occurs at $\alpha_0' = 3.4611$ a.u. (see the text for details).

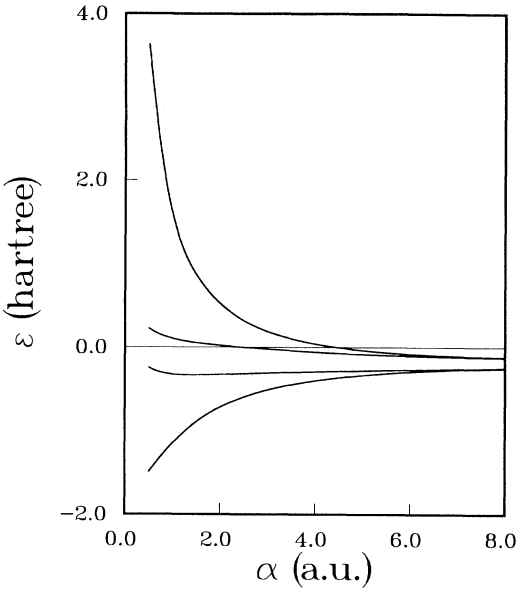

FIG. 3. Dependence of the Hartree-Fock orbital energies ε_i (in hartrees) that are associated with configuration $(\phi_1)^2(\phi_2)^2$ for the MBS S4 model on the parameter α. The orbital labeling ϕ_1, ϕ_2, ϕ_3, ϕ_4 corresponds to the increasing orbital energy. The same diagram would result if the $(\phi_1)^2(\phi_3)^2$ configuration was used as a reference, but the energies of MO's would increase in the order $\varepsilon_1 < \varepsilon_3 < \varepsilon_2 < \varepsilon_4$. Notice that the HOMO-LUMO energy gap never vanishes for finite values of α (cf. the text for details; see also Fig. 2).

The existence of a nonvanishing HOMO-LUMO gap for the square geometry, in spite of the fact that orbitals ϕ_2 and ϕ_3 belong to the same symmetry species of D_{4h}, is an indication of symmetry breaking. In fact, the Fock operator for the S4 model, associated with the solution $(\phi_1)^2(\phi_2)^2$ [or $(\phi_1)^2(\phi_3)^2$], does not commute with all symmetry operations of D_{4h}, but only with those belonging to D_{2h}. Symbolically, we can express this fact by writing

$$\begin{aligned} &[F[(\phi_1)^2(\phi_j)^2], D_{2h}] = 0 , \\ &[F[(\phi_1)^2(\phi_j)^2], D_{4h} \setminus D_{2h}] \neq 0, \quad (j = 2,3) . \end{aligned} \tag{63}$$

Relations (63) are an obvious consequence of the fact that both single-determinantal configurations $(\phi_1)^2(\phi_2)^2$ and $(\phi_1)^2(\phi_3)^2$ violate the D_{4h} symmetry of the S4 model. The e_u orbitals are only partially filled in either $(\phi_1)^2(\phi_2)^2$ or $(\phi_1)^2(\phi_3)^2$ configuration. In order to avoid this symmetry breaking while using a single-determinantal reference, we would have to use $(\phi_1)^2(\phi_4)^2$ configuration, in which both e_u orbitals remain unoccupied. In this case we would have

$$[F[(\phi_1)^2(\phi_4)^2], D_{4h}] = 0 , \tag{64}$$

and the empty orbitals ϕ_2 and ϕ_3 would be degenerate. This symmetry breaking has additional consequences for the MRCC formalism employing $(\phi_1)^2(\phi_2)^2$ and $(\phi_1)^2(\phi_3)^2$ as references, as will be shown later on. Let us

TABLE II. FCI coefficients of the configurations $|\Phi_1\rangle = |(\phi_1)^2(\phi_2)^2|$ and $|\Phi_2\rangle = |(\phi_1)^2(\phi_3)^2|$ for the ground-state wave function of the MBS H4 model with the H-H internuclear separations $a = 1.2$, 1.6, and 2.0 a.u. and different values of the parameter α.

a	Configuration \ α	0.500	0.200	0.150	0.100	0.050	0.010	0.005	0.000
1.2	$\|\Phi_1\rangle$	0.991	0.988	0.986	0.982	0.966	0.833	0.775	0.702
	$\|\Phi_2\rangle$	−0.106	−0.114	−0.123	−0.148	−0.228	−0.539	−0.619	−0.702
1.6	$\|\Phi_1\rangle$	0.983	0.979	0.976	0.970	0.948	0.811	0.760	0.697
	$\|\Phi_2\rangle$	−0.146	−0.153	−0.162	−0.187	−0.270	−0.560	−0.628	−0.697
2.0	$\|\Phi_1\rangle$	0.967	0.962	0.958	0.949	0.922	0.786	0.742	0.690
	$\|\Phi_2\rangle$	−0.193	−0.200	−0.209	−0.234	−0.317	−0.576	−0.632	−0.690

only mention that we encounter many more cases of symmetry breaking when studying nonplanar geometries [36,66].

C. Orbital and configurational degeneracies

We have seen that the RHF MO's associated with the $(\phi_1)^2(\phi_2)^2$ configuration display various degrees of quasidegeneracy, including the exact degeneracy of HOMO and LUMO levels for certain conformations. It is well known, however, that orbital degeneracy alone causes few problems for CC approaches [60]. Even the simplest L-CC methods give accurate correlation energies in such cases (cf., e.g., Refs. [67] and [68]). Configurational degeneracy, on the other hand, is of much greater concern. In this case, the linear SRCC (L-SRCC) approaches, such as L-CCD (CC with doubly excited amplitudes) or L-CCSD, suffer singular behavior due to the strong interaction of the ground-state configuration with the low-lying biexcited states [37,38,53,61,62,69], while the L-MRCC methods fail due to the presence of intruder states, which strongly interact with one or more model-space configurations [26,30] (see the next two sections). Inclusion of nonlinear terms in the CC formalism removes the L-CC singularities [26,30,37,38,53,61,62], but new serious problems arise when both types of quasidegeneracies (orbital and configurational) are simultaneously present or when the dimension of the quasidegenerate reference space becomes very large [60]. For example, in the linear metallike systems, even the full CCSD or CCSDT (CCSD with triply excited cluster amplitudes) approaches suffer singular behavior [61–63].

It is thus important to examine the effect of various configurational degeneracies. The H_4 models provide us with a useful example in this regard. In the case of H4, P4, and S4 models, we deal with a rather strong configurational quasidegeneracy involving configurations $(\phi_1)^2(\phi_2)^2$ and $(\phi_1)^2(\phi_3)^2$, as may be seen by examining the FCI ground-state wave function (cf. Tables II and III). As mentioned earlier, this quasidegeneracy becomes more pronounced with increasing internuclear distance a (see, e.g., the FCI coefficients for the H4, $a = 1.2$, 1.6, and 2.0 a.u. models in Table II). True degeneracy of $(\phi_1)^2(\phi_2)^2$ and $(\phi_1)^2(\phi_3)^2$ configurations is then reached for the square geometry $\alpha = a$ (cf., Table III). Thus, a challenging situation arises when the dissociation limit of the S4 model is studied. In this limit, orbital and configurational degeneracies are heavily mixed, producing a very severe test for various formalisms, including the MRCC theory investigated in this paper. Although the model space employed cannot properly describe the $H_4 \rightarrow 4H$ dissociation, this $a = \alpha \rightarrow \infty$ limit of the S4 model may be compared to a strongly correlated regime in the cyclic polyene model, where the increasing role of quadruply excited connected cluster components [70] causes the failure of highly sophisticated theories like CCSDT [63]. It is thus worthwhile to examine the behavior of the two-reference formalism in this limit.

The D4 model represents an entirely different situation, since the $(\phi_1)^2(\phi_3)^2$ configuration is relatively impor-

TABLE III. Same as Table II for the MBS D4, P4, and S4 models with $a = 2.0$ a.u.

Model	Configuration \ α	7.0	5.0	3.0	2.5	2.2	2.0	1.8	1.5
D4	$\|\Phi_1\rangle$	0.968	0.968	0.969	0.969	0.968	0.967	0.964	0.957
	$\|\Phi_2\rangle$	−0.088	−0.091	−0.123	−0.149	−0.173	−0.193	−0.216	−0.257
P4	$\|\Phi_1\rangle$	0.968	0.968	0.961	0.947	0.893	0.690	0.345	0.144
	$\|\Phi_2\rangle$	−0.088	−0.094	−0.143	−0.219	−0.386	−0.690	−0.916	−0.976
S4	$\|\Phi_1\rangle$	0.451	0.524	0.656	0.676	0.685	0.690	0.694	0.698
	$\|\Phi_2\rangle$	−0.451	−0.524	−0.656	−0.676	−0.685	−0.690	−0.694	−0.698

tant only for small α values (see Table III). For large α values, the dominant configuration in the FCI expansion of the ground-state wave function is $(\phi_1)^2(\phi_2)^2$, while almost all biexcited configurations relative to $(\phi_1)^2(\phi_2)^2$ contribute equally (a similar situation occurs in the case of the P4 model when $\alpha\rightarrow\infty$; see Ref. [37]). Thus, the D4 model essentially represents a single-reference case with an increasingly rich biexcited manifold for large α's.

D. Model spaces

The dominant role of CS configurations $(\phi_1)^2(\phi_2)^2$ and $(\phi_1)^2(\phi_3)^2$ suggests their choice as model states for our MRCC formalism. Such choice of the model space perfectly fits the two-reference theory described in the previous section. The lowest totally symmetric orbital ϕ_1 represents the core orbital and the next two orbitals, ϕ_2 and ϕ_3, the active orbitals. Since ϕ_2 and ϕ_3 belong to different symmetry species (see Table I), the two-configuration model space is complete. We thus have

$$|\Phi_1\rangle=|(\phi_1)^2(\phi_2)^2|\ , \tag{65}$$

$$|\Phi_2\rangle=|(\phi_1)^2(\phi_3)^2|\ , \tag{66}$$

so that [cf. Eqs. (51) and (52)]

$$|\Phi_2\rangle={}^{(1)}G^{33}_{22}(0)|\Phi_1\rangle,\quad |\Phi_1\rangle={}^{(2)}G^{22}_{33}(0)|\Phi_2\rangle\ . \tag{67}$$

Since we study the MBS models, there is only one virtual orbital ϕ_4.

The S4 model requires special attention. In this case, active orbitals ϕ_2 and ϕ_3 belong to the same symmetry species e_u of D_{4h}, so that the basic assumption of our two-reference formalism seems to be violated. It would seem that in order to obtain a complete model space, we must also consider the configuration [cf. Eqs. (35) and (36)]

$$|\Phi_3'\rangle={}^{(1)}\left|\begin{matrix}3\\2\end{matrix}\right\rangle\ , \tag{68}$$

and its triplet analog

$$|\Phi_3''\rangle={}^{(1)}\left|\begin{matrix}3\\2\end{matrix};10\right\rangle\ , \tag{69}$$

since the four states $|\Phi_1\rangle$, $|\Phi_2\rangle$, $|\Phi_3'\rangle$, and $|\Phi_3''\rangle$ span the representation e_u^2 of D_{4h}. The triplet state $|\Phi_3''\rangle$ cannot interact with the remaining three e_u^2 states since our Hamiltonian is spin independent. Since the enlarged model space $\tilde{\mathcal{M}}_0=\text{span}\{|\Phi_1\rangle,|\Phi_2\rangle,|\Phi_3'\rangle,|\Phi_3''\rangle\}$ breaks down into a direct sum of subspaces carrying different irreps of D_{4h}

$$\begin{aligned}\tilde{\mathcal{M}}_0&\equiv\text{span}\{|\Phi_1\rangle,|\Phi_2\rangle,|\Phi_3'\rangle,|\Phi_3''\rangle\}\\&=\mathcal{M}_{0,B_{1g}}\oplus\mathcal{M}_{0,A_{1g}}\oplus\mathcal{M}_{0,B_{2g}}\oplus\mathcal{M}_{0,A_{2g}}\ ,\end{aligned} \tag{70}$$

where

$$\mathcal{M}_{0,B_{1g}}=\text{span}\{(|\Phi_1\rangle-|\Phi_2\rangle)/\sqrt{2}\}\ , \tag{71}$$

$$\mathcal{M}_{0,A_{1g}}=\text{span}\{(|\Phi_1\rangle+|\Phi_2\rangle)/\sqrt{2}\}\ , \tag{72}$$

$$\mathcal{M}_{0,B_{2g}}=\text{span}\{|\Phi_3'\rangle\}\ , \tag{73}$$

$$\mathcal{M}_{0,A_{2g}}=\text{span}\{|\Phi_3''\rangle\}\ , \tag{74}$$

the CS configurations $|\Phi_1\rangle$ and $|\Phi_2\rangle$ do not interact with the state $|\Phi_3'\rangle$. Thus, the model space

$$\mathcal{M}_0=\text{span}\{|\Phi_1\rangle,|\Phi_2\rangle\}=\text{span}\{|\tilde{\Phi}_1\rangle,|\tilde{\Phi}_2\rangle\}\ , \tag{75}$$

where

$$|\tilde{\Phi}_1\rangle=(|\Phi_1\rangle-|\Phi_2\rangle)/\sqrt{2}\ , \tag{76}$$

and

$$|\tilde{\Phi}_2\rangle=(|\Phi_1\rangle+|\Phi_2\rangle)/\sqrt{2} \tag{77}$$

can be regarded as a complete reference space. Obviously, decomposition of the enlarged model space $\tilde{\mathcal{M}}_0$, Eq. (70), into a direct sum of four D_{4h}-invariant one-dimensional subspaces corresponds to the group-theoretical relation

$$e_u^2\equiv E_u^2=B_{1g}\oplus A_{1g}\oplus B_{2g}\oplus A_{2g}\ . \tag{78}$$

The RHF MO's (60) and (61) (where $a_2=a_3$) are adapted to the chain $D_{2h}\subset D_{4h}$, so that relations (63) hold. These relations imply that the proper symmetry group to be used for the S4 model is D_{2h}, which implies in turn the completeness of $\mathcal{M}_0$, Eq. (75), since ϕ_2 and ϕ_3 belong to different symmetry species of the D_{2h} group (cf., Table I). We immediately find that both configurations $|\Phi_1\rangle$ and $|\Phi_2\rangle$ [or $|\tilde{\Phi}_1\rangle$ and $|\tilde{\Phi}_2\rangle$, Eqs. (76) and (77)] are D_{2h} totally symmetric, while $|\Phi_3'\rangle$ and $|\Phi_3''\rangle$ transform as $B_{1g}(D_{2h})$ states, in agreement with relations

$$A_{1g}(D_{4h})\downarrow D_{2h}=B_{1g}(D_{4h})\downarrow D_{2h}=A_g(D_{2h})\ , \tag{79}$$

$$A_{2g}(D_{4h})\downarrow D_{2h}=B_{2g}(D_{4h})\downarrow D_{2h}=B_{1g}(D_{2h})\ . \tag{80}$$

We thus conclude that two-reference CC theory employing model space (75) for the S4 model will produce two solutions that are totally symmetric with respect to the symmetry of the Fock operator (D_{2h}), but at the same time belong to different symmetry species of the invariance group of the Hamiltonian (D_{4h}). This is related to the fact that for the model space $\mathcal{M}_0$, the corresponding MRCC wave operator U,

$$U=e^{T^{(1)}}P_1+e^{T^{(2)}}P_2\ , \tag{81}$$

and, in consequence, the effective Hamiltonian H^{eff}, Eq. (19), are invariant with respect to the D_{4h} symmetry operations, so that the resulting states

$$|\Psi_1\rangle=U|\tilde{\Phi}_1\rangle=U(|\Phi_1\rangle-|\Phi_2\rangle)/\sqrt{2}\ , \tag{82}$$

$$|\Psi_2\rangle=U|\tilde{\Phi}_2\rangle=U(|\Phi_1\rangle+|\Phi_2\rangle)/\sqrt{2}\ , \tag{83}$$

may be classified by the symmetry species of D_{4h}. We must remember, however, that the cluster operators $T^{(p)}$, $p=1,2$, break the D_{4h} symmetry in exactly the same way as does the Fock operator $F[(\phi_1)^2(\phi_2)^2]$. Thus, symbolically

TABLE IV. Excitation operators ${}^{(1)}G_i$ generating orthonormal spin-adapted configurations $|\Phi_i\rangle={}^{(1)}G_i|\Phi_1\rangle$ spanning the FCI totally symmetric singlet space for the MBS H4, D4, P4, and S4 models. See Refs. [23,26,29] for the definitions of orthogonally-spin-adapted configurations and excitation operators. As usual, S, D, T, and Q stand for single, double, triple, and quadruple excitations, respectively.

Configuration number i	Excitation operator ${}^{(1)}G_i$	Type	Excitation order	Model
1	1	REF	0	H4,D4,P4,S4
2	${}^{(1)}G^{33}_{22}(0)$	D	2	H4,D4,P4,S4
3	${}^{(1)}G^{44}_{22}(0)$	D	2	H4,D4,P4,S4
4	${}^{(1)}G^{33}_{11}(0)$	D	2	H4,D4,P4,S4
5	${}^{(1)}G^{44}_{11}(0)$	D	2	H4,D4,P4,S4
6	${}^{(1)}G^{34}_{12}(0)$	D	2	H4,D4,P4,S4
7	${}^{(1)}G^{34}_{12}(1)$	D	2	H4,D4,P4,S4
8	${}^{(1)}G^{3}_{1}$	S	1	H4,D4
9	${}^{(1)}G^{4}_{2}$	S	1	H4,D4
10	${}^{(1)}G^{443}_{221}(0,0,\frac{1}{2})={}^{(1)}G^{44}_{22}(0){}^{(1)}G^{3}_{1}$	T	3	H4,D4
11	${}^{(1)}G^{334}_{112}(0,0,\frac{1}{2})={}^{(1)}G^{33}_{11}(0){}^{(1)}G^{4}_{2}$	T	3	H4,D4
12	${}^{(1)}G^{3344}_{1122}(0,0,0,0,0,0)={}^{(1)}G^{33}_{11}(0){}^{(1)}G^{44}_{22}(0)$	Q	4	H4,D4,P4,S4

$$[U,D_{4h}]=0=[H^{\text{eff}},D_{4h}]\ , \tag{84}$$

while

$$\begin{aligned}&[T^{(p)},D_{4h}\setminus D_{2h}]\neq 0\ ,\\ &[T^{(p)},D_{2h}]=0\ ,\end{aligned} \tag{85}$$

which has interesting consequences for the general form of the effective Hamiltonian and the properties of the MRCC solutions for the MBS S4 model (see Sec. V D). Let us mention here that in more general situations even the invariance of the model space with respect to the maximum symmetry group of the Hamiltonian may not take place, and thus the relations analogous to Eq. (84) may not hold, so that the full symmetry group of the Hamiltonian cannot be used to classify the resulting states. Examples of such situations will be presented elsewhere [36]. As a final remark in this discussion, let us emphasize that the high symmetry of the S4 model uniquely determines the coefficients $c_{p\mu}$, Eq. (17) ($c_{11}=-c_{21}=c_{12}=c_{22}=1/\sqrt{2}$), so that we do not have to solve the secular problem (54) to get the eigenvectors $\mathbf{c}_\mu$ in this case.

E. CI results

To assess the performance of various MRCC solutions we compare them with the exact FCI results. For the totally symmetric singlet states considered, we only need twelve configurations. The excitation operators generating the required orthogonally-spin-adapted states $|\Phi_j\rangle$, $j=2-12$, through their action on the reference $|\Phi_1\rangle$ are listed in Table IV. In the case of the P4 and S4 models, monoexcited and triexcited configurations may be ignored, since they belong to other symmetry species than do $|\Phi_1\rangle$ and $|\Phi_2\rangle$ [namely, to $B_{3u}(D_{2h})$, while the remaining eight configurations belong to the totally symmetric $A_g(D_{2h})$ irrep]. Thus, for the MBS P4 and S4 models, the CI method limited to doubly and quadruply excited states and the FCI approach are equivalent (cf. Ref. [37]). An additional splitting of the $A_g(D_{2h})$ FCI matrix for the S4 model into $A_{1g}(D_{4h})$ and $B_{1g}(D_{4h})$ subproblems is not essential here, since the two-reference CC theory considered in this paper yields solutions belonging to different D_{4h} subproblems (see the above discussion).

F. MRCC equations and their solution

Singly and doubly excited operators ${}^{(p)}G^{\rho}_{\alpha}$ and ${}^{(p)}G^{\rho\sigma}_{\alpha\beta}(i)$, ($p=1,2$; $i=0,1$) which are required in the two-reference CCSD formalism, when applied to the MBS H4, D4, P4, and S4 models, are listed in Table V. Acting on model states $|\Phi_1\rangle$ and $|\Phi_2\rangle$, Eqs. (65) and (66), respectively, they generate totally symmetric singlet states in $\mathcal{M}_0^1$, so that all of them carry at least one nonvalence index (1 or 4). In general, we have sixteen excitations (seven for the first reference and nine for the second, see Table V), except for the P4 and S4 models, where the monoexcitations ${}^{(1)}G^3_1$ and ${}^{(1)}G^4_2$ do not contribute. This means that the MRCCSD and MRCCD methods are equivalent for the MBS P4 and S4 models (this will not be the case when larger basis sets are employed). It should also be noticed that for the P4 and S4 models, the biexcitations ${}^{(2)}G^{\rho\sigma}_{\alpha\alpha}(0)$, $\rho\neq\sigma$, and ${}^{(2)}G^{\rho\rho}_{\alpha\beta}(0)$, $\alpha\neq\beta$, are not totally symmetric (cf. Table V).

MRCCSD equations (40) represent an energy-independent system of nonlinear algebraic equations, which has the following general form:

$$a_I+\sum_{J=1}^{N}b_{IJ}t_J+\sum_{\substack{J,K=1\\(J\leq K)}}^{N}c_{IJK}t_Jt_K=0\ ,$$
$$(I=1,2,\ldots,N)\ , \tag{86}$$

where N designates the number of linearly independent singly and doubly excited cluster coefficients $\langle\rho|t_1^{(p)}|\alpha\rangle$

TABLE V. Monoexcitation and biexcitation operators ${}^{(p)}G^{\rho}_{\alpha}$ and ${}^{(p)}G^{\rho\sigma}_{\alpha\beta}(i)$, $(p=1,2;\ i=0,1)$ required in the two-reference CCSD formalism when applied to the MBS H4, D4, P4, and S4 models. Equation number I labels the equations in system (86), $N=16$.

p	Equation number (I)	${}^{(p)}G_i$	Model
1	1	${}^{(1)}G^{44}_{22}(0)$	H4,D4,P4,S4
	2	${}^{(1)}G^{33}_{11}(0)$	H4,D4,P4,S4
	3	${}^{(1)}G^{44}_{11}(0)$	H4,D4,P4,S4
	4	${}^{(1)}G^{34}_{12}(0)$	H4,D4,P4,S4
	5	${}^{(1)}G^{34}_{12}(1)$	H4,D4,P4,S4
	6	${}^{(1)}G^{3}_{1}$	H4,D4
	7	${}^{(1)}G^{4}_{2}$	H4,D4
2	8	${}^{(2)}G^{24}_{11}(0)$	H4,D4
	9	${}^{(2)}G^{22}_{13}(0)$	H4,D4
	10	${}^{(2)}G^{44}_{13}(0)$	H4,D4
	11	${}^{(2)}G^{24}_{33}(0)$	H4,D4
	12	${}^{(2)}G^{22}_{11}(0)$	H4,D4,P4,S4
	13	${}^{(2)}G^{44}_{11}(0)$	H4,D4,P4,S4
	14	${}^{(2)}G^{44}_{33}(0)$	H4,D4,P4,S4
	15	${}^{(2)}G^{24}_{13}(0)$	H4,D4,P4,S4
	16	${}^{(2)}G^{24}_{13}(1)$	H4,D4,P4,S4

and $\langle\rho\sigma|t_2^{(p)}|\alpha\beta\rangle_i$ (for brevity designated here as t_I) or operators ${}^{(p)}G^{\rho}_{\alpha}$ and ${}^{(p)}G^{\rho\sigma}_{\alpha\beta}(i)$, $(p=0,1;\ i=0,1)$. Since the order of the spin- and symmetry-adapted MRCCSD system of equations for all the models considered in the present paper is very small (cf. Table V), we can simply store the necessary coefficients a_I, b_{IJ}, and c_{IJK} and solve the system (86) for the unknown cluster amplitudes t_I by applying the standard Newton-Raphson procedure [see, e.g., Appendix B in Ref. 68(a)], while using Gaussian elimination to solve the linear system resulting in each iteration. Normally, only a few iterations (at most a dozen or so) are needed to achieve eight-digit accuracy for the cluster amplitudes, or better. The entire procedure is thus very similar to that used in our SRCC calculations [2,37,38,60–63,67,68,71–73]. The only essential difference is the presence of effective Hamiltonian matrix elements $H^{\rm eff}_{21}$ and $H^{\rm eff}_{12}$ in the linear and bilinear coupling terms, entering Eq. (86), which depend on cluster amplitudes and must be recalculated in every Newton-Raphson iteration (other algorithms, like allowing the Newton-Raphson procedure to converge first before updating the coupling term and then iterating in this fashion until convergence is achieved, were also examined, but finally we decided to update coupling terms after each Newton-Raphson iteration).

The convergence rate of the Newton-Raphson scheme strongly depends on the initial guess $\mathbf{t}^{(0)}=\|t_I^{(0)}\|_{1\le I\le N}$. Moreover, the system of nonlinear equations (86) may possess numerous solutions, in which case the actual solution that we obtain will depend on the choice of $\mathbf{t}^{(0)}$. As we have shown earlier [26,30] (cf. also Refs. [61] and [63]), an appropriate choice of $\mathbf{t}^{(0)}$ is very crucial. The L-MRCC solutions [obtained by solving system (86) with the nonlinear part neglected, $c_{IJK}=0$] are often useless due to their singular behavior caused by the presence of intruder states [26,30] (see the next two sections). Although it is possible that in some cases this situation can be remedied by employing other choices for $\mathbf{t}^{(0)}$ (cf. discussion in Refs. [61] and [63]), the best way to avoid convergence problems due to an appropriate choice of initial guess for cluster amplitudes is to exploit an "analytic continuation" of solutions from the region of geometries for which a good starting point is easily available. This procedure, which we often exploited in the past [26,30,37,38,60–63,71–73], employs as a first approximation $\mathbf{t}^{(0)}$, the converged solution for a sufficiently close geometry,

$$\mathbf{t}^{(0)}(\alpha+\Delta\alpha)=\mathbf{t}(\alpha)\ , \tag{87}$$

while choosing a sufficiently small step $\Delta\alpha$. This procedure is particularly helpful in the vicinity of singularities (most likely algebraic branch points; cf. Refs. [61] and [63]), that plague some of the nonlinear MRCCSD solutions (see the following sections). This analytic continuation is the only procedure that enables us to follow a particular solution of the system (86) while changing the geometry of the model. As far as we know, it is the only method that enables us to examine the analytic properties of CC potential-energy surfaces and the only efficient way to determine the limits of applicability of CC approaches (cf. Refs. [61] and [63]).

The actual computations were carried out with a set of programs exploiting both the spin and spatial symmetry common to all models. This was achieved by adapting the codes used in the original SR studies of the H_4 models [37] to the two-reference case. Correctness of these codes was checked by deriving explicit expressions for various terms occurring in the MRCCSD equations for the MBS H_4 models in different ways and checking them numerically. Exploitation of the available symmetries allowed us to reduce the dimension of the problem and thus to eliminate most of the difficulties which are normally associated with CC computations. The GAMESS electronic structure package [74] of computer programs was used for the initial RHF calculations. The one- and two-electron molecular integrals needed to construct the coefficients a_I, b_{IJ}, and c_{IJK} and the effective Hamiltonian matrix were evaluated using the transformation routines that form part of the GAMESS CI system.

V. RESULTS

We now focus on a comparison of MRCCSD energies with FCI data. Some specific problems, namely the breakdown of the L-MRCCSD method and the cluster analysis of the MRCCSD wave functions, are addressed in Secs. VI and VII.

A. H4 model

In the vicinity of the degenerate limit ($\alpha=0$), even the simplest L-MRCCSD formalism provides very good correlation energies. For $\alpha<0.05$, the energies (of the two lowest totally symmetric singlets) differ from the FCI energies by at most a couple of millihartrees (mhartree) [26]. This excellent performance of the L-MRCCSD

method in the degenerate region is apparent from Figs. 4(a)–4(c), which display the α dependence of the L-MRCCSD and MRCCSD-3 energies for three distinct internuclear separations $a=1.2$, 1.6, and 2.0 a.u. As the nondegenerate regime is approached, the second reference state energy becomes degenerate with the next lowest-lying state that acts as an intruder state and the L-MRCC theory undergoes singular behavior. This behavior is very similar to that of SR L-CCD and L-CCSD approaches in the vicinity of the $\alpha=0$ limit [37,38], in which case our second reference $|\Phi_2\rangle$ plays the role of an intruder. Clearly, inclusion of $|\Phi_2\rangle$ in our model space removes the singularity arising in the SR approach but at the same time increases the probability of encountering another intruder that interacts with $|\Phi_2\rangle$. This problem is even more acute for the D4, P4, and S4 models, where

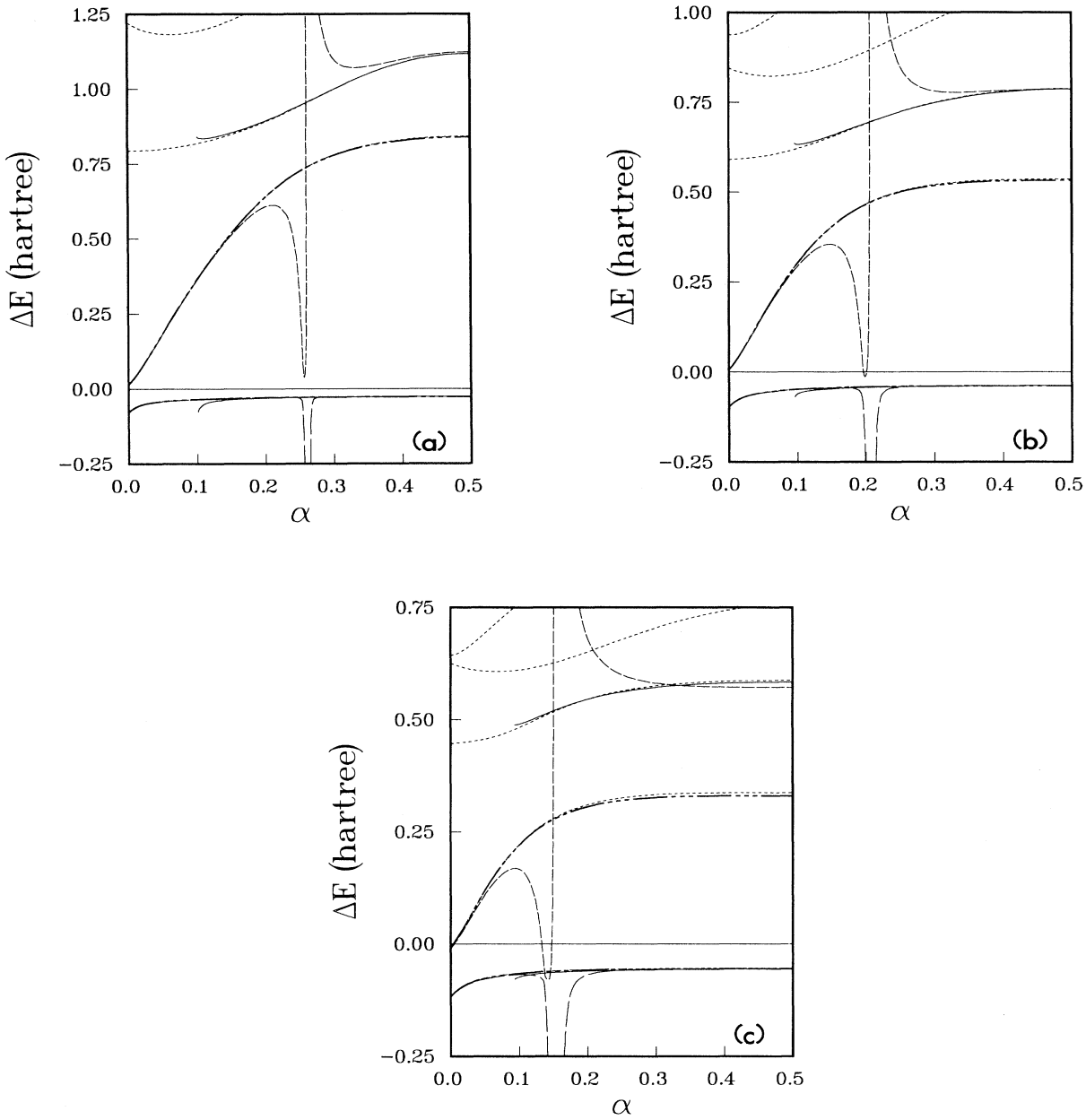

FIG. 4. A comparison of the FCI and various MRCCSD energies ΔE (in hartrees) relative to the ground-state RHF energy, $\Delta E=E-E_0^{\mathrm{RHF}}$, for the low-energy totally symmetric singlet states of the MBS H4 model considered over the whole range of the angular parameter α. Three distinct internuclear separations a are assumed, namely, $a=1.2$ a.u. [Fig. 4(a)], $a=1.6$ a.u. [Fig. 4(b)], and $a=2.0$ a.u. [Fig. 4(c)]. The L-MRCCSD energies that are represented by the long- and short-dashed lines display a singular behavior around $\alpha\cong 0.26$ (for $a=1.2$ a.u.), $\alpha\cong 0.21$ (for $a=1.6$ a.u.), and $\alpha\cong 0.16$ (for $a=2.0$ a.u.). Pairs of energies associated with two distinct solutions of the MRCCSD-3 equations are represented by the thick chain-dashed line (1st solution) and the thin solid line (2nd solution). The dotted lines represent the successive FCI eigenstates of the $^1A_1(C_{2v})$ symmetry.

the behavior of the L-MRCCSD method is indeed very complex (cf. Secs. V B–V D and Sec. VI). As we shall see in the next section, the L-MRCCSD singularity can be quite reliably predicted by observing the dependence of easily accessible diagonal CI matrix elements on the geometry of the nuclear framework.

Once we pass the region of singular behavior, the second root of the effective Hamiltonian describes the third (second excited) totally symmetric singlet state, to which the reference $|\Phi_2\rangle$ now primarily contributes (cf. Fig. 4). It is remarkable that the ground state is still very well described by the lowest root of H^{eff}. Thus, while the ground state is better and better approximated by $|\Phi_1\rangle$ as α increases, $|\Phi_2\rangle$ approximates successively higher and higher excited states (see also Secs. V B and V C). It is also interesting to observe (Fig. 4) that the "width" of the L-MRCCSD singularity becomes narrower and narrower as the nuclear framework is compressed together. This is precisely the reason why we consider slightly stretched ($a=2.0$ a.u.) H_2 molecules (cf. Ref. [26]). Notice that with increasing a, the first and second L-MRCCSD roots approach one another in the region of singular behavior, so that it may finally happen that the two energy curves will touch one another at some point. Further increase in the bond length a should thus lead to another type of L-MRCCSD breakdown, namely to the failure of the L-MRCCSD method to yield real energies (see Secs. V B and V C). Notice, finally, that with increasing internuclear distance a the L-MRCCSD singularity shifts towards the degenerate ($\alpha=0$) limit (see caption to Fig. 4).

Just as in the SR case [37,38], the singular behavior of the linear approximation is avoided when we account for nonlinear terms. This is illustrated graphically in Figs. 4(a)–4(c), and in greater detail in Tables VI–VIII, where three different nonlinear approximations MRCCSD-n, $n=1,2,3$, defined in Sec. III, are compared with FCI results. It is remarkable that already the direct $(T_2^{(p)})^2$ terms entirely eliminate the singular behavior of the L-MRCCSD approach. In fact, the ground-state energies provided by all three MRCCSD-n approximations differ by at most ~ 2 mhartree for $a=2.0$ a.u. and by less than ~ 0.5 mhartree for $a=1.2$ and 1.6 a.u. Even smaller differences are found for the second root corresponding to the first excited totally symmetric singlet (maximum difference in all cases is less than ~ 0.15 mhartree). The difference between the MRCCSD-2 and MRCCSD-3 approximations, which is entirely due to monoexcited clusters $T_1^{(p)}$ (cf. Sec. III), vanishes for $\alpha=0$ (recall that $T_1^{(p)}=0$ for the square configuration for symmetry reasons, cf. Sec. IV). The inclusion of bilinear terms involving singly excited clusters increases both the ground-state energy and the energy of the first excited state. However, for $a=1.2$ a.u., the energy of the ground state increases only up to $\alpha\approx 0.24-0.25$, while for $a=1.6$ a.u. this energy increase is observed up to $\alpha\approx 0.40-0.42$. Then, rapid decrease sets in.

The inclusion of nonlinear clusters involving $T_1^{(p)}$ [terms $Q_{11}^{(p)}(G_i^\dagger)$, $Q_{12}^{(p)}(G_i^\dagger)$, $B_{11}^{(p)}(G_i^\dagger)$, $B_{12}^{(p)}(G_i^\dagger)$, and $\tilde{B}_{12}^{(p)}(G_i^\dagger)$ given by Eqs. (43) with $n=1$, (44), (46) with $n=1$, (47), and (48), respectively] does not always improve the agreement with FCI results, just as the in-

TABLE VI. Comparison of the FCI and MRCCSD-n ($n=1,2,3$) energies relative to the ground-state RHF energy E_0^{RHF}, $\Delta E=E-E_0^{\text{RHF}}$ (in mhartree), for the lowest three totally symmetric singlet states of the MBS H4 model with $a=1.2$ a.u., as given by the two distinct solutions of the nonlinear MRCCSD problem. NC(↑) indicates no convergence when continued from the nondegenerate region. Critical α values for the second MRCCSD-1, MRCCSD-2, and MRCCSD-3 solutions are 0.1465, 0.1464, and 0.1011, respectively. See the text for details.

	FCI			MRCCSD-1				MRCCSD-2				MRCCSD-3			
				1st solution		2nd solution		1st solution		2nd solution		1st solution		2nd solution	
α	ΔE_1	ΔE_2	ΔE_3	ΔE_1	ΔE_2	ΔE_1	ΔE_3	ΔE_1	ΔE_2	ΔE_1	ΔE_3	ΔE_1	ΔE_2	ΔE_1	ΔE_3
0.000	−78.424	14.047	793.852	−78.384	14.029			−78.375	14.032			−78.375	14.032		
0.005	−69.161	26.034	793.932	−69.121	26.017			−69.112	26.020			−69.112	26.020		
0.010	−62.143	40.203	794.128	−62.106	40.191			−62.097	40.194			−62.096	40.194		
0.020	−53.014	73.139	794.860	−52.984	73.137			−52.974	73.140			−52.973	73.141		
0.050	−41.920	184.303	799.811	−41.904	184.329			−41.892	184.334			−41.887	184.334		
0.100	−35.363	363.174	817.872	−35.359	363.234	NC(↑)	NC(↑)	−35.340	363.239	NC(↑)	NC(↑)	−35.326	363.242	NC(↑)	NC(↑)
0.150	−31.924	516.791	848.277	−31.939	516.867	81.356	898.966	−31.911	516.871	82.475	898.027	−31.890	516.878	−35.822	853.693
0.200	−29.815	638.474	890.130	−29.864	638.475	−28.943	892.919	−29.819	638.477	−28.433	892.941	−29.798	638.489	−31.171	892.879
0.250	−28.508	724.844	942.018	−28.604	724.499	−28.160	943.123	−28.531	724.498	−27.934	943.133	−28.539	724.514	−29.089	943.087
0.300	−27.706	779.422	998.027	−27.847	778.421	−27.489	998.284	−27.733	778.416	−27.351	998.289	−27.832	778.433	−28.017	998.247
0.400	−26.938	830.174	1086.799	−27.113	827.952	−26.801	1086.614	−26.918	827.943	−26.711	1086.618	−27.301	827.955	−27.099	1086.580
0.500	−26.745	842.472	1117.916	−26.913	839.850	−26.624	1117.690	−26.689	839.840	−26.545	1117.693	−27.211	839.849	−26.879	1117.658

TABLE VII. Same as Table VI for the MBS H4 model with $a=1.6$ a.u. Critical α values for the second MRCCSD-1, MRCCSD-2, and MRCCSD-3 solutions are 0.1179, 0.1178, and 0.0961, respectively. Energies are in mhartree.

	FCI			MRCCSD-1				MRCCSD-2				MRCCSD-3			
				1st solution		2nd solution		1st solution		2nd solution		1st solution		2nd solution	
α	ΔE_1	ΔE_2	ΔE_3	ΔE_1	ΔE_2	ΔE_1	ΔE_3	ΔE_1	ΔE_2	ΔE_1	ΔE_3	ΔE_1	ΔE_2	ΔE_1	ΔE_3
0.000	−97.028	6.296	590.574	−96.964	6.278			−96.930	6.283			−96.930	6.283		
0.005	−87.970	17.646	591.183	−87.908	17.631			−87.873	17.636			−87.872	17.636		
0.010	−80.823	30.725	591.831	−80.768	30.718			−80.732	30.724			−80.730	30.724		
0.020	−70.887	60.553	593.293	−70.851	60.571			−70.813	60.578			−70.805	60.578		
0.050	−57.203	158.568	599.925	−57.216	158.650			−57.169	158.660			−57.131	158.663	NC(↑)	NC(↑)
0.100	−48.258	301.982	621.310	−48.363	302.076	NC(↑)	NC(↑)	−48.284	302.083	NC(↑)	NC(↑)	−48.190	302.099	−60.892	632.849
0.150	−43.792	403.492	653.690	−44.072	403.327	−46.354	658.035	−43.941	403.325	−44.805	658.133	−43.782	403.361	−46.783	657.420
0.200	−41.293	466.333	690.156	−41.830	465.466	−41.563	691.580	−41.627	465.453	−40.734	691.620	−41.410	465.505	−42.879	691.374
0.250	−39.844	501.676	723.266	−40.647	499.867	−39.646	723.238	−40.365	499.846	−39.022	723.256	−40.137	499.906	−40.910	723.036
0.300	−38.966	520.443	749.290	−39.971	517.801	−38.653	748.538	−39.620	517.774	−38.123	748.546	−39.442	517.835	−39.788	748.334
0.400	−38.073	534.222	799.938	−39.247	530.650	−37.751	778.751	−38.823	530.619	−37.320	778.752	−38.810	530.677	−38.678	778.561
0.500	−37.824	536.434	788.727	−39.019	532.632	−37.516	787.497	−38.579	532.602	−37.115	787.497	−38.644	532.658	−38.373	787.314

TABLE VIII. Same as Table VI for the MBS H4 model with $a=2.0$ a.u. Critical α values for the second MRCCSD-1, MRCCSD-2, and MRCCSD-3 solutions are 0.1036, 0.1033, and 0.0932, respectively. Energies are in mhartree.

	FCI			MRCCSD-1				MRCCSD-2				MRCCSD-3			
				1st solution		2nd solution		1st solution		2nd solution		1st solution		2nd solution	
α	ΔE_1	ΔE_2	ΔE_3	ΔE_1	ΔE_2	ΔE_1	ΔE_3	ΔE_1	ΔE_2	ΔE_1	ΔE_3	ΔE_1	ΔE_2	ΔE_1	ΔE_3
0.000	−117.621	−7.268	446.325	−117.686	−7.263			−117.575	−7.266			−117.575	−7.266		
0.005	−109.196	2.863	447.394	−109.280	2.874			−109.164	2.869			−109.161	2.870		
0.010	−102.307	14.250	448.304	−102.419	14.274			−102.299	14.270			−102.287	14.271		
0.020	−92.147	39.577	449.912	−92.327	39.631			−92.198	39.628			−92.152	39.631		
0.050	−76.429	118.950	456.798	−76.841	118.989			−76.673	118.987			−76.473	119.000	NC(↑)	NC(↑)
0.100	−65.321	221.428	482.682	−66.328	220.710	NC(↑)	NC(↑)	−66.023	220.678	NC(↑)	NC(↑)	−65.538	220.742	−73.284	490.042
0.150	−60.040	280.303	517.306	−61.953	277.783	−67.198	520.950	−61.440	277.711	−64.948	521.103	−60.665	277.819	−63.576	519.587
0.200	−57.260	310.816	545.685	−60.074	306.354	−59.168	546.455	−59.349	306.252	−57.102	546.512	−58.363	306.376	−60.288	545.412
0.250	−55.698	326.171	564.010	−59.136	320.341	−55.954	563.048	−58.259	320.224	−53.869	563.044	−57.188	320.352	−58.627	561.866
0.300	−54.775	333.480	575.126	−58.539	326.890	−54.459	573.096	−57.579	326.768	−52.451	573.056	−56.522	326.899	−57.507	571.873
0.400	−53.905	337.503	585.372	−57.806	330.428	−53.389	582.527	−56.808	330.309	−51.616	582.463	−55.876	330.447	−56.216	581.397
0.500	−53.690	337.643	587.722	−57.567	330.525	−53.179	584.741	−56.573	330.409	−51.498	584.675	−55.705	330.550	−55.855	583.661

clusion of higher-order terms in the effective Hamiltonian does not necessarily improve the accuracy of the MRCCSD-3 method [30] (cf. Sec. III). This is particularly apparent for the compressed $a=1.2$ a.u. geometry in the vicinity of the degenerate ($\alpha=0$) limit. This contrasts with the observation made in Ref. [27], whose authors find that the inclusion of $T_1^{(p)}$ clusters invariably improves the agreement with exact energies in the whole range of the parameter α. Indeed, more thorough investigation of the degenerate $\alpha\approx 0$ region as well as of various bond lengths a shows that this is not necessarily the case. On the whole, however, there is excellent agreement between our MRCCSD-3 and MRCC results of Ref. [27]. Small differences (at most 0.05 mhartree) for $\alpha\neq 0$ geometries are due to higher than quadratic terms in $T_1^{(p)}$ clusters that are accounted for in the MRCC results of Ref. [27], while our MRCCSD-3 approximation is strictly quadratic. An earlier reported [30] slight discrepancy between these MRCC energies for square geometry ($\alpha=0$), in which case $T_1^{(p)}$ clusters do not contribute, was due to rounding off errors. No difference is found when data of the same accuracy are compared.

It is not uncommon that a higher-level approximation yields less accurate results than a simpler version of a theory. Among many reasons for such seemingly contradictory behavior may be the fact that a simpler theory provides a more balanced truncation scheme, while a theoretically preferable approach may overestimate certain effects. We have demonstrated such a situation in Ref. [30], showing that the MRCCSD-3*a* energies are superior to the 3*b* and 3*c* approximations. Sometimes, the simplest method of accounting for nonlinear terms, MRCCSD-1, gives the best result [cf. e.g., $a=1.2$ a.u. and $\alpha<0.15$ for the ground state and $\alpha\leq 0.2$ for the first excited state). However, the differences between various MRCCSD-*n* energies are too small to allow definite conclusions to be made. To get a better understanding of the differences between these methods, we also analyze the resulting wave functions in Sec. VII.

We can thus conclude that agreement is best in the highly quasidegenerate region and deteriorates as the nondegenerate limit ($\alpha=0.5$) is approached. Overall agreement also deteriorates with increasing internuclear separation a [cf. Tables VI–VIII and Figs. 4(a)–4(c)]. For this reason we consider slightly stretched H_2 molecules in our models [26,37] to make the comparison more demanding. We also note that in the degenerate region, we invariably get better results for the second state rather than for the ground state, while the opposite is true in the nondegenerate limit. Since the description of the first excited $^1A_1(C_{2v})$ state worsens with increasing α [cf. e.g., Fig. 4(c)], we must expect rather poor results for this state in the dissociation limit of the D4 and P4 models, when the second H—H bond gets broken. Clearly, the manifold $\{|\Phi_1\rangle,|\Phi_2\rangle\}$ is too small to properly describe this process (see Secs. V B and V C).

The MRCCSD solutions (Tables VI–VIII) were obtained using the analytic continuation procedure described in the preceding section. Even in the highly degenerate $\alpha\approx 0$ region, where the L-MRCCSD method represents a very good approximation, this procedure was faster since it required fewer iterations. We thus used the L-MRCCSD solution as an initial guess only for one of the values near $\alpha=0$ and then continued the resulting solution of nonlinear MRCCSD equations toward the nondegenerate limit. In this way, we could obtain MRCCSD results matching the two lowest $^1A_1(C_{2v})$ eigenstates of the Hamiltonian (referred to as the 1st solution in Tables VI–VIII) over the entire range of the parameter α. Once the $\alpha=0.5$ limit was reached, we could immediately start varying the H(2)-H(3) distance (see Fig. 1) and continue this solution towards the $\alpha\rightarrow\infty$ and $\alpha\rightarrow 0$ limits of the D4 model, despite the problem with the L-MRCCSD method, which for the H4 $\alpha=0.5$ model (or D4 $\alpha=a$ model) describes the ground and the *second* excited states (see Sec. V B).

When we employ the L-MRCCSD solution for $\alpha=0.5$ as a starting guess, the Newton-Raphson iterative procedure converges to another solution of system (86) (referred to as the 2nd solution in Tables VI–VIII), which describes the ground and the second excited states (cf. Fig. 4). This solution can then be continued towards the degenerate limit, yielding an amazingly good description of the second excited totally symmetric state over a broad range of geometries (cf. Fig. 4 and Tables VI–VIII), the error for all MRCCSD-*n* methods being at most a couple of mhartree (again, the three MRCCSD-*n*, $n=1,2,3$, approximations yield almost identical results). Remarkably enough, the ground-state energy is best described by the simplest approximation MRCCSD-1. Only when the highly degenerate regime is reached ($\alpha\approx 0.1$), the rate of convergence of the Newton-Raphson scheme rapidly worsens (tens, hundreds, or even thousands of iterations are needed to achieve convergence), and the energies begin to deviate from FCI results. Very soon no converged solutions can be obtained even when very small steps $\Delta\alpha$ (such as $\Delta\alpha=10^{-5}$) are used.

This behavior is very much reminiscent of that found in the strongly correlated limit of cyclic polyene models, where no real solution of the SRCC [CCD, CCSD, CCSDT-1 (CCSDT with the second-order perturbative estimate for triples [75,76]), ACPTQ (coupled pair theory with an approximate estimate of connected triples and quadruples [58,63], see also [77,78])] equations, that is continuous as a function of the resonance integral β from the weakly correlated side, can be found beyond a certain critical value β_c of the resonance integral β (see Refs. [61–63]). In this case we were able to prove that this critical value $\beta=\beta_c$ represents an algebraic branch point of the first order, so that the SRCC energy bifurcates into two complex solutions that have no physical meaning [61–63]. It seems that the critical values α_c of parameter α, beyond which further continuation of the MRCCSD-*n* solutions is not possible (cf. Tables VI–VIII), also represent algebraic branch points. Indeed, careful numerical inspection indicates that the Jacobian of system (86), i.e., the determinant

$$J(\alpha)\equiv\det\left\|\frac{\partial f_I[\alpha,\mathbf{t}(\alpha)]}{\partial t_J(\alpha)}\right\|_{1\leq I,J\leq N}, \tag{88}$$

where

$$f_I(\alpha,\mathbf{t})=a_I(\alpha)+\sum_{J=1}^{N} b_{IJ}(\alpha)t_J+\sum_{\substack{J,K=1\\(J\le K)}}^{N} c_{IJK}(\alpha)t_J t_K \qquad (89)$$

represents the left-hand side of Eq. (86) and $\mathbf{t}(\alpha)$ is the second solution of the system (86), vanishes for $\alpha=\alpha_c$. This invalidates the Newton-Raphson procedure and causes its failure in the immediate vicinity of α_c in the same way as in the SRCC approach to cyclic polyenes [61–63]. Because of the algebraic nature of system (86), the cluster amplitudes $t_J(\alpha)$ are algebraic functions of α, so that $\mathbf{t}(\alpha)$ is defined for all complex α with the possible exception of a finite number of poles and algebraic branch points (cf. Sec. VI in Ref. [63]). The critical values α_c do not represent poles [none of the components $t_J(\alpha)$ tends to infinity as $\alpha\to\alpha_c$], so that they must be algebraic branch points. The situation is much easier in the case of L-MRCCSD singularities, since they appear whenever the corresponding solution $\mathbf{t}(\alpha)$ has a pole (cf. Sec. VI). The problem of an analytic continuation of the 2nd solution of nonlinear MRCCSD equations towards the degenerate limit of the H4 model will be discussed in Sec. V C.

It is certainly remarkable that the nonlinear MRCCSD equations possess multiple solutions that describe higher excited states of a given symmetry species (SRCC equations also possess multiple solutions, but it is rather hard to associate them with physically meaningful eigenstates [63]). Existence of a solution matching the ground and the second excited state suggests that there exist other solutions of system (86) that match other pairs of totally symmetric FCI eigenstates. Results for the H4 model indicate that the lowest root of the effective Hamiltonian always provides a good approximation to the ground-state energy, while the second root approximates energies of the successive excited states. Examples of such further solutions of nonlinear MRCCSD equations will be given in Sec. VIII.

B. D4 model

Results for the H4 model indicate that most of the problems encountered by MRCC theories appear when we use them to describe weakly degenerate or nondegenerate states. The best illustration of this fact is provided by the singular behavior of the L-MRCCSD approach. In weakly degenerate situations, a given state is relatively well described by a single dominant configuration, while other configurations, differing in one or two orbitals, contribute more or less equally. Consequently, the choice of a *multidimensional* model space becomes problematic. Including only a few configurations that dominate in quasidegenerate situations is often unsatisfactory, since it increases the probability of encountering intruder states dut to a strong interaction of model-space configurations with configurations belonging to $\mathcal{M}_0^{\perp}$. This is exactly what happens when we employ our two-reference L-CCSD formalism for the "nondegenerate" D4 model. With increasing intermolecular distance α we observe an increasingly strong interaction of the second reference $|\Phi_2\rangle$ with various configurations from $\mathcal{M}_0^{\perp}$ (see the next section for details). As a result, the L-MRCCSD method is plagued by numerous singularities, since the second root of H^{eff} successively approximates higher and higher excited states (see Fig. 5), even though the lowest root of H^{eff}, to which $|\Phi_1\rangle$ primarily contributes, invariably describes the ground state. Exceptions are the regions of the singular behavior of the L-MRCCSD theory, where both eigenvalues of H^{eff} tend to infinity.

Thus, for compressed geometries ($\alpha\approx 0.5$ a.u.), the L-MRCCSD energies match rather well the two energetically lowest ${}^1\Sigma_g^+$ states, since $|\Phi_2\rangle$ is relatively important here (cf. Table III and recall similar behavior in the H4 model). Once we pass the region of the first singularity ($\alpha\approx 1.18$ a.u.), the second root of H^{eff} begins to approximate the second ${}^1\Sigma_g^+$ excited state, and soon another singularity is reached (at $\alpha\approx 2.41$ a.u.), after which the second root begins to approximate the third excited ${}^1\Sigma_g^+$ state. Once the next singularity (at $\alpha\approx 3.03$ a.u.) is passed, the second root begins to approximate the fourth excited ${}^1\Sigma_g^+$ state. The last and broadest singularity appears at $\alpha\approx 6.20$ a.u., following which the second root approximates the group of the fifth, sixth, and seventh excited states of ${}^1\Sigma_g^+$ symmetry.

We must also note that in the range of examined geometries there exist two regions where the L-MRCCSD method fails to provide real energies (for 2.37 a.u. $<\alpha<$ 2.40 a.u. and 6.00 a.u. $<\alpha<$ 6.12 a.u.; cf. Fig. 5). Both regions appear in the vicinity of

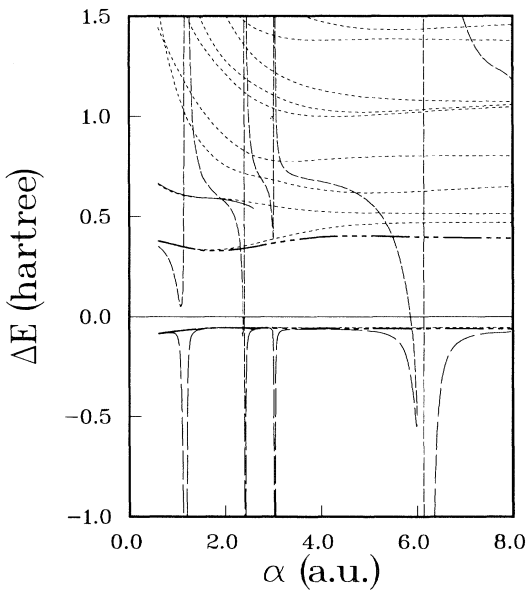

FIG. 5. Same as Fig. 4 for the MBS D4 model with $a=2.0$ a.u. and 0.6 a.u. $\le\alpha\le$ 8.0 a.u. For $\alpha=1.18$, 2.41, 3.03, and 6.20 a.u., L-MRCCSD method becomes singular. For $\alpha\in(2.37$ a.u., 2.40 a.u.) and $\alpha\in(6.00$ a.u., 6.12 a.u.), the energies resulting from the L-MRCCSD theory become complex (cf. text for details). The dotted lines correspond to successive FCI eigenstates of ${}^1\Sigma_g^+$ symmetry.

L-MRCCSD singularities. Their existence is related to the fact that in the vicinity of L-MRCCSD singularities the off-diagonal matrix elements of H^{eff} assume large values (see the next section). It thus happens that the discriminant of the secular equation for H^{eff},

$$\Delta=(H_{22}^{\text{eff}}-H_{11}^{\text{eff}})^2+4H_{12}^{\text{eff}}H_{21}^{\text{eff}}\ , \tag{90}$$

becomes negative. Since in the vicinity of the L-MRCCSD singularities the non-Hermiticity of the effective Hamiltonian, as measured by the difference $H_{12}^{\text{eff}}-H_{21}^{\text{eff}}$, becomes extremely large (see the next section), it is not surprising that H^{eff} may posses complex eigenvalues. We have mentioned this possibility in a previous subsection and we now see that the L-MRCCSD method does indeed fail to produce real energies in some regions $\Omega_\alpha=(\alpha_1,\alpha_2)$ near singularities. This type of breakdown of the L-MRCCSD formalism distinguishes MR linear theory from the SR one, which may become singular, but can never yield complex energies. Note that at the terminal points of the interval Ω_α, i.e., at $\alpha=\alpha_1$ and $\alpha=\alpha_2$, the energies E_1 and E_2 become identical (see Fig. 5), since $\Delta<0$ for $\alpha_1<\alpha<\alpha_2$ while $\Delta>0$ for $\alpha<\alpha_1$ and $\alpha>\alpha_2$, so that $\Delta=0$ for $\alpha=\alpha_1$ and $\alpha=\alpha_2$, and

$$E_1=E_2=\tfrac{1}{2}(H_{11}^{\text{eff}}+H_{22}^{\text{eff}})\ . \tag{91}$$

Just as in the case of the H4 model, singular behavior of the linear approximation is overcome by accounting for nonlinear terms. Results of these calculations are shown in Fig. 5 and in Table IX. The analytic continuation procedure (see Sec. IV) yields MRCCSD energies matching the two lowest $^1\Sigma_g^+$ states (so-called 1st solution of MRCCSD equations) for the entire region of parameter α. This was accomplished by employing the converged MRCCSD amplitudes for the H4 $\alpha=0.5$ model as a starting approximation. Using these amplitudes, we can continue the first solution, obtained for the H4 model, toward both the $\alpha\to 0$ and $\alpha\to\infty$ limits of the D4 model. Only for large values of α are many iterations needed to achieve convergence. For intermediate and small α values, convergence of the Newton-Raphson scheme is very fast.

Again, to obtain a nonsingular formalism providing reasonable results, it is entirely sufficient to include the direct $(T_2^{(p)})^2$ terms. It is, however, the MRCCSD-3 formalism that provides the best results. Remarkably, a good description of the first excited $^1\Sigma_g^+$ state in the quasidegenerate ($\alpha<a$) region by all three MRCCSD-n methods begins to deteriorate when $\alpha\approx a$. Consequently, this state is poorly described in the $\alpha\to\infty$ limit: the error of MRCCSD-n results for $\alpha=8$ a.u. is almost 80 mhartree. This confirms an earlier observation that the two-dimensional model space is not rich enough to describe nondegenerate states. It seems that we either have to increase the dimension of $\mathcal{M}_0$ or to go beyond the CCSD approximation in order to achieve a more accurate description of the low-lying states of $^1\Sigma_g^+$ symmetry in the nondegenerate limit of the D4 model. Indeed, the

TABLE IX. Same as Table VI for the MBS D4 model with $a=2.0$ a.u. NC(↓) designates no convergence when continued toward the $\alpha\to\infty$ limit. Corresponding critical α values for the second MRCCSD-1, MRCCSD-2, and MRCCSD-3 solutions are 2.7422, 2.6949, and 2.6011 a.u., respectively. Energies are in mhartree.

	FCI			MRCCSD-1					MRCCSD-2					MRCCSD-3				
				1st solution		2nd solution			1st solution		2nd solution			1st solution		2nd solution		
α	ΔE_1	ΔE_2	ΔE_3	ΔE_1	ΔE_2	ΔE_1	ΔE_3		ΔE_1	ΔE_2	ΔE_1	ΔE_3		ΔE_1	ΔE_2	ΔE_1	ΔE_3	
0.6	−83.683	378.379	660.656	−83.916	378.512	−79.237	667.842		−83.851	378.518	−78.501	667.987		−83.877	378.507	−87.870	665.734	
0.8	−77.376	367.634	633.138	−77.887	367.753	−75.934	639.185		−77.774	367.757	−75.166	639.328		−77.719	367.743	−81.056	637.515	
1.0	−70.896	356.324	613.986	−71.875	356.230	−70.768	618.991		−71.683	356.228	−69.954	619.124		−71.462	356.220	−74.088	617.566	
1.2	−65.060	345.936	602.275	−66.666	345.260	−65.304	606.111		−66.361	345.242	−64.427	606.225		−65.909	345.258	−67.838	604.882	
1.5	−58.517	335.590	594.092	−61.134	333.183	−58.561	595.870		−60.603	333.131	−57.539	595.940		−59.838	333.204	−60.805	594.880	
2.0	−53.690	337.643	587.722	−57.567	330.525	−53.179	584.741		−56.573	330.409	−51.498	584.675		−55.705	330.550	−55.855	583.661	
2.5	−53.319	358.475	572.878	−57.942	345.408	−54.119	557.476		−56.430	345.245	−49.563	556.622		−55.803	345.371	−59.585	553.501	
3.0	−54.018	386.593	552.508	−59.301	366.613	NC(↓)	NC(↓)		−57.194	366.394	NC(↓)	NC(↓)		−56.814	366.480	NC(↓)	NC(↓)	
4.0	−54.754	436.245	525.103	−61.862	397.842				−58.245	397.341				−58.123	397.363			
5.0	−54.779	461.181	517.354	−64.193	402.937				−58.920	401.944				−58.888	401.942			
6.0	−54.718	468.118	515.861	−65.966	398.821				−59.446	397.435				−59.440	397.434			
8.0	−54.666	469.714	512.999	−67.500	393.448				−59.923	391.735				−59.923	391.735			

FCI calculations indicate that for large α values we find almost equal participation of reference configuration $|\Phi_2\rangle = {}^{(1)}G^{33}_{22}(0)|\Phi_1\rangle$ and double excitations ${}^{(1)}G^{44}_{22}(0)|\Phi_1\rangle$, ${}^{(1)}G^{33}_{11}(0)|\Phi_1\rangle$, ${}^{(1)}G^{44}_{11}(0)|\Phi_1\rangle$ and ${}^{(1)}G^{34}_{12}(1)|\Phi_1\rangle$ in the first excited-state wave function (for $\alpha=8$ a.u., the corresponding FCI expansion coefficients equal 0.438, −0.430, −0.436, 0.428, and 0.500, respectively), while $|\Phi_1\rangle$ is almost totally absent. Only when α approaches small values, configurations $|\Phi_1\rangle$ and $|\Phi_2\rangle$ begin to dominate. In this region (small α values) the CCSD approximation is perfectly adequate, since triply and quadruply excited clusters $T_3^{(p)}$ and $T_4^{(p)}$, respectively, are very small. When α increases, $T_3^{(p)}$ clusters remain small while $T_4^{(p)}$ clusters increase rapidly. To provide better insight, we have carried out a detailed cluster analysis of two energetically lowest FCI eigenstates of ${}^1\Sigma_g^+$ symmetry, using our reference space $\mathcal{M}_0$ and cluster Ansatz of Eq. (27) (for details, see Sec. VII and Appendix), obtaining exact values of the orthogonally-spin-adapted cluster amplitudes defining the operators $T_i^{(p)}$, $i=1-4$, $p=1,2$. Thanks to the high symmetry of our models and small dimension of the MBS CI space, there are only two triexcited and two quadruply excited cluster amplitudes, namely,

$$\langle t_3^{(1)}\rangle_1 \equiv \langle 443|t_3^{(1)}|221\rangle_{0,0,1/2} ,$$

$$\langle t_3^{(1)}\rangle_2 \equiv \langle 334|t_3^{(1)}|112\rangle_{0,0,1/2} ,$$

$$\langle t_4^{(1)}\rangle \equiv \langle 3344|t_4^{(1)}|1122\rangle_{0,0,0,0,0} ,$$

and

$$\langle t_4^{(2)}\rangle \equiv \langle 2244|t_4^{(2)}|1133\rangle_{0,0,0,0,0} .$$

Just like the monoexcited clusters $T_1^{(2)}$, all triexcited cluster coefficients associated with reference $|\Phi_2\rangle$ vanish (cf. Table V). Amplitudes $\langle t_3^{(1)}\rangle_1$ and $\langle t_3^{(1)}\rangle_2$ are associated with excitation operators ${}^{(1)}G^{443}_{221}(0,0,\frac{1}{2})$ and ${}^{(1)}G^{334}_{112}(0,0,\frac{1}{2})$, respectively, while the amplitudes $\langle t_4^{(1)}\rangle$ and $\langle t_4^{(2)}\rangle$ are associated with quadruple excitations ${}^{(1)}G^{3344}_{1122}(0,0,0,0,0)$ and ${}^{(2)}G^{2244}_{1133}(0,0,0,0,0)$ (cf. Table IV). Their exact values for the MBS D4 model and several values of α are given in Table X. It is seen that both tetraexcited cluster amplitudes increase by about two orders of magnitude when α changes from 1 to 8 a.u.'s. Especially large becomes the amplitude $\langle t_4^{(2)}\rangle$ defining $T_4^{(2)}$. It is thus not surprising that the two-reference CCSD formalism provides a poor description of the first excited state when $\alpha\to\infty$ and that the description of the first excited state is much worse than the description of the ground state. Just as in the case of the SR formalism [37], the role of $T_4^{(1)}$ is rather unessential. The corresponding amplitude $\langle t_4^{(1)}\rangle$ never becomes large.

When approaching a nondegenerate regime, we could, of course, switch to the SR formalism [37,38] that here provides excellent results. However, apart from small discontinuities that would necessarily arise in this way, we would lose all information about the excited states that is provided by MR theories. It should be noted that our two-reference CCSD method yields a qualitatively correct shape of the potential-energy surface for the first excited ${}^1\Sigma_g^+$ state. On the other hand, for large α values the FCI energies, as well as the MRCCSD results, saturate and do not change with a further increase in the internuclear distance, whereas for smaller α values these methods yield almost identical energies (see Fig. 5 and Table IX).

In the quasidegenerate region of the D4 model, the three nonlinear approaches MRCCSD-n, $n=1,2,3$, provide identical results. Differences arise when the intermolecular distance α becomes larger than the intramolecular bond length a. Differences between MRCCSD-2 and MRCCSD-3 energies remain small over the entire region of α. In fact, energies provided by these two methods differ by at most ~0.9 mhartree for the ground state and less than ~0.15 mhartree for the first ${}^1\Sigma_g^+$ excited state. Maximum difference between MRCCSD-2 and MRCCSD-3 energies appears for $\alpha\approx a$ and decreases when α approaches zero or infinity. For $\alpha=8$ a.u., the energies provided by the MRCCSD-2 and MRCCSD-3 methods are identical up to 1 μhartree. This indicates that the role of nonlinear terms involving $T_1^{(p)}$ clusters is relatively small, even though they do improve final results. Except for $\alpha\le 0.6$ a.u., their inclusion only slightly increases the ground-state energy. The situation is, however, different when we examine the role of the $(T_2^{(p)})^2$ coupling terms. Except for the small values of α, the MRCCSD-2 and MRCCSD-3 approaches yield energies, that are visibly closer to FCI data than those provided by the MRCCSD-1 method. For example, for $\alpha=8$ a.u., the difference between the MRCCSD-1 and MRCCSD-2 or MRCCSD-3 energies is almost 7.6 mhartree for the ground state and about 1.7 mhartree for the first excited state. It is thus essential to include nonlinear coupling

TABLE X. Exact values of the orthogonally-spin-adapted triply and quadruply excited cluster amplitudes (see Appendix) associated with reference states $|\Phi_1\rangle$ and $|\Phi_2\rangle$ for the MBS D4 model with $a=2.0$ a.u., as obtained by cluster analysis of two energetically lowest FCI eigenstates of ${}^1\Sigma_g^+$ symmetry. In view of the symmetry of the model, triexcited cluster coefficients associated with reference $|\Phi_2\rangle$ vanish.

α	1.0	2.0	3.0	4.0	5.0	6.0	8.0
t_{17}	−0.006 562	−0.009 225	−0.001 980	0.002 179	0.002 080	0.000 933	0.000 020
t_{18}	0.008 084	0.005 176	−0.003 506	−0.006 052	−0.004 035	−0.001 884	−0.000 360
t_{19}	0.000 439	−0.003 592	−0.009 661	−0.013 542	−0.016 676	−0.019 057	−0.021 144
t_{20}	−0.011 258	−0.112 314	−0.249 141	−0.375 868	−0.482 481	−0.571 382	−0.651 044

terms. However, as pointed out earlier, we must not forget about the necessity of enlarging the model space or including higher-order terms for large values of α.

As for the H4 model, we found another solution of the nonlinear system (86), matching the ground and the *second* excited totally symmetric states. We obtained it by applying the analytic continuation procedure to the second solution of system (86), that was found earlier for the H4 model. Contrary to the H4 model, however, we could only penetrate the quasidegenerate $\alpha < a$ region (cf. Fig. 5 and Table IX). Once we increased α beyond $\alpha \approx a$, the resulting energies began to deviate from FCI results and the rate of convergence of the Newton-Raphson procedure began to deteriorate, so that soon we were unable to obtain a converged solution, even when very small steps $\Delta\alpha$ were used (such as $\Delta\alpha = 10^{-5}$ a.u.). As in the case of the H4 model, we approached the singular point α_c, beyond which further continuation of the second solution of system (86) was impossible due to the vanishing of the Jacobian (88) (critical points α_c for all three nonlinear approximations MRCCSD-n are given in Table IX).

The fact that we cannot proceed very far beyond the region $\alpha \approx a$ seems to indicate that our model space is not rich enough to describe the second excited state in the nondegenerate limit of the D4 model, at least at the CCSD level of approximation. This becomes clear when we examine the FCI expansion of the second excited state for $\alpha > a$. Indeed, monoexcited states ${}^{(1)}G_1^3|\Phi_1\rangle$ and ${}^{(1)}G_2^4|\Phi_1\rangle$ are far more important than references $|\Phi_1\rangle$ and $|\Phi_2\rangle$ in this region. In fact, for $\alpha \to \infty$ they become dominant configurations (the corresponding FCI expansion coefficients for $\alpha = 8$ a.u. are -0.706 and -0.683, respectively). It is thus remarkable that our two-reference formalism is capable of providing rather good results for the second excited ${}^1\Sigma_g^+$ state for $\alpha < a$. For both the ground and second excited states, differences between MRCCSD-n and FCI data do not exceed a few mhartree (see Table IX).

As in the case of the H4 model, the best ground-state energy from among those provided by the 2nd solution of system (86) results from the simplest MRCCSD-1 approximation. Contrary to the 1st solution, the fully quadratic MRCCSD-3 approach yields the worst ground-state energies. As a matter of fact, we observe that $E_1^{\text{MRCCSD-3}} < E_1^{\text{MRCCSD-1}} < E_1^{\text{MRCCSD-2}}$.

Quadratic MRCCSD equations for the D4 model possess several other solutions. As we shall see in Sec. VIII, some of them describe highly excited states. This is not surprising when we realize that even the linear two-reference theory may approximate higher excitations (cf. Fig. 5).

C. P4 model

By proceeding from a square configuration toward the $\alpha \to \infty$ limit of the D4 model, we describe a consecutive breaking of two chemical bonds. Another type of dissociation of two chemical bonds is modeled by the P4 system. In this case, when α increases, the H(1)—H(4) and H(2)—H(3) bonds are broken simultaneously (cf. Fig. 1). For $\alpha \to \infty$, the dominant configuration in the FCI expansion of the ground-state wave function is $|\Phi_1\rangle$, while configurations of the type ${}^{(1)}G_{\alpha\alpha}^{\rho\rho}(0)|\Phi_1\rangle$ contribute with more or less equal weight. The doubly excited configuration ${}^{(1)}G_{12}^{34}(0)|\Phi_1\rangle$ is also quite important, whereas its triplet coupled counterpart ${}^{(1)}G_{12}^{34}(1)|\Phi_1\rangle$ plays a negligible role [37]. The importance of the latter configuration increases, however, when we consider the first excited state (cf. the FCI expansion of the first excited state for the D4 model described in Sec. V B). When $\alpha \to 0$, $|\Phi_2\rangle$ begins to dominate and a strong quasidegeneracy involving $|\Phi_1\rangle$ and $|\Phi_2\rangle$ is achieved for $\alpha \approx a$. In fact, for the square geometry ($\alpha = a$), $|\Phi_1\rangle$ and $|\Phi_2\rangle$ are exactly degenerate (cf. Sec. IV and Table III). Thus, for $\alpha \approx a$ we can expect similar behavior as observed in the degenerate limit of the H4 model, whereas for α approaching infinity we should observe similarities with the nondegenerate D4 model.

Although configuration $(\phi_1)^2(\phi_2)^2$ does not represent the ground-state RHF solution for $\alpha < a$, we use it to determine MO's and MO energies for both $\alpha \geq a$ and $\alpha < a$. As explained in Sec. IV, switching to MO's associated with configuration $(\phi_1)^2(\phi_3)^2$ would not be very instructive, since the orbital energy picture associated with configuration $(\phi_1)^2(\phi_3)^2$ for $\alpha \leq a$ is equivalent to the orbital energy picture associated with configuration $(\phi_1)^2(\phi_2)^2$ for $\alpha \geq a$. By employing MO's associated with configuration $(\phi_1)^2(\phi_2)^2$ for both $\alpha \geq a$ and $\alpha < a$, we can examine various types of orbital quasidegeneracy ranging from the nondegenerate $\alpha \to \infty$ limit to the exact degeneracy of active orbitals ϕ_2 and ϕ_3 (cf. Fig. 2). We would never attain the exact degeneracy of orbitals ϕ_2 and ϕ_3 by switching to MO's associated with configuration $(\phi_1)^2(\phi_3)^2$ in the region of $\alpha < a$.

For the MBS P4 model, the monoexcited clusters $T_1^{(p)}$ vanish, so that MRCCSD-2 and MRCCSD-3 approximations become equivalent (and will thus be designated as MRCCSD-2,3). For the same reason, the fully quadratic MRCCSD approach is equivalent to the quadratic MRCCD method considered by Meissner and co-workers [24]. Likewise, the FCI manifold is smaller and consists of only eight states (see Table IV). Since monoexcited and triexcited states now belong to other symmetry species than do $|\Phi_1\rangle$ and $|\Phi_2\rangle$ (cf. Sec. IV and Table IV), we can expect the number of singularities encountered in the L-MRCCSD approach to also be smaller than in the D4 model, in spite of similarities between both models for large values of α. Indeed, only two singularities are found for the P4 model (see Fig. 6).

As for the H4 and D4 models, the lowest root of the L-MRCCSD effective Hamiltonian describes the ground state, while the second root approximates higher and higher excited states of ${}^1A_g(D_{2h})$ symmetry. In the region of strong quasidegeneracy (configurational or orbital), the L-MRCCSD energies match the two energetically lowest ${}^1A_g(D_{2h})$ states. Once we pass the region of the first singularity ($\alpha \approx 3.46$ a.u.), the second root begins to approximate the second excited state of ${}^1A_g(D_{2h})$ symmetry. Following the second singularity (at $\alpha \approx 6.80$ a.u.), the second root begins to approximate a group of

the third, fourth, and fifth excited states of $^1A_g(D_{2h})$ symmetry. As in the case of the D4 model, this singularity is very broad. For symmetry reasons, the L-MRCCSD energies cannot describe the two $^1B_{3u}(D_{2h})$ FCI states, spanned by monoexcited and triexcited configurations, that appear between the first and the second excited $^1A_g(D_{2h})$ states. For reasons of greater clarity, these, as well as the other two $^1B_{3u}(D_{2h})$ FCI states, are not shown in Fig. 6.

Again, in the vicinity of the L-MRCCSD singularities, there exist two regions Ω_α where the L-MRCCSD method fails to provide real energies (for 3.41 a.u. $<\alpha<$ 3.43 a.u. and 6.54 a.u. $<\alpha<$ 6.70 a.u., cf. Fig. 6). As for the D4 model, the existence of these regions is related to a large non-Hermiticity of H^{eff} and for a given region $\Omega_\alpha=(\alpha_1,\alpha_2)$ we observe that discriminant Δ, Eq. (90), vanishes for $\alpha=\alpha_1$ and $\alpha=\alpha_2$. Consequently, for $\alpha=\alpha_1$ and $\alpha=\alpha_2$, two L-MRCCSD roots are equal [cf. Eq. (91) and Fig. 6].

Inclusion of nonlinear terms removes the singular behavior of L-MRCCSD theory, and we can easily continue the solution of the nonlinear MRCCSD equations, which matches two energetically lowest $^1A_g(D_{2h})$ states, over the entire region of α. Only for large values of α, many iterations are needed to achieve convergence. The resulting energies are shown in Fig. 6 and, in greater detail, in Table XI. As the initial iteration in the Newton-Raphson scheme, we can either use the L-MRCCSD amplitudes for $\alpha\approx a$ or the converged MRCCSD amplitudes obtained for the H4 $\alpha=0$ model (which coincides with the P4 $\alpha=a$ model).

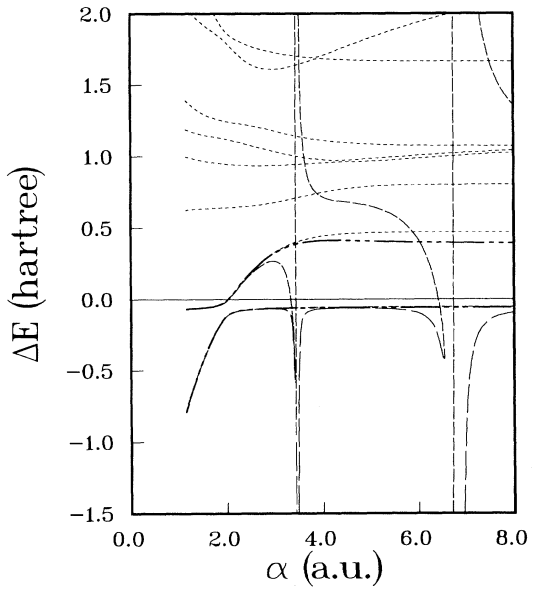

FIG. 6. Same as Fig. 4 for the MBS P4 model with $a=2.0$ a.u. and 1.1428 a.u. $\le\alpha\le$ 8.0 a.u. For both $\alpha\ge a$ and $\alpha<a$, we employ the RHF MO's associated with configuration $(\phi_1)^2(\phi_2)^2$, so that for $\alpha=1.1428$ a.u. active orbitals ϕ_2 and ϕ_3, Eqs. (60) and (61), become degenerate. All energies are evaluated relative to the RHF energy of $(\phi_1)^2(\phi_2)^2$ configuration, which represents the RHF ground state for $\alpha\ge a$. Dotted lines correspond to successive FCI eigenstates of $^1A_g(D_{2h})$ symmetry [$^1B_{3u}(D_{2h})$ states are not displayed] and only one MRCCSD-3 solution is shown. The L-MRCCSD method becomes singular for $\alpha=3.46$ a.u. and $\alpha=6.80$ a.u. For $\alpha\in$(3.41 a.u., 3.43 a.u.) and $\alpha\in$(6.54 a.u., 6.70 a.u.), the energies resulting from the L-MRCCSD theory become complex (cf. text for details).

For obvious reasons, we cannot find the second $^1A_g(D_{2h})$ solution following the same strategy as we did for the D4 model. In fact, the second solution for the H4 model describes the second excited state of $^1A_1(C_{2v})$ symmetry, that becomes the lowest state of $^1B_{3u}(D_{2h})$ symmetry in the square configuration. Clearly, for symmetry reasons, $|\Phi_1\rangle$ and $|\Phi_2\rangle$ do not contribute at all to the latter state. This is also why the second solution for the H4 model could not be continued toward the degenerate $\alpha=0$ limit. Participation of $|\Phi_1\rangle$ and $|\Phi_2\rangle$ in the FCI expansion of the second excited $^1A_1(C_{2v})$ state of the H4 model decreases with decreasing value of the parameter α. Already for $\alpha=0.05$, the corresponding FCI expansion coefficients equal 0.096 and 0.176, respectively. When the square geometry is reached, they simply vanish and the symmetry of this state changes to $^1B_{3u}(D_{2h})$.

As in the case of the D4 model, the best results are provided by the MRCCSD-2,3 approach. The behavior of MRCCSD-n formalisms for the P4 model is in fact almost identical to that found for the previously discussed D4 model, particularly for large α's, when all nonlinear approximations give a rather poor description of the first excited $^1A_g(D_{2h})$ state. Again, while the $(T_2^{(p)})^2$ direct terms entirely remove the singular behavior of the linear approximation, the nonlinear coupling terms play a substantial role. For example, for $\alpha=10$ a.u., the MRCCSD-1 error in the ground-state energy is almost 13.3 mhartree, whereas with the MRCCSD-2,3 approach it is only about 5.4 mhartree (see Table XI). Even the latter result, however, is not satisfactory, indicating that our model space is too small to describe low-lying electronic states of the P4 model in the nondegenerate limit. This is especially the case for excited states. Similarly as in the case of the D4 model, for $\alpha=10$ a.u., the error in the first excited-state energy is almost 80 mhartree, indicating an increasing importance of configurations belonging to $\mathcal{M}_0^\perp$ when $\alpha\to\infty$. These are not necessarily the dominant configurations, but—as already pointed out—their contribution to low-lying eigenstates of the Hamiltonian is substantial. For example, for $\alpha=10$ a.u., the FCI expansion coefficients at $|\Phi_1\rangle$, $|\Phi_2\rangle$, $^{(1)}G^{44}_{22}(0)|\Phi_1\rangle$, $^{(1)}G^{33}_{11}(0)|\Phi_1\rangle$, $^{(1)}G^{44}_{11}(0)|\Phi_1\rangle$, $^{(1)}G^{34}_{12}(0)|\Phi_1\rangle$, and $^{(1)}G^{34}_{12}(1)|\Phi_1\rangle$ configurations for the ground state are 0.968, −0.087, −0.088, −0.088, −0.087, −0.175, and −0.001, respectively, and for the first excited $^1A_g(D_{2h})$ state 0.000, 0.433, −0.433, −0.433, 0.433, 0.000, and 0.500, respectively.

Another indication of an increasing importance of configurations belonging to $\mathcal{M}_0^\perp$ for large α's is the increasing role of $T_4^{(p)}$ clusters that are neglected in the MRCCSD formalism ($T_3^{(p)}$ clusters are also neglected, but for the MBS P4 model these do not appear for symmetry reasons). A detailed cluster analysis of the two energetically lowest FCI eigenstates of $^1A_g(D_{2h})$ symmetry (see Sec. VII) indicates that the exact values of tetraexcit-

TABLE XI. Comparison of the FCI and MRCCSD-n ($n=1,2,3$) energies, relative to the energy of $|\Phi_1\rangle=|(\phi_1)^2(\phi_2)^2|$, $\Delta E=E-H_{11}$ (in mhartree), for the two lowest totally symmetric singlet states of the MBS P4 model with $a=2.0$ a.u. RHF MO's associated with configuration $(\phi_1)^2(\phi_2)^2$ are employed throughout (see the text for details). For $\alpha=1.1428$ a.u. active orbitals ϕ_2 and ϕ_3 become degenerate.

	FCI		MRCCSD-1		MRCCSD-2,3	
α	ΔE_1	ΔE_2	ΔE_1	ΔE_2	ΔE_1	ΔE_2
1.1428	−791.128	−67.990	−791.152	−67.794	−791.113	−67.790
1.145	−788.553	−67.953	−788.577	−67.757	−788.538	−67.753
1.15	−782.719	−67.867	−782.742	−67.673	−782.704	−67.668
1.20	−725.733	−66.978	−725.756	−66.795	−725.716	−66.790
1.30	−618.873	−65.001	−618.896	−64.842	−618.852	−64.836
1.40	−520.896	−62.696	−520.918	−62.563	−520.870	−62.555
1.60	−349.331	−56.397	−349.349	−56.318	−349.290	−56.307
1.80	−210.047	−44.008	−210.065	−43.982	−209.988	−43.974
1.90	−155.978	−30.868	−156.010	−30.859	−155.917	−30.857
1.95	−134.584	−20.648	−134.629	−20.643	−134.527	−20.644
1.98	−123.867	−13.009	−123.924	−13.004	−123.816	−13.007
1.99	−120.655	−10.202	−120.716	−10.197	−120.606	−10.201
2.00	−117.621	−7.268	−117.686	−7.263	−117.575	−7.266
2.01	−114.760	−4.209	−114.830	−4.203	−114.717	−4.207
2.02	−112.069	−1.030	−112.143	−1.024	−112.029	−1.028
2.05	−104.949	9.171	−105.038	9.178	−104.920	9.174
2.10	−95.815	27.951	−95.930	27.959	−95.806	27.956
2.20	−84.443	68.960	−84.613	68.959	−84.475	68.958
2.50	−70.873	187.247	−71.256	187.012	−71.039	187.000
3.00	−63.061	327.960	−64.154	324.820	−63.600	324.720
4.00	−57.269	441.613	−62.072	410.376	−59.529	409.908
5.00	−55.391	464.667	−64.236	407.406	−59.283	406.416
7.00	−54.701	469.618	−67.143	395.450	−59.856	393.807
10.00	−54.650	469.740	−67.914	391.961	−60.078	390.161

ed amplitudes $\langle t_4^{(1)}\rangle$ and $\langle t_4^{(2)}\rangle$ (see Sec. V B) increase by a few orders of magnitude when α changes from 2 to 10 a.u. (cf. Table XII). While amplitude $\langle t_4^{(1)}\rangle$ remains small over the entire region of α, amplitude $\langle t_4^{(2)}\rangle$ assumes large values when $\alpha\rightarrow\infty$. Thus, to obtain a correct description of the first excited state, we must account for the $T_4^{(2)}$ cluster component or increase the dimension of $\mathcal{M}_0$. As in the case of SR theory [37], the connected cluster components $T_4^{(1)}$ are far less important, so that there is no need to include them to achieve a relatively good description of the ground-state wave function.

In view of these facts, it is quite remarkable that simple nonlinear MRCCSD methods, employing only a two-dimensional model space, are capable of providing a rather good description of the two energetically lowest $^1A_g(D_{2h})$ states even for large α values. Description of the ground state remains particularly good over the entire range of geometries considered. At the same time we obtain important information about the shape of the potential-energy curve for the first excited state.

In the degenerate region, where either configurational ($\alpha\approx a$) or orbital ($\alpha<a$) quasidegeneracy is present, the difference between the MRCCSD-1 and MRCCSD-2,3 approximations is very small, both providing an excellent description of the two energetically lowest $^1A_g(D_{2h})$ states. For example, for $\alpha<a=2.0$ a.u., the maximal error of MRCCSD-n energies is 61 μhartree for the ground state and less than 0.2 mhartree for the first excited state. The fact that we are able to obtain remarkably good results for $\alpha<a$, where configurational quasidegeneracy is

TABLE XII. Exact values of the quadruply excited cluster amplitudes (see Appendix) associated with reference states $|\Phi_1\rangle$ and $|\Phi_2\rangle$ for the MBS P4 model with $a=2.0$ a.u., as obtained by cluster analysis of two energetically lowest FCI eigenstates of $^1A_g(D_{2h})$ symmetry. Triexcited clusters vanish due to symmetry. RHF MO's associated with configuration $(\phi_1)^2(\phi_2)^2$ are used throughout. Orbitals ϕ_2 and ϕ_3 become degenerate for $\alpha=1.1428$ a.u.

α	1.1428	1.5	2.0	3.0	4.0	5.0	7.0	10.0
t_{19}	0.003 112	0.002 115	0.000 398	−0.004 544	−0.011 740	−0.017 036	−0.020 794	−0.021 674
t_{20}	0.000 146	0.000 327	0.000 398	−0.027 128	−0.212 660	−0.436 216	−0.625 927	−0.665 191

absent (cf. Table III), seems to indicate the importance of a proper choice of an MO basis. Here we do not mean the size of the basis, which is another problem that remains to be investigated [27,79], but the type of MO's employed. In our case, MO's are fully determined by the symmetry [cf. Eqs. (60) and (61)]. However, we do not employ the ground-state RHF MO's for all values of α. In order to employ the ground-state RHF MO's for $\alpha < a$, we would have to switch to orbitals associated with configuration $(\phi_1)^2(\phi_3)^2$. In this way, active orbitals ϕ_2 and ϕ_3 would never become degenerate and, consequently, we would obtain a poor description of the first excited state, just as in the case of large α's. The use of MO's associated with configuration $(\phi_1)^2(\phi_2)^2$ leads to a strong quasidegeneracy of active orbitals and, as our cluster analysis indicates (see Table XII), to very small values of the connected tetraexcited cluster components. This results in a very good description of the lowest two eigenstates of the Hamiltonian by the two-reference CCSD formalism, despite the nondegenerate character of the P4 model for $\alpha < a$ (cf. Sec. VII). It would thus be interesting to examine other choices of molecular bases [such as multiconfiguration self-consistent field (MCSCF) orbitals, triplet orbitals [42], etc.]. This problem was already addressed in the context of the multireference many-body perturbation theory (MRMBPT) study of the P4 model, where it was shown that various shifting techniques of one-particle energy levels speed up convergence of perturbation-theory series and extend the range of applicability of MR theories [42].

D. S4 model

The most challenging situation arises when we study the simultaneous breaking of all four chemical bonds in our H_4 models. For this reason we examine the S4 model, in which the four protons form a square, and we increase the nearest-neighbor separation α toward the fully dissociated limit $\alpha \rightarrow \infty$, where, similarly as in the strongly correlated regime of the cyclic polyene model [60–63,70–72], all orbital energies are identical (cf. Fig. 3) so that a strong mixing of orbital and configurational degeneracies sets in.

For small and intermediate values of α, the model space employed is perfectly adequate: as shown in Table XIII, the reference configurations $|\Phi_1\rangle$ and $|\Phi_2\rangle$ dominate in the FCI expansions of the two lowest singlets [recall that these states belong to different symmetry species of the invariance group of the Hamiltonian D_{4h}; they are totally symmetric only with respect to invariance group of the Fock operator (D_{2h}); see Sec. IV]. Their weights, as measured by the sum of squares of the FCI expansion coefficients, exceed 50% up to $\alpha \approx 5$ a.u. for the ground state [which is a $^1B_{1g}(D_{4h})$ state] and up to $\alpha \approx 3$ a.u. for the first excited state [the lowest state of $^1A_{1g}(D_{4h})$ symmetry]. For $\alpha < 2$ a.u., the weight of the remaining configurations does not exceed 8%.

For larger values of α, the situation becomes far more complex. The reference configurations $|\Phi_1\rangle$ and $|\Phi_2\rangle$ are still exactly degenerate (cf. Tables III and XIII), but the role of other states dramatically increases. For $\alpha = 7$ a.u., the weight of other configurations is about 60% for the ground state and 86% for the first excited state (see Table XIII). Thus it is inappropriate to use our $\mathcal{M}_0$ as a reference space in this region. It is, in fact, impossible to find a low-dimensional model space in this case, since such a space would have to be identical with the FCI space (cf. Tables IV and XIII). Alternatively, we must go beyond the CCSD approximation. The cluster analysis of the exact wave functions $|\Psi_1\rangle$ and $|\Psi_2\rangle$ [assuming the cluster Ansatz of Eq. (81); see Sec. VII and Appendix] indicates a rapid increase in the importance of $T_4^{(1)}$ and $T_4^{(2)}$ clusters with increasing α (see Table XIV). These clusters remain small up to $\alpha \approx 3$ a.u. Then, a rapid increase sets in and the ratio of the connected tetraexcited component $T_4^{(p)}$ to its disconnected counterpart $\frac{1}{2}(T_2^{(p)})^2$ becomes as large as 0.4 for $\alpha \rightarrow \infty$. Contrary to the previously discussed D4 and P4 models, both quadruply excited components $T_4^{(1)}$ and $T_4^{(2)}$ become large (actually $\langle t_4^{(1)} \rangle = \langle t_4^{(2)} \rangle$ in this case; cf. later part of this section), so that we can expect the two-reference CCSD theory to fail in the dissociation limit of the S4 model. Just as in the case of the SRCCSD formalism and the strongly correlated regime of cyclic polyenes [60–63] neglect of connected quadruply excited clusters should result in singular behavior of our two-reference formalism for α sufficiently large.

This is precisely what we find. All three MRCCSD-n formalisms provide good results only up to the region of the first L-MRCCSD singularity, which appears at $\alpha \approx 3.30$ a.u. (see Fig. 7 and Table XV). For $\alpha > 3.3$ a.u., the MRCCSD-n energies begin to deviate from the FCI results, the rate of convergence of the Newton-Raphson procedure deteriorates, and soon a point is reached where

TABLE XIII. FCI expansion coefficients for the two lowest singlet eigenstates $|\Psi_1\rangle$ and $|\Psi_2\rangle$ of the MBS S4 model [see Table IV and Eqs. (114) and (115)]. Monoexcited and triexcited coefficients $d'_{j,\mu}$, $j = 8-11$ vanish. Recall that $|\Psi_1\rangle$ and $|\Psi_2\rangle$ belong to different symmetry species of the symmetry group of the Hamiltonian D_{4h} but are totally symmetric with respect to the invariance group of the Fock operator D_{2h} (see Sec. IV). Since $|\Psi_1\rangle$ is a $B_{1g}(D_{4h})$ state and the symmetry of $|\Psi_2\rangle$ is $A_{1g}(D_{4h})$, the coefficients $d'_{j,\mu}$ satisfy the following relations: $d'_{1,1} = -d'_{2,1}$, $d'_{3,1} = d'_{4,1} = 0$, $d'_{5,1} = -d'_{12,1}$, $d'_{6,1} = \sqrt{3}d'_{7,1}$, $d'_{1,2} = d'_{2,2}$, $d'_{5,2} = d'_{12,2}$, $d'_{7,2} = -\sqrt{3}d'_{6,2}$. Only independent coefficients are listed.

	α	$d'_{1,\mu}$	$d'_{3,\mu}$	$d'_{4,\mu}$	$d'_{5,\mu}$	$d'_{6,\mu}$
$\mu=1$	1.0	0.703	0.0	0.0	−0.013	−0.086
	2.0	0.690	0.0	0.0	−0.045	−0.183
	3.0	0.656	0.0	0.0	−0.118	−0.290
	4.0	0.594	0.0	0.0	−0.230	−0.376
	5.0	0.524	0.0	0.0	−0.330	−0.417
	6.0	0.476	0.0	0.0	−0.388	−0.430
	7.0	0.451	0.0	0.0	−0.415	−0.432
$\mu=2$	1.0	0.702	−0.053	−0.100	−0.005	−0.005
	2.0	0.678	−0.169	−0.205	0.002	−0.049
	3.0	0.554	−0.374	−0.369	0.058	−0.162
	4.0	0.392	−0.482	−0.459	0.141	−0.230
	5.0	0.312	−0.500	−0.487	0.195	−0.246
	6.0	0.276	−0.501	−0.496	0.225	−0.249
	7.0	0.260	−0.500	−0.499	0.240	−0.250

TABLE XIV. Exact values of the quadruply excited cluster amplitudes associated with reference states $|\Phi_1\rangle$ and $|\Phi_2\rangle$ and the ratio of the connected tetraexcited components $T_4^{(p)}$ and their disconnected counterparts $\frac{1}{2}(T_2^{(p)})^2$, $p=1,2$ for the MBS S4 model, as obtained by cluster analysis of two energetically lowest FCI eigenstates of $^1A_g(D_{2h})$ symmetry. As in the case of the P4 model, $T_3^{(p)}=0$. The quantities $k^{(i)}$ designate the ratio: $k^{(i)}=|\langle {}^{(i)}\Phi_{20}|T_4^{(i)}|\Phi_i\rangle/\langle {}^{(i)}\Phi_{20}|\frac{1}{2}(T_2^{(i)})^2|\Phi_i\rangle|$, where

$$|{}^{(1)}\Phi_{20}\rangle={}^{(1)}G^{3344}_{1122}(0,0,0,0,0,0)|\Phi_1\rangle ,$$

$$|{}^{(2)}\Phi_{20}\rangle={}^{(2)}G^{2244}_{1133}(0,0,0,0,0,0)|\Phi_2\rangle .$$

Recall that (see Appendix)

$$t_{19}\equiv\langle t_4^{(1)}\rangle=\langle 3344|t_4^{(1)}|1122\rangle_{0,0,0,0,0,0}=\langle {}^{(1)}\Phi_{20}|T_4^{(1)}|\Phi_1\rangle$$

and similarly for $t_{20}=\langle t_4^{(2)}\rangle$.

α	$t_{19}=t_{20}$	$k^{(1)}=k^{(2)}$
1.0	0.000 335	0.064 023
2.0	0.000 398	0.011 975
3.0	−0.045 623	0.243 360
4.0	−0.224 885	0.376 118
5.0	−0.413 843	0.397 457
6.0	−0.542 887	0.399 741
7.0	−0.613 546	0.399 973

no converged solution can be obtained, even when the analytical continuation procedure with a very small step $\Delta\alpha$ is used. With the MRCCSD-1 scheme, we can pass the region of the second L-MRCCSD singularity ($\alpha\approx 5.86$ a.u.), but this does not help much: the solution cannot be continued beyond $\alpha=6.4682$ a.u. (cf. Table XV).

As explained in Sec. V A, singularities encountered in MRCCSD-n approaches are most likely algebraic branch points. Our experience with SR theories [60–63,71–73] tells us that there is only one way in which to overcome this type of singularity in the CC formalism while employing low dimensional reference space, namely, by accounting for the connected quadruple excitations. We should thus consider the MRCCSDTQ or MRCCDQ theory (as usual, T and Q stand for the connected triply and quadruply excited clusters). Since, however, the MRCCSDTQ formalism is equivalent to the full (not truncated) MRCC theory in our case, it would be more instructive to develop and test an approximate method of accounting for connected quadruply excited clusters. Our preliminary observations indicate that we can obtain such a formalism by generalizing the so-called ACPQ theory (coupled pair theory with an approximate account of connected quadruply excited clusters [77,78]) to the MR case [80].

In the region of small values of α, where $|\Phi_1\rangle$ and $|\Phi_2\rangle$ are the dominant configurations, all three MRCCSD-n methods provide remarkably good energies. For $\alpha\leq 2$ a.u., the difference between the MRCCSD-1 and MRCCSD-2,3 energies is less than ~ 0.1 mhartree for the ground state and at most 5 μhartree for the first excited state of $^1A_g(D_{2h})$ symmetry. For $\alpha\leq 1.5$ a.u., the best ground-state energies are provided by the simplest MRCCSD-1 method. As for the H4 model with small α values, when our $\mathcal{M}_0$ is perfectly adequate, the second $^1A_g(D_{2h})$ state [i.e., the lowest state of $^1A_{1g}(D_{4h})$ symmetry] is better described than the ground state (the errors in MRCCSD-n energies for the first excited state do not exceed 20 μhartree). Actually, for $\alpha\leq 2$ a.u., very good results are already provided by linear theory (cf. Fig. 7). Only when α becomes larger, the linear theory becomes singular. As already mentioned, the L-MRCCSD formalism has singularities at $\alpha\approx 3.30$ and 5.86 a.u. In the region of geometries that we examined, there is one more singularity for $\alpha\approx 8.41$ a.u. As in the case of the D4 and P4 models, this singularity is very broad (cf. Fig. 7). For example, for $\alpha=10$ a.u., the L-MRCCSD energies $E_i^{\text{L-MRCCSD}}$, $i=1,2$, are still very large: $\Delta E_1^{\text{L-MRCCSD}}=E_1^{\text{L-MRCCSD}}-E_0^{\text{RHF}}=-66.081$ hartree, $\Delta E_2^{\text{L-MRCCSD}}=E_2^{\text{L-MRCCSD}}-E_0^{\text{RHF}}=101.149$ hartree. As we shall see in the next section, we deal with a very strong interaction of both model states with configurations belonging to $\mathcal{M}_0^{\perp}$, when α approaches infinity.

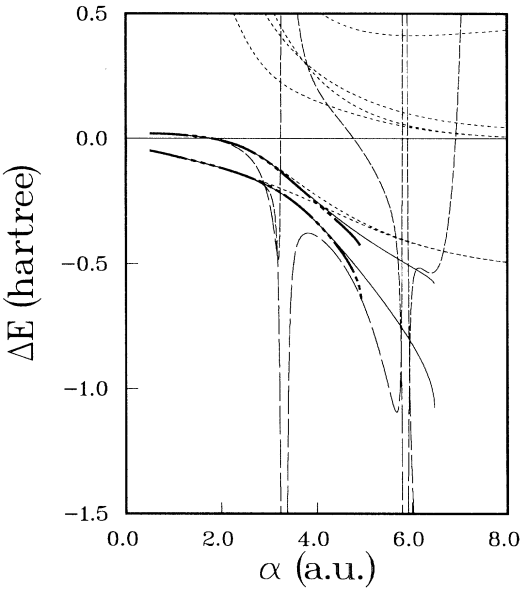

FIG. 7. Same as Fig. 4 for two energetically lowest $^1A_g(D_{2h})$ states of the MBS S4 model with 0.5 a.u. $\leq\alpha\leq$ 8.0 a.u. The ground state of $^1A_g(D_{2h})$ symmetry is the lowest eigenstate of $^1B_{1g}(D_{4h})$ symmetry, whereas the first excited state of $^1A_g(D_{2h})$ symmetry is the lowest eigenstate of $^1A_{1g}(D_{4h})$ symmetry. For $\alpha<3.72$ a.u. the fourth- and the sixth-excited states of $^1A_g(D_{2h})$ symmetry belong to $^1B_{1g}(D_{4h})$ subproblem, while the third, fourth, sixth, and eighth $^1A_g(D_{2h})$ states belong to $^1A_{1g}(D_{4h})$ subproblem. For $\alpha\approx 3.72$ a.u., the fourth and fifth states of $^1A_g(D_{2h})$ symmetry cross one another, so that for $\alpha>3.72$ a.u. the ground, the third-, and the sixth-excited $^1A_g(D_{2h})$ states belong to $^1B_{1g}(D_{4h})$ subproblem. The dotted lines correspond to successive FCI eigenstates of $^1A_g(D_{2h})$ symmetry (recall that proper symmetry for the two-reference CC theory is D_{2h}). The thin solid line represents MRCCSD-1 solution and the thick chain-dashed line the MRCCSD-2,3 solution. The L-MRCCSD method becomes singular for $\alpha=3.30$, 5.86, and 8.41 a.u. For $\alpha=2.92$, 3.18, 5.77, and 5.95 a.u., L-MRCCSD energies become identical.

TABLE XV. Same as Table VI for the two lowest $^1A_g(D_{2h})$ states of the MBS S4 model (see the text for details). Critical α values for MRCCSD-1 and MRCCSD-2,3 methods are 6.4682 and 4.9356 a.u., respectively. Energies are in mhartree.

	FCI		MRCCSD-1		MRCCSD-2,3	
α	ΔE_1	ΔE_2	ΔE_1	ΔE_2	ΔE_1	ΔE_2
0.50	−48.273	19.546	−48.269	19.543	−48.269	19.544
1.00	−69.211	16.635	−69.187	16.622	−69.183	16.624
1.50	−92.259	8.633	−92.197	8.613	−92.172	8.618
2.00	−117.621	−7.268	−117.686	−7.263	−117.575	−7.266
2.50	−147.058	−39.076	−148.677	−39.261	−148.261	−39.386
3.00	−180.605	−92.530	−190.088	−95.251	−188.987	−95.978
3.50	−218.530	−159.780	−250.747	−170.718	−249.089	−172.927
4.00	−260.289	−226.728	−334.156	−250.712	−333.663	−256.103
4.50	−303.762	−286.517	−436.032	−326.007	−445.870	−340.078
5.00	−345.874	−337.639	−550.991	−394.272	NC(↓)	NC(↓)
6.00	−416.160	−414.523	−819.264	−512.415		
7.00	−463.410	−463.119	NC(↓)	NC(↓)		

It is interesting to observe that L-MRCCSD energies become identical for several values of α, but unlike the D4 and P4 models, the eigenvalues of the L-MRCCSD effective Hamiltonian never become complex. There are four points where L-MRCCSD energies become identical: $\alpha_1=2.92$ a.u., $\alpha_2=3.18$ a.u., $\alpha_3=5.77$ a.u., and $\alpha_4=5.95$ a.u. At all these points, energies $E_i^{\text{L-MRCCSD}}$, $i=1,2$ (E_1 is always the lower eigenvalue) have discontinuous first derivatives with respect to α. To see these discontinuities better, we plotted the α dependence of the L-MRCCSD eigenvalues in separate Figs. 8(a) and 8(b). We note that both L-MRCCSD energies can easily be transformed into smooth functions of α (except, of course, for the poles at $\alpha=3.30$, 5.86, and 8.41 a.u.) by defining new energies $\tilde{E}_i^{\text{L-MRCCSD}}$, $i=1,2$ as follows:

$$\tilde{E}_1^{\text{L-MRCCSD}}=\begin{cases} E_1^{\text{L-MRCCSD}} & \text{for } \alpha<\alpha_1,\alpha_2<\alpha<\alpha_3,\alpha_4<\alpha \\ E_2^{\text{L-MRCCSD}} & \text{for } \alpha_1<\alpha<\alpha_2,\alpha_3<\alpha<\alpha_4 \end{cases}, \tag{92}$$

$$\tilde{E}_2^{\text{L-MRCCSD}}=\begin{cases} E_2^{\text{L-MRCCSD}} & \text{for } \alpha<\alpha_1,\alpha_2<\alpha<\alpha_3,\alpha_4<\alpha \\ E_1^{\text{L-MRCCSD}} & \text{for } \alpha_1<\alpha<\alpha_2,\alpha_3<\alpha<\alpha_4 \end{cases}. \tag{93}$$

To understand this behavior, we note that for the MBS S4 model the effective Hamiltonian matrix is Hermitian and has the following highly symmetric form:

$$\mathbf{H}^{\text{eff}}=\begin{bmatrix} a & b \\ b & a \end{bmatrix}, \tag{94}$$

where

$$a=H_{11}^{\text{eff}}=H_{22}^{\text{eff}},\quad b=H_{12}^{\text{eff}}=H_{21}^{\text{eff}}, \tag{95}$$

so that MRCCSD-n and L-MRCCSD energies are given by

$$E_1=a-|b|, \tag{96}$$

$$E_2=a+|b|. \tag{97}$$

In the case of MRCCSD-n methods, the off-diagonal matrix element b is always positive, so that the energies (96) and (97) are smooth functions of α in the region of existence of MRCCSD-n solutions. However, for the L-MRCCSD approach, b changes sign, being positive for $\alpha<\alpha_1$, $\alpha_2<\alpha<\alpha_3$, and $\alpha_4<\alpha$ and negative otherwise. For $\alpha=\alpha_i$, $i=1$–4, $b=0$, so that $E_1^{\text{L-MRCCSD}}=E_2^{\text{L-MRCCSD}}=a$. Clearly, if we redefine the energies (96) and (97) as follows:

$$\tilde{E}_1=a-b, \tag{98}$$

$$\tilde{E}_2=a+b, \tag{99}$$

we obtain two smooth functions of α defined by Eqs. (92) and (93).

It thus remains to explain why Eq. (95) holds for the MBS S4 model. We have seen in Sec. IV that our two-reference CC theory yields two states of different symmetry with respect to the invariance group of the Hamiltonian (D_{4h}). This is a consequence of the fact that our MO basis is adapted to the chain $D_{2h}\subset D_{4h}$, so that $\mathcal{M}_0\equiv\text{span}\{|\Phi_1\rangle,|\Phi_2\rangle\}$ represents an invariant subspace that is embedded in a larger space $\tilde{\mathcal{M}}_0$, Eq. (70), and the operations belonging to D_{4h} leave $|\Phi_1\rangle$ and $|\Phi_2\rangle$ unchanged, or transform them one into the other. The two states resulting from the two-reference CC formalism are given by Eqs. (82) and (83). The symmetry of the lower energy solution $|\Psi_1\rangle$ is $B_{1g}(D_{4h})$, so that rotation $C_4\in D_{4h}$ acts on $|\Psi_1\rangle$ as

$$C_4|\Psi_1\rangle=-|\Psi_1\rangle. \tag{100}$$

The second state $|\Psi_2\rangle$ is totally symmetric [$A_{1g}(D_{4h})$], so that

$$C_4|\Psi_2\rangle=|\Psi_2\rangle. \tag{101}$$

From Eqs. (81)–(83), (100), and (101), and the fact that C_4 transforms $|\Phi_1\rangle$ into $|\Phi_2\rangle$ (as pointed out in Sec. IV, none of the reference states spans a single irrep of D_{4h}), it

follows that

$$\sqrt{2}|\Psi_1\rangle = e^{T^{(1)}}|\Phi_1\rangle - e^{T^{(2)}}|\Phi_2\rangle$$
$$= -C_4 e^{T^{(1)}}|\Phi_1\rangle + C_4 e^{T^{(2)}}|\Phi_2\rangle$$
$$= e^{C_4 T^{(2)} C_4^{-1}}|\Phi_1\rangle - e^{C_4 T^{(1)} C_4^{-1}}|\Phi_2\rangle \ , \qquad (102)$$

$$\sqrt{2}|\Psi_2\rangle = e^{T^{(1)}}|\Phi_1\rangle + e^{T^{(2)}}|\Phi_2\rangle$$
$$= C_4 e^{T^{(1)}}|\Phi_1\rangle + C_4 e^{T^{(2)}}|\Phi_2\rangle$$
$$= e^{C_4 T^{(2)} C_4^{-1}}|\Phi_1\rangle + e^{C_4 T^{(1)} C_4^{-1}}|\Phi_2\rangle \ . \qquad (103)$$

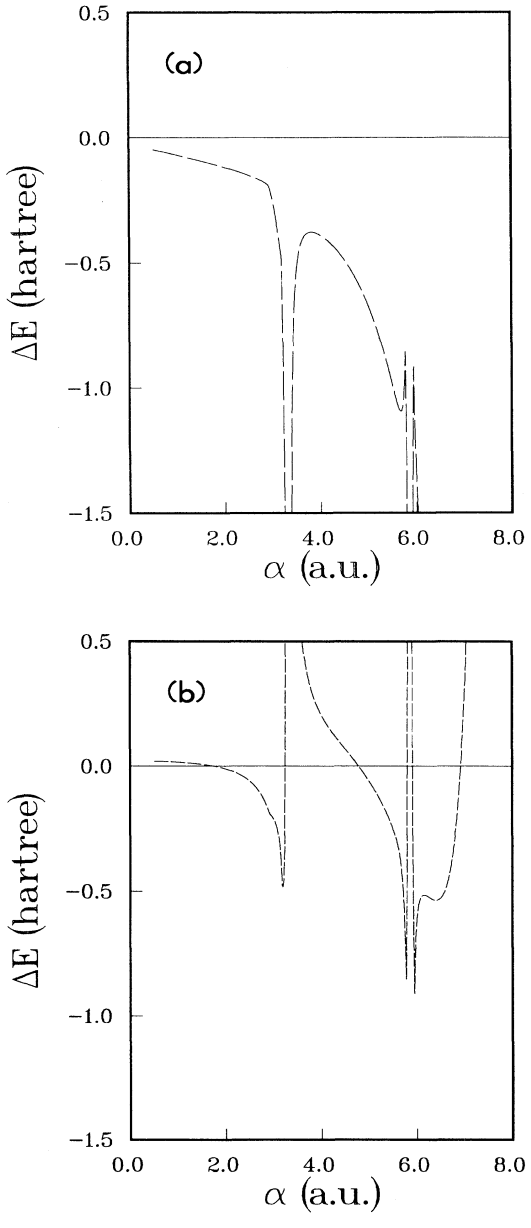

FIG. 8. Dependence of the L-MRCCSD energies on the parameter α for the MBS S4 model. The α dependence of the first (lower energy) root of the effective Hamiltonian $\mathbf{H}^{\text{eff}}$ is displayed in Fig. 8(a), whereas Fig. 8(b) displays the α dependence of the second (higher-energy) root of $\mathbf{H}^{\text{eff}}$.

This implies that cluster operators break the D_{4h} symmetry, since we can write [cf. Eq. (85)]

$$C_4 T^{(p)} C_4^{-1} = T^{(q)}, \quad p=1,2, \quad q=3-p \ . \qquad (104)$$

There is no such symmetry breaking when we consider the wave operator U, Eq. (81), i.e., we have

$$C_4 U C_4^{-1} = U \ . \qquad (105)$$

Notice that relation (104) follows directly from Eq. (105). Indeed, since

$$C_4|\Phi_p\rangle = |\Phi_q\rangle, \quad p=1,2, \quad q=3-p \ , \qquad (106)$$

we can write

$$C_4 P_p C_4^{-1} = P_q \ , \qquad (107)$$

so that

$$e^{T^{(1)}}P_1 + e^{T^{(2)}}P_2 \equiv U = C_4 U C_4^{-1}$$
$$= e^{C_4 T^{(2)} C_4^{-1}}P_1 + e^{C_4 T^{(1)} C_4^{-1}}P_2 \ . \qquad (108)$$

Now, relations (95) are an immediate consequence of Eqs. (105) and (106): for the diagonal matrix elements we get

$$H_{11}^{\text{eff}} = \langle \Phi_1|HU|\Phi_1\rangle = \langle C_4^{-1}\Phi_2|HU|C_4^{-1}\Phi_2\rangle$$
$$= \langle \Phi_2|(C_4 H C_4^{-1})(C_4 U C_4^{-1})|\Phi_2\rangle$$
$$= \langle \Phi_2|HU|\Phi_2\rangle = H_{22}^{\text{eff}} \ , \qquad (109)$$

while for the off-diagonal elements we find

$$H_{12}^{\text{eff}} = \langle \Phi_1|HU|\Phi_2\rangle = \langle C_4^{-1}\Phi_2|HU|C_4^{-1}\Phi_1\rangle$$
$$= \langle \Phi_2|(C_4 H C_4^{-1})(C_4 U C_4^{-1})|\Phi_1\rangle$$
$$= \langle \Phi_2|HU|\Phi_1\rangle = H_{21}^{\text{eff}} \ , \qquad (110)$$

so that indeed $\mathbf{H}^{\text{eff}}$ has the form (94). Clearly, $\mathbf{H}^{\text{eff}}$ must have this highly symmetric form, since the effective Hamiltonian operator H^{eff}, Eq. (19), is invariant with respect to all symmetry operations belonging to D_{4h}, in particular C_4 [cf. Eq. (84)].

There are further interesting consequences of Eq. (104). We can apply it to specific many-body components of cluster operators $T^{(p)}$ and thus find useful relations between individual pair-cluster coefficients associated with distinct reference configurations, namely,

$$\begin{aligned} &\langle 44|t_2^{(1)}|22\rangle_0 = \langle 44|t_2^{(2)}|33\rangle_0 \ , \\ &\langle 44|t_2^{(1)}|11\rangle_0 = \langle 44|t_2^{(2)}|11\rangle_0 \ , \\ &\langle 33|t_2^{(1)}|11\rangle_0 = \langle 22|t_2^{(2)}|11\rangle_0 \ , \\ &\langle 34|t_2^{(1)}|12\rangle_i = \langle 24|t_2^{(2)}|13\rangle_i, \quad i=0,1 \ . \end{aligned} \qquad (111)$$

Monoexcited clusters and pair-cluster amplitudes associated with excitations ${}^{(p)}G_{\alpha\alpha}^{\rho\sigma}(0)$, $\rho \neq \sigma$, and ${}^{(p)}G_{\alpha\beta}^{\rho\rho}(0)$, $\alpha \neq \beta$ vanish for the MBS S4 model (cf. Sec. IV). For qua-

druply excited components $T_4^{(p)}$ we then get

$$\langle t_4^{(1)} \rangle \equiv \langle 3344|t_4^{(1)}|1122\rangle_{0,0,0,0,0} = \langle 2244|t_4^{(2)}|1133\rangle_{0,0,0,0,0} \equiv \langle t_4^{(2)} \rangle , \quad (112)$$

which is employed in Table XIV. Our calculations confirm the above results. Relations (111) hold for both the full CC theory (equivalent to FCI) and the CCSD approximation.

Results of this section confirm our expectations that the S4 model represents the most severe test for the two-reference version of the MRCC theory employed here. Clearly, a two-reference model space is insufficient to describe the breaking of all four bonds in our model.

VI. L-MRCCSD BREAKDOWN

Our calculations reveal that L-MRCC formalisms are more likely to suffer from singular behavior than SRCC theories. Including only a few (in our case, two) configurations that dominate the quasidegenerate regime in the model space is generally insufficient to yield a meaningful description of nondegenerate or strongly correlated states. In the vicinity of the square geometry of the nuclear framework with H—H bond lengths close to their equilibrium value, where the ground-state configuration $|\Phi_1\rangle$ strongly interacts only with biexcited $|\Phi_2\rangle$ configuration, the model space $\mathcal{M}_0 \equiv \text{span}\{|\Phi_1\rangle, |\Phi_2\rangle\}$ is perfectly adequate. Absence of $|\Phi_2\rangle$ from $\mathcal{M}_0$ would certainly lead to the appearance of a singularity in this region as was first found by Jankowski and Paldus in their SRCC study of various H_4 models [37]. Unfortunately, the presence of $|\Phi_2\rangle$ in $\mathcal{M}_0$ increases the probability of encountering intruder states in other regions of the nuclear coordinate space, characterized by a strong interaction of $|\Phi_2\rangle$ with configurations belonging to $\mathcal{M}_0^{\perp}$. As a consequence, the L-MRCCSD coefficient matrix $\mathbf{b} \equiv \mathbf{b}(\alpha) \equiv \|b_{IJ}(\alpha)\|_{1 \le I,J \le N}$ [cf. Eqs. (86) or (89)] becomes singular [37,38,53,69] (cf. also Refs. [6] and [7]) and the solution vector $\mathbf{t} \equiv \mathbf{t}(\alpha)$, as well as the corresponding energies $E_i^{\text{L-MRCCSD}}(\alpha)$, $i=1,2$ regarded as functions of the parameter α, have one or more poles [63].

As mentioned in Sec. V A, the appearance of these poles may be approximately predicted by examining the dependence of easily accessible diagonal CI matrix elements $H_{jj} = \langle \Phi_j|H|\Phi_j \rangle$ on the geometry of the nuclear framework. Figure 9 shows this dependence for the models considered in this paper. Every crossing indicates a strong interaction of corresponding configurations. Thus, crossings of curves H_{11} or H_{22} with H_{jj}, $j=3-12$, imply the possibility of appearance of L-MRCCSD singularities.

For the MBS H4 model [Fig. 9(a)], we observe a crossing of $H_{22} = \langle {}^{(1)}G^{33}_{22}(0)\Phi_1|H|{}^{(1)}G^{33}_{22}(0)\Phi_1\rangle$ with $H_{88} = \langle {}^{(1)}G^{3}_{1}\Phi_1|H|{}^{(1)}G^{3}_{1}\Phi_1\rangle$ (cf. Table IV). For $a=2.0$ a.u., this crossing takes place at $\alpha \approx 0.26$, which correlates quite well with the appearance of the L-MRCCSD singularity at $\alpha \approx 0.16$ (cf. Sec. V A). Actually, the region where L-MRCCSD energies significantly deviate from the FCI data ($\alpha \approx 0.1-0.25$) is much larger than the immediate vicinity of the singularity, so that the crossing of H_{22} and H_{88} at $\alpha \approx 0.26$ provides us with valuable information where this region may appear. Notice that the matrix elements H_{22} and H_{88} remain close in a much broader region $\alpha \approx 0.15-0.5$. In this region, $|\Phi_2\rangle$ and $|\Phi_8\rangle = {}^{(1)}G^{3}_{1}|\Phi_1\rangle$ are the dominant configurations in the FCI expansion of the second excited ${}^1A_1(C_{2v})$ state $|\Psi_3\rangle$ (see Table XVI), with almost equal weights at $\alpha \approx 0.5$. It is thus not surprising that once we pass the region of singular behavior, the second root of the L-MRCCSD effective Hamiltonian begins to describe the second rather than the first excited state. The lowest root of the effective Hamiltonian invariably describes the ground state, since the reference state $|\Phi_1\rangle$ never becomes degenerate with configurations belonging to $\mathcal{M}_0^{\perp}$ [cf. Fig. 9(a)].

Although the situation for the MBS D4 model is much more complicated, we can carry out a similar analysis. In this case H_{22} crosses H_{88} at $\alpha \approx 1.7$ a.u., $H_{99} = \langle {}^{(1)}G^{4}_{2}\Phi_1|H|{}^{(1)}G^{4}_{2}\Phi_1\rangle$ at $\alpha \approx 2.7$ a.u., and $H_{77} = \langle {}^{(1)}G^{34}_{12}(1)\Phi_1|H|{}^{(1)}G^{34}_{12}(1)\Phi_1\rangle$ at $\alpha \approx 5.1$ a.u. [Fig. 9(b)]. Moreover, we observe a strong interaction of $|\Phi_2\rangle$ with configurations $|\Phi_3\rangle = {}^{(1)}G^{44}_{22}(0)|\Phi_1\rangle$, $|\Phi_4\rangle = {}^{(1)}G^{33}_{11}(0)|\Phi_1\rangle$, and $|\Phi_5\rangle = {}^{(1)}G^{44}_{11}(0)|\Phi_1\rangle$ for $\alpha \to \infty$ [H_{22}, H_{33}, H_{44}, and H_{55} are very close already for $\alpha \approx 7$ a.u.; cf. Fig. 9(b)]. Interaction of $|\Phi_2\rangle$ with $|\Phi_8\rangle$ results in the appearance of a L-MRCCSD singularity at $\alpha \approx 1.18$ a.u. Indeed, in this region $|\Phi_2\rangle$ and $|\Phi_8\rangle$ are dominant configurations in the FCI expansions of the first and second excited states and participation of $|\Phi_1\rangle$ in the FCI expansion of the second excited state reaches its maximum (Table XVII). Since $|\Phi_2\rangle$ and $|\Phi_8\rangle$ become nearly degenerate, the second root of the L-MRCCSD effective Hamiltonian, $E_2^{\text{L-MRCCSD}}$, begins to approximate the second rather than the first excited state of ${}^1\Sigma_g^+$ sym-

TABLE XVI. Selected FCI expansion coefficients for the first and the second excited states of ${}^1A_1(C_{2v})$ symmetry, $|\Psi_2\rangle$ and $|\Psi_3\rangle$, respectively, for the MBS H4 model with $a=2.0$ a.u. As in Table XIII, $|\Psi_\mu\rangle = \sum_j d'_{j\mu}|\Phi_j\rangle$, $\langle \Psi_\mu|\Psi_\mu\rangle = 1$.

α	$d'_{1,2}$	$d'_{2,2}$	$d'_{8,2}$	$d'_{1,3}$	$d'_{2,3}$	$d'_{8,3}$
0.000	0.678	0.678	0.000	0.000	0.000	−0.894
0.050	0.296	0.884	0.126	0.096	0.176	−0.858
0.100	0.194	0.847	0.275	0.134	0.352	−0.826
0.150	0.150	0.769	0.410	0.146	0.481	−0.805
0.200	0.127	0.700	0.504	0.145	0.539	−0.785
0.500	0.106	0.593	0.650	0.143	0.609	−0.693

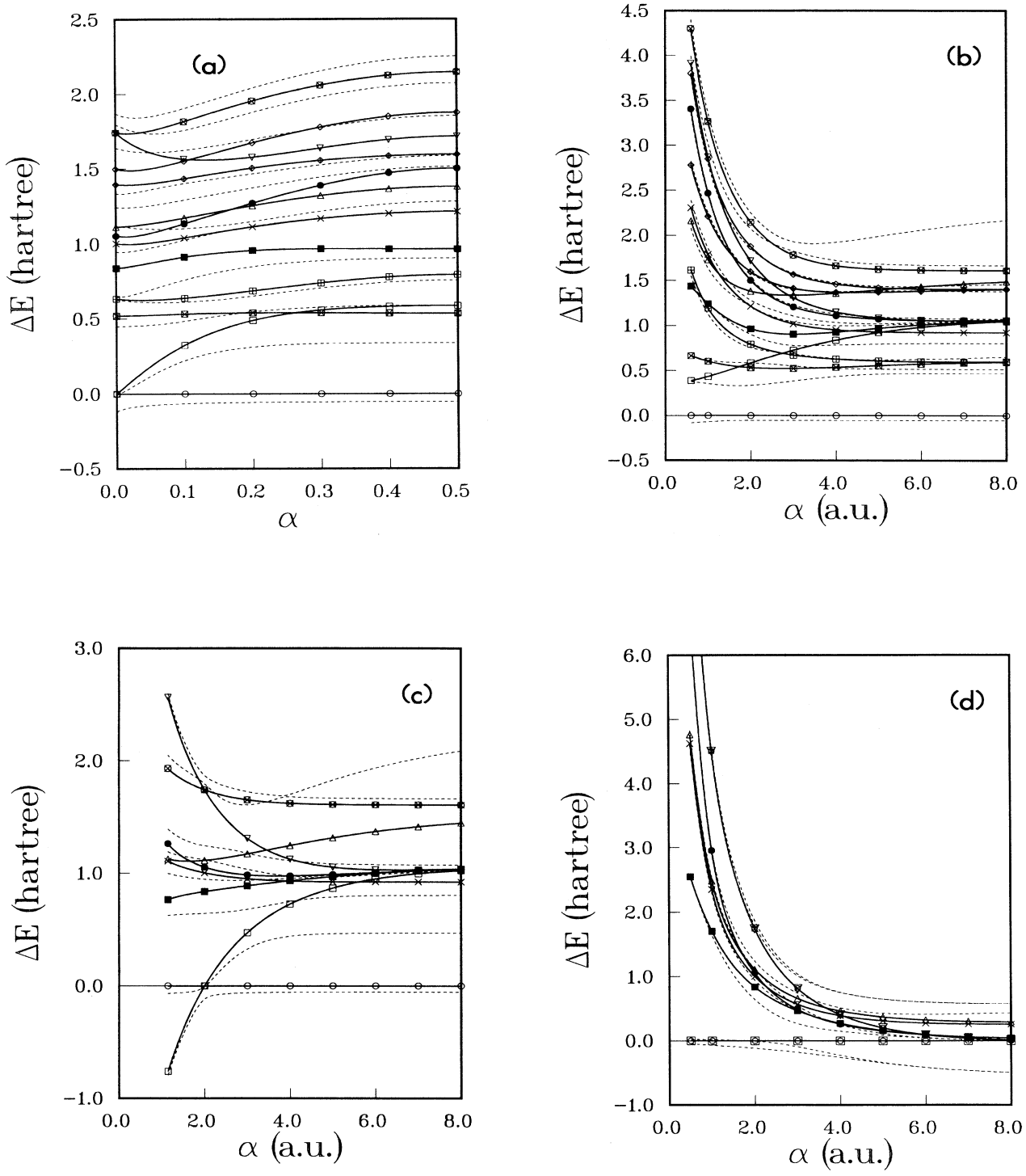

FIG. 9. Dependence of the diagonal CI matrix elements $H_{jj}=\langle\Phi_j|H|\Phi_j\rangle$, $j=1-12$, relative to the RHF energy $H_{11}=\langle\Phi_1|H|\Phi_1\rangle=\langle(\phi_1)^2(\phi_2)^2|H|(\phi_1)^2(\phi_2)^2\rangle$ (except for the MBS P4 model with $\alpha<a$, H_{11} represents the ground-state RHF energy), on the geometry of the nuclear framework, as measured by the parameter α (solid lines), for the MBS H4 model with $a=2.0$ a.u. and $0\le\alpha\le0.5$ (a), MBS D4 model with $a=2.0$ a.u. and 0.6 a.u. $\le\alpha\le8$ a.u. (b), MBS P4 model with $a=2.0$ a.u. and 1.1428 a.u. $\le\alpha\le8$ a.u. (c), and MBS S4 model with 0.5 a.u. $\le\alpha\le8$ a.u. (d). Open circles and squares (○ and □) represent matrix elements H_{11} and H_{22}, respectively, whereas solid circles and squares (● and ■) represent H_{33} and H_{44}. The remaining matrix elements H_{jj}, $j=5-12$, are represented by ▽, △, ×, ⊠, ⊗, ◇, ⊗, and ⊗, respectively. In the case of the P4 and S4 models, configurations $|\Phi_j\rangle$, $j=8-11$, belong to different symmetry species than do $|\Phi_1\rangle$ and $|\Phi_2\rangle$. Thus, the corresponding matrix elements H_{jj}, $j=8-11$, are not displayed in (c) and (d). The dotted lines correspond to successive FCI eigenstates of $^1A_1(C_{2v})$ (a), $^1\Sigma_g^+$ (b), and $^1A_g(D_{2h})$ [(c) and (d)] symmetry. As in Fig. 7, we do not distinguish between $^1B_{1g}(D_{4h})$ and $^1A_{1g}(D_{4h})$ states in part (d).

TABLE XVII. Same as Table XVI for the first, second, and third excited states of $^1\Sigma_g^+$ symmetry, $|\Psi_2\rangle$, $|\Psi_3\rangle$, and $|\Psi_4\rangle$, respectively, for the MBS D4 model with $a=2.0$ a.u.

α	$d'_{1,2}$	$d'_{2,2}$	$d'_{8,2}$	$d'_{9,2}$	$d'_{1,3}$	$d'_{2,3}$	$d'_{8,3}$	$d'_{9,3}$	$d'_{1,4}$	$d'_{2,4}$	$d'_{8,4}$	$d'_{9,4}$
1.0	0.294	0.750	0.536	−0.164	0.156	0.538	−0.795	−0.025	0.040	0.129	0.139	0.914
1.5	0.192	0.656	0.628	−0.231	0.170	0.632	−0.705	−0.107	0.073	0.221	0.158	0.883
2.0	0.106	0.593	0.650	−0.265	0.143	0.609	−0.693	−0.249	0.112	0.363	0.090	0.834
2.5	0.052	0.552	0.639	−0.271	0.091	0.485	−0.715	−0.393	0.125	0.469	−0.069	0.794
3.0	0.023	0.525	0.611	−0.256	0.049	0.364	−0.734	−0.450	0.081	0.389	−0.206	0.816
4.0	0.004	0.502	0.491	−0.188	0.014	0.209	−0.790	−0.454	0.020	0.170	−0.330	0.852
5.0	0.001	0.489	0.267	−0.112	0.005	0.081	−0.820	−0.511	0.008	0.062	−0.483	0.837
8.0	0.000	0.438	0.012	−0.011	0.001	0.001	−0.706	−0.683	0.001	−0.025	−0.695	0.718

metry and this transition results in the appearance of a singularity. Crossing of H_{22} and H_{99} nicely correlates with the appearance of the next singularity at $\alpha\approx 2.41$ a.u. In this case, the energy $E_2^{\text{L-MRCCSD}}$ begins to match the energy of the third excited state $|\Psi_4\rangle$, since the FCI expansion of $|\Psi_4\rangle$ for $\alpha\approx 2.5$ a.u. results from a strong interaction of $|\Phi_2\rangle$ and $|\Phi_9\rangle$ with a substantial participation of $|\Phi_1\rangle$ (see Table XVII). The third singularity appears at $\alpha\approx 3.03$ a.u., so that it is hard to associate it with the crossing of H_{22} with H_{77}. However, for $\alpha\approx 3-4$ a.u. we observe a strong interaction of $|\Phi_2\rangle$, $|\Phi_4\rangle$, and $|\Phi_7\rangle$ [see Fig. 9(b)], and this seems to correlate with the fact that the FCI expansion of the fourth excited state $|\Psi_5\rangle$ results from a strong interaction of $|\Phi_2\rangle$, $|\Phi_4\rangle$, $|\Phi_6\rangle = {}^{(1)}G_{12}^{34}(0)|\Phi_1\rangle$ and $|\Phi_7\rangle$ (the corresponding FCI expansion coefficients for $\alpha=3$ a.u. equal 0.470, 0.587, 0.457, and 0.291, respectively). In consequence, once we pass the singularity at $\alpha\approx 3.03$ a.u., the second root begins to describe $|\Psi_5\rangle$. The last and the broadest singularity at $\alpha\approx 6.20$ a.u. seems to be related with both the crossing of H_{22} with H_{77} and strong interaction of $|\Phi_2\rangle$ with $|\Phi_3\rangle$, $|\Phi_4\rangle$, and $|\Phi_5\rangle$. Once we pass it, the second root begins to describe the group of fifth, sixth, and seventh excited states, to which configurations $|\Phi_j\rangle$, $j=2-5$, and $|\Phi_7\rangle$ contribute substantially. This can be most easily seen by looking at the FCI expansions of $|\Psi_6\rangle$, $|\Psi_7\rangle$, and $|\Psi_8\rangle$ for $\alpha > 6.20$ a.u. (Table XVIII for $\alpha=8$ a.u.).

For the P4 model, H_{22} crosses H_{77} at $\alpha\approx 5.6$ a.u. and we observe a strong interaction of $|\Phi_2\rangle$ with $|\Phi_3\rangle$, $|\Phi_4\rangle$, and $|\Phi_5\rangle$ for α approaching infinity [see Fig. 9(c)]. Proximity of H_{22}, H_{33}, H_{44}, and H_{55}, and the crossing of H_{22} and H_{77}, result in the appearance of two singularities at $\alpha\approx 3.46$ a.u. and $\alpha\approx 6.80$ a.u. For $\alpha > 3.46$ a.u., the second root $E_2^{\text{L-MRCCSD}}$ begins to approximate the second excited $^1A_g(D_{2h})$ state, to which $|\Phi_2\rangle$, $|\Phi_4\rangle$, $|\Phi_6\rangle$, and $|\Phi_7\rangle$ contribute most substantially [recall that the second excited $^1A_g(D_{2h})$ state for the P4 model corresponds to the fourth excited $^1\Sigma_g^+$ state for the D4 model]. Then, beyond the singularity at $\alpha\approx 6.80$ a.u., $E_2^{\text{L-MRCCSD}}$ begins to approximate the energy of the fourth, fifth, and sixth states of $^1A_g(D_{2h})$ symmetry, which result from a strong mixing of configurations $|\Phi_j\rangle$, $j=2-5$, and $|\Phi_7\rangle$ (other configurations practically do not contribute to the FCI expansions of these states). For symmetry reasons, $|\Phi_2\rangle$ cannot interact with $^1B_{3u}(D_{2h})$ configurations $|\Phi_8\rangle$ and $|\Phi_9\rangle$. Thus, two singularities appearing in the short-range region of the D4 model do not show up for the P4 model.

As in the other cases, singularities appearing for the S4 model can also be associated with a strong interaction of the model-space configurations $|\Phi_1\rangle$ and $|\Phi_2\rangle$ with configurations belonging to $\mathcal{M}_0^{\perp}$. Again, we can predict their occurrence by observing the α dependence of diagonal matrix elements H_{jj}. Figure 9(d) shows that $|\Phi_1\rangle$ and $|\Phi_2\rangle$ do not interact with $\mathcal{M}_0^{\perp}$ only for small values of α, but become degenerate with $|\Phi_3\rangle$, $|\Phi_4\rangle$, $|\Phi_5\rangle$, and $|\Phi_{12}\rangle$ when $\alpha\rightarrow\infty$, causing singularities in this region [cf. Figs. 7, 8, and 9(d)].

The singular character of the L-MRCCSD coefficient matrix $\mathbf{b}$ is also reflected in the structure of the effective Hamiltonian matrix. Since in the vicinity of the singularity the cluster amplitudes become large, so do the t-dependent contributions to $\mathbf{H}^{\text{eff}}$. This is illustrated by the α dependence of the individual contributions to $\mathbf{H}^{\text{eff}}$ for the MBS H4 model with $a=2.0$ a.u. in Tables XIX and XX. In the immediate vicinity of the singularity at $\alpha\approx 0.155$, we observe a rapid increase in the absolute values of all t-dependent contributions to $\mathbf{H}^{\text{eff}}$. Simultaneously, we observe a dramatic increase in the absolute values of cluster amplitudes, particularly t_6, t_9, t_{11}, t_{12}, t_{14}, and t_{16} (cf. Table V).

TABLE XVIII. FCI expansion coefficients for the fifth, sixth, and seventh excited states of $^1\Sigma_g^+$ symmetry, $|\Psi_6\rangle$, $|\Psi_7\rangle$, and $|\Psi_8\rangle$, respectively, for the MBS D4 model with $a=2.0$ a.u. and $\alpha=8$ a.u.

μ	$d'_{1,\mu}$	$d'_{2,\mu}$	$d'_{3,\mu}$	$d'_{4,\mu}$	$d'_{5,\mu}$	$d'_{6,\mu}$	$d'_{7,\mu}$	$d'_{8,\mu}$	$d'_{9,\mu}$	$d'_{10,\mu}$	$d'_{11,\mu}$	$d'_{12,\mu}$
6	0.004	−0.633	0.337	−0.307	0.621	0.013	0.044	0.029	−0.030	−0.027	0.027	−0.006
7	0.001	−0.348	−0.586	0.661	0.277	0.001	0.140	0.015	−0.013	−0.014	0.017	−0.003
8	0.011	−0.157	0.339	0.171	−0.320	0.017	0.853	−0.005	0.004	0.007	−0.003	−0.021

TABLE XX. Same as Table XIX for the off-diagonal elements of H^{eff} (in hartree). We define $\langle (T^{(1)})^k \rangle = (k!)^{-1} \langle \Phi_2 | H (T^{(1)})^k | \Phi_1 \rangle$ and $\langle (T^{(2)})^k \rangle \equiv (k!)^{-1} \langle \Phi_1 | H (T^{(2)})^k | \Phi_2 \rangle$.

α	H_{12}^{eff}	H_{12}	$\langle T^{(2)} \rangle$	$\langle (T^{(2)})^2 \rangle$	H_{21}^{eff}	H_{21}	$\langle T^{(1)} \rangle$	$\langle (T^{(1)})^2 \rangle$	$\langle (T^{(1)})^3 \rangle$	$\langle (T^{(1)})^4 \rangle$
0.000	0.053 927	0.056 970	−0.005 256	0.002 212	0.053 927	0.056 970	−0.005 256	0.002 212	0.000 000	0.000 000
0.005	0.053 868	0.057 282	−0.005 768	0.002 353	0.054 113	0.057 282	−0.005 396	0.002 227	0.000 000	0.000 000
0.010	0.053 886	0.057 749	−0.006 370	0.002 507	0.054 420	0.057 749	−0.005 582	0.002 254	0.000 000	0.000 000
0.020	0.054 058	0.059 066	−0.007 866	0.002 858	0.055 318	0.059 066	−0.006 089	0.002 343	−0.000 002	0.000 000
0.050	0.054 075	0.064 975	−0.015 329	0.004 430	0.059 024	0.064 975	−0.008 847	0.002 902	−0.000 006	0.000 000
0.100	0.039 624	0.076 690	−0.050 778	0.013 712	0.061 483	0.076 690	−0.022 467	0.007 252	0.000 002	0.000 006
0.110	0.031 165	0.078 940	−0.067 854	0.020 079	0.060 302	0.078 940	−0.029 132	0.010 452	0.000 027	0.000 015
0.120	0.019 277	0.081 111	−0.094 824	0.032 990	0.058 534	0.081 111	−0.039 718	0.016 985	0.000 107	0.000 047
0.130	0.005 145	0.083 194	−0.143 580	0.065 531	0.058 276	0.083 194	−0.058 944	0.033 375	0.000 444	0.000 207
0.140	0.016 716	0.085 181	−0.258 244	0.189 779	0.080 644	0.085 181	−0.104 324	0.095 136	0.002 841	0.001 811
0.150	1.159 837	0.087 066	−0.854 725	1.927 495	0.979 589	0.087 066	−0.340 921	0.941 541	0.109 544	0.182 359
0.155	715.030 315	0.087 970	16.469 974	698.472 371	22 549.192 728	0.087 970	6.534 837	335.088 328	−804.373 122	23 011.854 716
0.160	2.601 714	0.088 848	0.817 666	1.695 200	1.234 127	0.088 848	0.322 935	0.795 595	−0.100 965	0.127 714
0.170	0.608 692	0.090 523	0.296 424	0.221 745	0.301 793	0.090 523	0.116 198	0.098 337	−0.005 087	0.001 822
0.180	0.370 535	0.092 093	0.187 343	0.091 099	0.201 491	0.092 093	0.073 033	0.037 510	−0.001 379	0.000 234
0.190	0.286 753	0.093 559	0.139 605	0.053 589	0.167 336	0.093 559	0.054 209	0.020 140	−0.000 627	0.000 056
0.200	0.245 235	0.094 922	0.112 496	0.037 817	0.150 907	0.094 922	0.043 565	0.012 773	−0.000 371	0.000 017
0.250	0.179 027	0.100 319	0.058 880	0.019 828	0.126 304	0.100 319	0.022 706	0.003 426	−0.000 146	0.000 000
0.300	0.161 924	0.103 748	0.039 934	0.018 243	0.120 595	0.103 748	0.015 309	0.001 674	−0.000 139	0.000 002
0.400	0.151 696	0.106 915	0.027 291	0.017 490	0.117 905	0.106 915	0.010 216	0.000 905	−0.000 135	0.000 003
0.500	0.149 790	0.107 635	0.025 186	0.016 970	0.117 686	0.107 635	0.009 365	0.000 811	−0.000 128	0.000 003

TABLE XIX. Individual contributions to diagonal elements of the effective Hamiltonian H^{eff} (in hartree) for the MBS H4 model with $a=2.0$ a.u. and various values of α, as obtained by using the L-MRCCSD method. Zero contributions are not listed.

α	H_{11}^{eff}	H_{11}	$\langle\Phi_1\vert HT^{(1)}\vert\Phi_1\rangle$	$\frac{1}{2}\langle\Phi_1\vert H(T^{(1)})^2\vert\Phi_1\rangle$	H_{22}^{eff}	H_{22}	$\langle\Phi_2\vert HT^{(2)}\vert\Phi_2\rangle$
0.000	−4.630 173	−4.565 348	−0.064 825	0.000 000	−4.630 173	−4.565 348	−0.064 825
0.005	−4.622 269	−4.557 786	−0.064 481	−0.000 001	−4.604 625	−4.537 695	−0.066 930
0.010	−4.614 628	−4.550 596	−0.064 026	−0.000 005	−4.579 876	−4.510 730	−0.069 147
0.020	−4.600 051	−4.537 155	−0.062 876	−0.000 020	−4.532 786	−4.458 811	−0.073 975
0.050	−4.560 944	−4.502 001	−0.058 844	−0.000 099	−4.411 439	−4.318 257	−0.093 183
0.100	−4.509 876	−4.452 611	−0.056 747	−0.000 519	−4.297 034	−4.129 176	−0.167 859
0.110	−4.502 788	−4.443 614	−0.058 406	−0.000 767	−4.299 417	−4.097 419	−0.201 998
0.120	−4.498 012	−4.434 875	−0.061 927	−0.001 211	−4.322 827	−4.067 514	−0.255 313
0.130	−4.497 944	−4.426 387	−0.069 413	−0.002 144	−4.390 299	−4.039 386	−0.350 913
0.140	−4.511 703	−4.418 154	−0.088 685	−0.004 865	−4.587 507	−4.012 962	−0.574 545
0.150	−4.632 959	−4.410 175	−0.193 503	−0.029 281	−5.722 593	−3.988 169	−1.734 424
0.155	−7.615 032	−4.406 282	2.879 793	−6.088 543	27.954 804	−3.976 360	31.931 164
0.160	−4.300 922	−4.402 454	0.104 021	−0.002 490	−2.450 254	−3.964 931	1.514 677
0.170	−4.379 269	−4.394 992	0.012 393	0.003 331	−3.442 122	−3.943 175	0.501 053
0.180	−4.390 945	−4.387 792	−0.006 199	0.003 045	−3.634 463	−3.922 828	0.288 365
0.190	−4.391 999	−4.380 853	−0.013 973	0.002 827	−3.708 936	−3.903 819	0.194 883
0.200	−4.389 599	−4.374 177	−0.018 144	0.002 722	−3.744 596	−3.886 078	0.141 481
0.250	−4.366 974	−4.344 672	−0.025 165	0.002 862	−3.780 723	−3.814 129	0.033 406
0.300	−4.345 164	−4.321 356	−0.026 920	0.003 112	−3.772 329	−3.764 811	−0.007 518
0.400	−4.316 092	−4.291 522	−0.027 604	0.003 034	−3.749 129	−3.711 618	−0.037 510
0.500	−4.306 601	−4.281 903	−0.027 599	0.002 901	−3.739 733	−3.696 814	−0.042 919

It is interesting to compare the effective Hamiltonians resulting from the L-MRCCSD (Tables XIX and XX) and nonlinear MRCCSD-3 (Tables XXI and XXII) calculations. It is seen that the off-diagonal matrix elements are especially sensitive to the appearance of singularities. They contain highly nonlinear (even quartic) terms, such as $\frac{1}{24}\langle\Phi_2\vert H(T^{(1)})^4\vert\Phi_1\rangle$, and these terms are much more sensitive to variations in cluster coefficients than other t-dependent contributions. In nonsingular regions, where cluster amplitudes are small, these terms practically do not contribute. However, when we approach a singularity, cluster coefficients increase and highly nonlinear terms, such as $\frac{1}{6}\langle\Phi_2\vert H(T^{(1)})^3\vert\Phi_1\rangle$ or $\frac{1}{24}\langle\Phi_2\vert H(T^{(1)})^4\vert\Phi_1\rangle$, increase by many orders of magni-

TABLE XXI. Individual contributions to diagonal elements of the effective Hamiltonian H^{eff} (in hartree) for the MBS H4 model with $a=2.0$ a.u. and various values of α, as obtained by using the fully quadratic MRCCSD-3 approach. As in Tables XIX and XX, zero contributions are not listed.

α	H_{11}^{eff}	H_{11}	$\langle\Phi_1\vert HT^{(1)}\vert\Phi_1\rangle$	$\frac{1}{2}\langle\Phi_1\vert H(T^{(1)})^2\vert\Phi_1\rangle$	H_{22}^{eff}	H_{22}	$\langle\Phi_2\vert HT^{(2)}\vert\Phi_2\rangle$
0.000	−4.627 769	−4.565 348	−0.062 421	0.000 000	−4.627 769	−4.565 348	−0.062 421
0.005	−4.619 856	−4.557 786	−0.062 069	−0.000 001	−4.602 007	−4.537 695	−0.064 312
0.010	−4.612 206	−4.550 596	−0.061 605	−0.000 004	−4.577 003	−4.510 730	−0.066 273
0.020	−4.597 592	−4.537 155	−0.060 424	−0.000 013	−4.529 240	−4.458 811	−0.070 429
0.050	−4.558 076	−4.502 001	−0.056 019	−0.000 057	−4.403 399	−4.318 257	−0.085 142
0.100	−4.502 419	−4.452 611	−0.049 656	−0.000 152	−4.247 600	−4.129 176	−0.118 424
0.110	−4.492 488	−4.443 614	−0.048 701	−0.000 172	−4.223 655	−4.097 419	−0.126 236
0.120	−4.482 910	−4.434 875	−0.047 844	−0.000 192	−4.201 793	−4.067 514	−0.134 280
0.130	−4.473 670	−4.426 387	−0.047 073	−0.000 210	−4.181 848	−4.039 386	−0.142 462
0.140	−4.464 760	−4.418 154	−0.046 379	−0.000 227	−4.163 648	−4.012 962	−0.150 686
0.150	−4.456 170	−4.410 175	−0.045 753	−0.000 242	−4.147 027	−3.988 169	−0.158 858
0.155	−4.451 993	−4.406 282	−0.045 462	−0.000 248	−4.139 258	−3.976 360	−0.162 898
0.160	−4.447 893	−4.402 454	−0.045 185	−0.000 254	−4.131 825	−3.964 931	−0.166 894
0.170	−4.439 926	−4.394 992	−0.044 670	−0.000 264	−4.117 897	−3.943 175	−0.174 722
0.180	−4.432 262	−4.387 792	−0.044 200	−0.000 270	−4.105 110	−3.922 828	−0.182 282
0.190	−4.424 899	−4.380 853	−0.043 772	−0.000 273	−4.093 348	−3.903 819	−0.189 529
0.200	−4.417 831	−4.374 177	−0.043 381	−0.000 273	−4.082 508	−3.886 078	−0.196 430
0.250	−4.386 788	−4.344 672	−0.041 885	−0.000 231	−4.039 392	−3.814 129	−0.225 263
0.300	−4.362 463	−4.321 356	−0.040 965	−0.000 141	−4.009 873	−3.764 811	−0.245 062
0.400	−4.331 621	−4.291 522	−0.040 144	0.000 045	−3.976 853	−3.711 618	−0.265 234
0.500	−4.321 751	−4.281 903	−0.039 967	0.000 119	−3.967 210	−3.696 814	−0.270 396

TABLE XXII. Same as Table XXI for the off-diagonal elements of $H^{\rm eff}$ (in hartree). We define $\langle (T^{(1)})^k \rangle \equiv (k!)^{-1} \langle \Phi_2 | H (T^{(1)})^k | \Phi_1 \rangle$ and $\langle (T^{(2)})^k \rangle \equiv (k!)^{-1} \langle \Phi_1 | H (T^{(2)})^k | \Phi_2 \rangle$.

α	$H_{12}^{\rm eff}$	H_{12}	$\langle T^{(2)} \rangle$	$\langle (T^{(2)})^2 \rangle$	$H_{21}^{\rm eff}$	H_{21}	$\langle T^{(1)} \rangle$	$\langle (T^{(1)})^2 \rangle$	$\langle (T^{(1)})^3 \rangle$	$\langle (T^{(1)})^4 \rangle$
0.000	0.055 154	0.056 970	−0.003 830	0.002 013	0.055 154	0.056 970	−0.003 830	0.002 013	0.000 000	0.000 000
0.005	0.055 237	0.057 282	−0.004 174	0.002 128	0.055 363	0.057 282	−0.003 942	0.002 023	0.000 000	0.000 000
0.010	0.055 426	0.057 749	−0.004 574	0.002 251	0.055 689	0.057 749	−0.004 099	0.002 039	0.000 000	0.000 000
0.020	0.056 048	0.059 066	−0.005 540	0.002 522	0.056 624	0.059 066	−0.004 533	0.002 092	−0.000 001	0.000 000
0.050	0.058 844	0.064 975	−0.009 688	0.003 558	0.060 688	0.064 975	−0.006 638	0.002 355	−0.000 003	0.000 000
0.100	0.063 069	0.076 690	−0.019 810	0.006 188	0.067 481	0.076 690	−0.012 275	0.003 068	−0.000 003	0.000 000
0.110	0.063 731	0.078 940	−0.022 068	0.006 859	0.068 541	0.078 940	−0.013 649	0.003 252	−0.000 003	0.000 001
0.120	0.064 365	0.081 111	−0.024 315	0.007 569	0.069 484	0.081 111	−0.015 072	0.003 446	−0.000 002	0.000 001
0.130	0.064 991	0.083 194	−0.026 513	0.008 310	0.070 316	0.083 194	−0.016 526	0.003 648	−0.000 001	0.000 001
0.140	0.065 623	0.085 181	−0.028 630	0.009 072	0.071 046	0.085 181	−0.017 989	0.003 853	0.000 000	0.000 001
0.150	0.066 271	0.087 066	−0.030 639	0.009 844	0.071 682	0.087 066	−0.019 445	0.004 059	0.000 001	0.000 001
0.155	0.066 603	0.087 970	−0.031 597	0.010 230	0.071 969	0.087 970	−0.020 165	0.004 161	0.000 001	0.000 002
0.160	0.066 939	0.088 848	−0.032 522	0.010 614	0.072 237	0.088 848	−0.020 876	0.004 262	0.000 002	0.000 002
0.170	0.067 626	0.090 523	−0.034 268	0.011 371	0.072 719	0.090 523	−0.022 269	0.004 460	0.000 002	0.000 002
0.180	0.068 328	0.092 093	−0.035 873	0.012 107	0.073 138	0.092 093	−0.023 612	0.004 651	0.000 003	0.000 002
0.190	0.069 036	0.093 559	−0.037 336	0.012 813	0.073 501	0.093 559	−0.024 897	0.004 833	0.000 004	0.000 003
0.200	0.069 744	0.094 922	−0.038 662	0.013 484	0.073 816	0.094 922	−0.026 119	0.005 005	0.000 005	0.000 003
0.250	0.072 996	0.100 319	−0.043 511	0.016 189	0.074 841	0.100 319	−0.031 188	0.005 700	0.000 007	0.000 004
0.300	0.075 368	0.103 748	−0.046 203	0.017 823	0.075 271	0.103 748	−0.034 633	0.006 145	0.000 006	0.000 005
0.400	0.077 570	0.106 915	−0.048 358	0.019 012	0.075 366	0.106 915	−0.038 108	0.006 551	0.000 002	0.000 005
0.500	0.078 010	0.107 635	−0.048 786	0.019 162	0.075 292	0.107 635	−0.038 991	0.006 643	0.000 001	0.000 005

tude (see Table XX). By observing these highly nonlinear terms we can forecast the breakdown of the L-MRCCSD method very early. Visible differences between the L-MRCCSD and MRCCSD-3 results and a rapid increase of matrix elements $\frac{1}{6}\langle \Phi_2 | H (T^{(1)})^3 | \Phi_1 \rangle$ and $\frac{1}{24}\langle \Phi_2 | H (T^{(1)})^4 | \Phi_1 \rangle$ begin to appear already at $\alpha \approx 0.11$ (cf. Tables XX and XXII).

The presence of cubic and quartic terms in $H_{21}^{\rm eff}$ and their absence in $H_{12}^{\rm eff}$ lead to a large non-Hermiticity of the effective Hamiltonian in the vicinity of L-MRCCSD singularities, which may even lead to complex energies (see Secs. V B and V C). Interestingly enough, the non-Hermiticity of $\mathbf{H}^{\rm eff}$ for a very accurate MRCCSD-3 method also reaches its local maximum in the vicinity of the L-MRCCSD singularity (see Table XXIII). The effective Hamiltonian matrix is nearly Hermitian only in the highly quasidegenerate region, where the interaction of the model-space configurations with those belonging to $\mathcal{M}_0^{\perp}$ is small (cf. Table XXIII).

VII. CLUSTER ANALYSIS OF MRCC WAVE FUNCTIONS

Our models are sufficiently simple so that we are able to carry out an explicit cluster analysis of exact FCI wave functions and thus obtain exact values of cluster amplitudes. Comparing these with the MRCCSD amplitudes we obtain deeper insight into the nature of various MRCCSD-n approximations, since the differences in energy are much less sensitive than those in the wave function. In this way we can also better assess the effectiveness of various MRCCSD-n methods in describing low-lying excited states.

To obtain exact values of cluster amplitudes, we first transform the relevant FCI wave functions into the form required by MRCC theory [see Eq. (28)]. Thus, we consider a group of FCI eigenstates $|\Psi_\mu\rangle$, $\mu=1,\ldots,M$, whose CI expansions have the form

$$|\Psi_\mu\rangle = \sum_{p=1}^{M} d'_{p,\mu} |\Phi_p\rangle + \sum_{j=M+1}^{N_{\rm tot}} d'_{j,\mu} |\Phi_j\rangle \ , \quad (\mu=1,\ldots,M) \ , \tag{113}$$

with M and $N_{\rm tot}$ being the dimensions of $\mathcal{M}_0$ and of the FCI configuration space $\mathcal{M}_0 \oplus \mathcal{M}_0^{\perp}$, and transform them into the functions $|\tilde{\Psi}_p\rangle$, $p=1,\ldots,M$, Eq. (14). In this way [cf. Eq. (15)] we can find the family of excitation operators $\{C^{(p)}\}_{p=1}^{M}$ that is used to define cluster operators $T^{(p)}$, $p=1,\ldots,M$, through the logarithmic relationship (26). We could, of course, compare the FCI expansions (113) directly with the corresponding MRCC expansions (28). However, this would be more cumbersome than to transform first $|\Psi_\mu\rangle$'s into $|\tilde{\Psi}_p\rangle$'s, and subsequently to use Eq. (26).

In the two-reference case considered, we must transform a given pair of FCI eigenstates (not necessarily the lowest-energy states)

$$|\Psi_1\rangle = d'_{1,1}|\Phi_1\rangle + d'_{2,1}|\Phi_2\rangle + \sum_{j=3}^{N_{\rm tot}} d'_{j,1}|\Phi_j\rangle \ , \tag{114}$$

$$|\Psi_2\rangle = d'_{1,2}|\Phi_1\rangle + d'_{2,2}|\Phi_2\rangle + \sum_{j=3}^{N_{\rm tot}} d'_{j,2}|\Phi_j\rangle \ , \tag{115}$$

TABLE XXIII. Comparison of the L-MRCCSD and MRCCSD-3 effective Hamiltonian matrices and their non-Hermiticities, as measured by the difference $H_{21}^{\text{eff}}-H_{12}^{\text{eff}}$, for the MBS H4 model with $a=2.0$ a.u. and various values of α. All numbers, except for the values of α, are in hartree.

	L-MRCCSD					MRCCSD-3				
α	H_{11}^{eff}	H_{22}^{eff}	H_{12}^{eff}	H_{21}^{eff}	$H_{21}^{\text{eff}}-H_{12}^{\text{eff}}$	H_{11}^{eff}	H_{22}^{eff}	H_{12}^{eff}	H_{21}^{eff}	$H_{21}^{\text{eff}}-H_{12}^{\text{eff}}$
0.000	−4.630 173	−4.630 173	0.053 927	0.053 927	0.000 000	−4.627 769	−4.627 769	0.055 154	0.055 154	0.000 000
0.005	−4.622 269	−4.604 625	0.053 868	0.054 113	0.000 245	−4.619 856	−4.602 007	0.055 237	0.055 363	0.000 126
0.010	−4.614 628	−4.579 876	0.053 886	0.054 420	0.000 535	−4.612 206	−4.577 003	0.055 426	0.055 689	0.000 263
0.020	−4.600 051	−4.532 786	0.054 058	0.055 318	0.001 261	−4.597 592	−4.529 240	0.056 048	0.056 624	0.000 576
0.050	−4.560 944	−4.411 439	0.054 075	0.059 024	0.004 948	−4.558 076	−4.403 399	0.058 844	0.060 688	0.001 844
0.100	−4.509 876	−4.297 034	0.039 624	0.061 483	0.021 858	−4.502 419	−4.247 600	0.063 069	0.067 481	0.004 413
0.110	−4.502 788	−4.299 417	0.031 165	0.060 302	0.029 137	−4.492 488	−4.223 655	0.063 731	0.068 541	0.004 810
0.120	−4.498 012	−4.322 827	0.019 277	0.058 534	0.039 256	−4.482 910	−4.201 793	0.064 365	0.069 484	0.005 119
0.130	−4.497 944	−4.390 299	0.005 145	0.058 276	0.053 131	−4.473 670	−4.181 848	0.064 991	0.070 316	0.005 325
0.140	−4.511 703	−4.587 507	0.016 716	0.080 644	0.063 928	−4.464 760	−4.163 648	0.065 623	0.071 046	0.005 422
0.150	−4.632 959	−5.722 593	1.159 837	0.979 589	−0.180 248	−4.456 170	−4.147 027	0.066 271	0.071 682	0.005 411
0.155	−7.615 032	27.954 804	715.030 315	22 549.192 728	21 834.162 413	−4.451 993	−4.139 258	0.066 603	0.071 969	0.005 367
0.160	−4.300 922	−2.450 254	2.601 714	1.234 127	−1.367 587	−4.447 893	−4.131 825	0.066 939	0.072 237	0.005 298
0.170	−4.379 269	−3.442 122	0.608 692	0.301 793	−0.306 899	−4.439 926	−4.117 897	0.067 626	0.072 719	0.005 093
0.180	−4.390 945	−3.634 463	0.370 535	0.201 491	−0.169 044	−4.432 262	−4.105 110	0.068 328	0.073 138	0.004 810
0.190	−4.391 999	−3.708 936	0.286 753	0.167 336	−0.119 416	−4.424 899	−4.093 348	0.069 036	0.073 501	0.004 465
0.200	−4.389 599	−3.744 596	0.245 235	0.150 907	−0.094 328	−4.417 831	−4.082 508	0.069 744	0.073 816	0.004 072
0.250	−4.366 974	−3.780 723	0.179 027	0.126 304	−0.052 723	−4.386 788	−4.039 392	0.072 996	0.074 841	0.001 845
0.300	−4.345 164	−3.772 329	0.161 924	0.120 595	−0.041 330	−4.362 463	−4.009 873	0.075 368	0.075 271	−0.000 097
0.400	−4.316 092	−3.749 129	0.151 696	0.117 905	−0.033 792	−4.331 621	−3.976 853	0.077 570	0.075 366	−0.002 204
0.500	−4.306 601	−3.739 733	0.149 790	0.117 686	−0.032 104	−4.321 751	−3.967 210	0.078 010	0.075 292	−0.002 719

into states $|\tilde{\Psi}_1\rangle$ and $|\tilde{\Psi}_2\rangle$, where [cf. Eqs. (15) and (26)]

$$|\tilde{\Psi}_p\rangle = e^{T^{(p)}}|\Phi_p\rangle, \quad (p=1,2) , \tag{116}$$

are related with $|\Psi_1\rangle$ and $|\Psi_2\rangle$ as follows [cf. Eq. (28)]:

$$|\Psi_\mu\rangle = d'_{1,\mu}|\tilde{\Psi}_1\rangle + d'_{2,\mu}|\tilde{\Psi}_2\rangle, \quad (\mu=1,2) . \tag{117}$$

The required transformation is given by the inverse of the 2×2 matrix

$$\mathbf{D} = \begin{bmatrix} d'_{1,1} & d'_{1,2} \\ d'_{2,1} & d'_{2,2} \end{bmatrix} , \tag{118}$$

with coefficients given by expansions (114) and (115), i.e., by

$$\mathbf{D}^{-1} = \frac{1}{D}\begin{bmatrix} d'_{2,2} & -d'_{1,2} \\ -d'_{2,1} & d'_{1,1} \end{bmatrix} , \tag{119}$$

where $D = \det\mathbf{D}$. We thus get

$$|\tilde{\Psi}_p\rangle = |\Phi_p\rangle + \sum_{j=3}^{N_{\rm tot}} d_{j,p}|\Phi_j\rangle, \quad (p=1,2) , \tag{120}$$

where

$$d_{j,1} = (d'_{j,1}d'_{2,2} - d'_{j,2}d'_{2,1})/D , \tag{121}$$

$$d_{j,2} = (-d'_{j,1}d'_{1,2} + d'_{j,2}d'_{1,1})/D , \tag{122}$$

are the expansion coefficients of $|\tilde{\Psi}_p\rangle$ in terms of states $|\Phi_j\rangle$, $j=3,\ldots,N_{\rm tot}$. Clearly, every state $|\Phi_j\rangle$, $j=3,\ldots,N_{\rm tot}$, may be written in the form

$$|\Phi_j\rangle = {}^{(1)}G_j|\Phi_1\rangle \tag{123}$$

or

$$|\Phi_j\rangle = {}^{(2)}G_{j'}|\Phi_2\rangle , \tag{124}$$

where the excitation operators ${}^{(1)}G_j$, $j=3-12$, are listed in Table IV and ${}^{(2)}G_j$ when acting on $|\Phi_2\rangle$ are given by [cf. Eq. (67)]

$${}^{(2)}G_{j'} = {}^{(1)}G_j\,{}^{(2)}G^{22}_{33}(0) . \tag{125}$$

We can thus cast the transformed FCI wave functions $|\tilde{\Psi}_1\rangle$ and $|\tilde{\Psi}_2\rangle$ into the form of Eq. (15), where

$$C^{(1)} = \sum_{j=3}^{N_{\rm tot}} d_{j,1}\,{}^{(1)}G_j = C_1^{(1)} + C_2^{(1)} + \cdots , \tag{126}$$

$$C^{(2)} = \sum_{j=3}^{N_{\rm tot}} d_{j,2}\,{}^{(2)}G_{j'} = C_1^{(2)} + C_2^{(2)} + \cdots , \tag{127}$$

with $C_i^{(p)}$, $i=1,2,\ldots,$ designating the i-particle component of the excitation operator $C^{(p)}$ relative to the reference $|\Phi_p\rangle$, $p=1,2$. Since the cluster operators $T^{(p)}$ are related with the FCI excitation operators $C^{(p)}$ in exactly the same way as in SRCC theory, Eq. (26), we immediately find the exact cluster amplitudes $\langle\rho|t_1^{(p)}|\alpha\rangle$, $\langle\rho\sigma|t_2^{(p)}|\alpha\beta\rangle_i$, $(i=0,1)$, etc., using the well-known relations

$$T_1^{(p)} = C_1^{(p)} , \tag{128}$$

$$T_2^{(p)} = C_2^{(p)} - \tfrac{1}{2}(C_1^{(p)})^2 , \tag{129}$$

$$T_3^{(p)} = C_3^{(p)} - C_1^{(p)}C_2^{(p)} + \tfrac{1}{3}(C_1^{(p)})^3 , \tag{130}$$

$$T_4^{(p)} = C_4^{(p)} - C_1^{(p)}C_3^{(p)} - \tfrac{1}{2}(C_2^{(p)})^2 + (C_1^{(p)})^2C_2^{(p)} - \tfrac{1}{4}(C_1^{(p)})^4 . \tag{131}$$

Explicit expressions for the cluster amplitudes are given in the Appendix. We shall now compare their exact FCI values with those obtained by various approximations studied in this paper. Note that higher than biexcited amplitudes, which are neglected in our MRCCSD approaches, are listed in Tables X, XII, and XIV.

Comparison of various cluster components for the MBS H4 model with $a=2.0$ a.u. is given in Tables XXIV

TABLE XXIV. Comparison of the exact (FCI) and MRCCSD-n (designated as M-n) amplitudes with respect to $|\Phi_1\rangle$ for the MBS H4 model with $a=2.0$ a.u. and three values of α, corresponding to the quasidegenerate region (0.05), the vicinity of the L-MRCCSD singularity (0.155) and the nondegenerate region (0.5). See Appendix for the definition of cluster amplitudes t_i.

α	Method	t_1	t_2	t_3	t_4	t_5	t_6	t_7
0.050	FCI	−0.121 831	−0.145 114	−0.034 102	−0.163 816	−0.008 764	0.042 327	−0.037 137
	M-1	−0.120 765	−0.144 048	−0.036 381	−0.164 410	−0.010 326	0.047 962	−0.042 370
	M-2	−0.121 012	−0.144 362	−0.034 283	−0.164 246	−0.010 076	0.048 071	−0.042 462
	M-3	−0.121 547	−0.145 029	−0.034 366	−0.163 081	−0.008 799	0.042 456	−0.037 995
0.155	FCI	−0.111 048	−0.147 155	−0.033 219	−0.151 820	0.001 915	0.113 826	−0.080 208
	M-1	−0.108 179	−0.142 369	−0.038 553	−0.156 622	−0.004 872	0.126 984	−0.090 421
	M-2	−0.108 820	−0.143 216	−0.031 746	−0.155 979	−0.004 268	0.127 264	−0.090 711
	M-3	−0.111 574	−0.148 592	−0.032 037	−0.150 224	0.002 993	0.114 473	−0.081 863
0.500	FCI	−0.088 544	−0.178 959	−0.028 746	−0.141 348	0.010 731	0.201 743	−0.076 554
	M-1	−0.086 895	−0.163 740	−0.034 728	−0.150 058	0.000 355	0.222 405	−0.086 908
	M-2	−0.087 772	−0.165 011	−0.022 967	−0.148 690	0.001 064	0.222 117	−0.087 249
	M-3	−0.089 987	−0.181 905	−0.023 459	−0.138 994	0.012 568	0.199 892	−0.078 156

TABLE XXV. Same as Table XXIV for cluster amplitudes associated with $|\Phi_2\rangle$.

α	Method	t_8	t_9	t_{10}	t_{11}	t_{12}	t_{13}	t_{14}	t_{15}	t_{16}
0.050	FCI	0.018 638	−0.128 002	0.021 676	−0.102 618	−0.193 571	−0.033 752	−0.159 577	−0.199 092	0.007 366
	M-1	0.018 181	−0.128 994	0.021 217	−0.103 408	−0.193 707	−0.034 919	−0.159 665	−0.199 505	0.007 198
	M-2	0.018 217	−0.129 074	0.021 224	−0.103 486	−0.193 943	−0.033 777	−0.159 844	−0.199 438	0.007 386
	M-3	0.018 342	−0.128 131	0.021 293	−0.102 826	−0.193 865	−0.033 794	−0.159 782	−0.199 454	0.007 263
0.155	FCI	0.030 634	−0.531 405	0.053 718	−0.359 324	−0.306 270	−0.027 979	−0.223 537	−0.212 579	0.115 177
	M-1	0.032 437	−0.536 904	0.055 057	−0.363 935	−0.313 716	−0.030 971	−0.228 814	−0.219 988	0.114 390
	M-2	0.032 538	−0.537 186	0.055 104	−0.364 172	−0.314 098	−0.029 799	−0.229 075	−0.219 982	0.114 647
	M-3	0.032 866	−0.533 921	0.055 330	−0.362 293	−0.313 622	−0.029 855	−0.228 790	−0.220 015	0.113 940
0.500	FCI	0.007 773	−1.058 944	0.081 087	−0.432 528	−0.465 717	−0.018 659	−0.214 244	−0.196 510	0.222 856
	M-1	0.018 979	−1.051 412	0.086 693	−0.439 950	−0.485 197	−0.026 772	−0.226 759	−0.216 725	0.212 840
	M-2	0.019 101	−1.051 487	0.086 754	−0.440 111	−0.485 604	−0.025 670	−0.226 968	−0.216 766	0.212 973
	M-3	0.019 501	−1.045 909	0.087 145	−0.438 520	−0.484 652	−0.025 693	−0.226 704	−0.216 716	0.211 880

and XXV. Cluster amplitudes resulting from the MRCCSD-n, $n=1,2,3$, calculations are compared with their exact counterparts for three characteristic values of parameter α, namely, for $\alpha=0.05$ (quasidegenerate region), $\alpha=0.155$ (vicinity of the L-MRCCSD singularity), and $\alpha=0.5$ (nondegenerate region). In the quasidegenerate region all three MRCCSD-n methods provide an excellent description of corresponding FCI wave functions. The best results are usually provided by the fully quadratic MRCCSD-3 approach, although the remaining two MRCCSD-n methods give very good results as well. Comparing MRCCSD-3 results with MRCCSD-1 and MRCCSD-2 data indicates that the inclusion of bilinear terms involving $T_1^{(p)}$ clusters definitely improves the description of monoexcited components, both in the quasidegenerate region (cf. values of $\langle 3|t_1^{(1)}|1\rangle$ and $\langle 4|t_1^{(1)}|2\rangle$ for $\alpha=0.05$) and in the vicinity of the L-MRCCSD singularity ($\alpha\approx 0.155$) as well as in the nondegenerate region ($\alpha\approx 0.5$). In a few cases we observe a spectacular improvement when going to the fully quadratic approach. The best example is the amplitude $\langle 34|t_2^{(1)}|12\rangle_1$. MRCCSD-1 and MRCCSD-2 methods provide a rather poor description of this amplitude, especially in the nondegenerate region. For $\alpha=0.155$ they give the wrong sign, while for $\alpha=0.5$ MRCCSD-1 and MRCCSD-2 results are smaller in comparison with FCI value by an order of magnitude. The fully quadratic MRCCSD-3 method corrects these results substantially, yielding the results that are very close to the FCI values.

The amplitudes associated with the second reference $|\Phi_2\rangle$ are rather insensitive to the type of approximation employed, independently of the value of α. As a result, the energy of the second root, to which the second reference primarily contributes, is almost the same in all MRCCSD-n formalisms (cf. Table VIII). There are, however, a few pair-cluster amplitudes associated with this reference, namely $\langle 24|t_2^{(2)}|11\rangle_0$ and $\langle 44|t_2^{(2)}|11\rangle_0$, that are very poorly represented by all three MRCCSD-n approximations in the nondegenerate ($\alpha\approx 0.5$) region. In the case of $\langle 24|t_2^{(2)}|11\rangle_0$, the error of any of the MRCCSD-n result amounts to about 150%, whereas the error for $\langle 44|t_2^{(2)}|11\rangle_0$ is about 40%. The amplitude $\langle 44|t_2^{(2)}|13\rangle_0$ is also poorly represented by all three MRCCSD-n methods in the nondegenerate region (the error for $\alpha=0.5$ is about 7%). For a few other pair-cluster amplitudes associated with $|\Phi_2\rangle$ (i.e., $\langle 44|t_2^{(2)}|33\rangle_0$, $\langle 22|t_2^{(2)}|11\rangle_0$, $\langle 24|t_2^{(2)}|13\rangle_i$, $i=0,1$), the differences between the MRCCSD-n and FCI results are small and do not reduce when going from the simplest MRCCSD-1 approach to the more sophisticated MRCCSD-2 or MRCCSD-3 methods. This is consistent with our earlier observation that the MRCCSD description of the first excited $^1A_1(C_{2v})$ state for the MBS H4 model worsens with increasing α (cf. Sec. V A). For $\alpha=0.5$, the difference between the FCI and MRCCSD-n results is about 7 mhartree, compared to at most 5 μhartree for $\alpha=0$ (Table VIII). As pointed out in Secs. V B and V C, the situation gets even worse when we approach the $\alpha\rightarrow\infty$ limit of the D4 and P4 models. Let us therefore examine how closely various cluster components are approximated by the MRCCSD-n methods in this case.

Comparison of various cluster components for the MBS D4 model with $a=2.0$ a.u. is given in Tables XXVI and XXVII, and for the P4 model with $a=2.0$ a.u. in Table XXVIII. For the D4 model, we do not report the results covering the well-behaved quasidegenerate region ($\alpha<a$), where all three MRCCSD-n approaches provide an excellent description of both states $|\Psi_1\rangle$ and $|\Psi_2\rangle$, since we wish to concentrate on the difficulties encountered by the MRCCSD methods. We thus consider three values of α belonging to the region $\alpha>a$. For the P4 model, we consider four different values of α, including the region of configurational degeneracy ($\alpha=2$ a.u.), the region of orbital degeneracy ($\alpha=1.1428$ a.u.), and two values of α belonging to the nondegenerate $\alpha>a$ region ($\alpha=4$ and 10 a.u.).

Let us first note that in the long-range limit of both models, it is usually the simplest MRCCSD-1 approximation that yields the best results. This is particularly evident for cluster amplitudes associated with reference $|\Phi_1\rangle$ and is slightly surprising in view of the fact that the best energies are provided by the fully quadratic MRCCSD-3 approach (cf. Secs. V B and V C). We must not forget, however, that in this region all three

TABLE XXVI. Same as Table XXIV for the MBS D4 model with $a=2.0$ a.u. and $\alpha=3$, 5, and 8 a.u. Comparison of FCI and MRCCSD-n (designated as M-n) results for amplitudes associated with $|\Phi_1\rangle$. See Appendix for the definition of cluster amplitudes t_i.

α	Method	t_1	t_2	t_3	t_4	t_5	t_6	t_7
3.0	FCI	−0.125 198	−0.191 368	−0.030 996	−0.170 650	0.048 181	0.153 765	−0.064 653
	M-1	−0.125 763	−0.183 975	−0.042 449	−0.176 278	0.043 082	0.158 092	−0.073 699
	M-2	−0.128 198	−0.186 772	−0.016 648	−0.172 658	0.045 087	0.155 201	−0.073 152
	M-3	−0.129 194	−0.194 085	−0.017 078	−0.167 749	0.050 664	0.138 056	−0.064 650
5.0	FCI	−0.161 576	−0.184 015	−0.016 639	−0.180 584	0.081 880	0.054 232	−0.023 137
	M-1	−0.161 631	−0.182 695	−0.047 698	−0.183 220	0.081 223	0.036 852	−0.025 347
	M-2	−0.166 904	−0.188 006	0.010 237	−0.174 533	0.085 032	0.033 516	−0.023 421
	M-3	−0.167 038	−0.188 344	0.010 308	−0.174 247	0.085 430	0.030 680	−0.021 369
8.0	FCI	−0.179 800	−0.181 436	−0.001 269	−0.181 251	0.099 566	0.002 705	−0.002 217
	M-1	−0.177 271	−0.178 919	−0.046 266	−0.184 771	0.097 982	0.000 850	−0.001 035
	M-2	−0.182 974	−0.184 876	0.027 965	−0.172 582	0.101 508	−0.000 065	−0.000 152
	M-3	−0.182 974	−0.184 876	0.027 965	−0.172 582	0.101 508	−0.000 064	−0.000 144

MRCCSD-n methods provide relatively poor energies (especially for the first excited state) and rather poor values of several cluster coefficients, particularly those which are associated with the second reference $|\Phi_2\rangle$ (cf. Tables IX, XI, XXVII, and XXVIII). Recall that the energies of the first excited state for D4 and P4 models are almost identical in all MRCCSD-n approximations (Tables IX and XI) and the $t_2^{(2)}$ amplitudes are also practically independent of the method employed. In the quasidegenerate region, the latter are practically identical with the FCI amplitudes. For $\alpha\rightarrow\infty$, however, the errors for most $t_2^{(2)}$ amplitudes are large. Inclusion of $(T_2^{(p)})^2$ terms in the coupling term or of nonlinear cluster components involving $T_1^{(p)}$ and $T_2^{(p)}$ does not seem to reduce these discrepancies. The $t_2^{(2)}$ amplitudes resulting from various truncation schemes saturate rather than approach exact values. For example, when $\alpha\rightarrow\infty$, the amplitude $\langle 44|t_2^{(2)}|11\rangle_0$ vanishes, whereas its absolute value obtained with MRCCSD formalisms increases with α, so that for the D4 model with $\alpha=8$ a.u. or the P4 model with $\alpha=10$ a.u. all three MRCCSD-n approaches give about (-0.06) to (-0.07) for this amplitude. The FCI value of the amplitude $\langle 24|t_2^{(2)}|13\rangle_1$ for the D4 model with $\alpha=8$ a.u. or the P4 model with $\alpha=10$ a.u. equals about 0.57–0.58, whereas all three MRCCSD-n approaches give about 0.40. Similar discrepancies are observed for the remaining $t_2^{(2)}$ amplitudes for $\alpha>a$. It even happens that all MRCCSD-n approaches give the wrong sign (see $\langle 24|t_2^{(2)}|11\rangle_0$ for the D4 model with $\alpha=3$ and 5 a.u. or $\langle 22|t_2^{(2)}|13\rangle_0$ and $\langle 24|t_2^{(2)}|33\rangle_0$ for the same model with $\alpha=8$ a.u.) or give errors of a few orders of magnitude (e.g., $\langle 24|t_2^{(2)}|11\rangle_0$ and $\langle 24|t_2^{(2)}|33\rangle_0$ for the D4 model with $\alpha=8$ a.u. or $\langle 44|t_2^{(2)}|11\rangle_0$ for the same model with $\alpha=5$ a.u.).

Large errors in $t_2^{(2)}$ amplitudes that result when MRCCSD-n methods are employed explain why the two-reference CCSD method provides a rather poor description of the first excited state in the $\alpha\rightarrow\infty$ limit of D4 and P4 models. We cannot obtain good results for this state when the $T_2^{(2)}$ cluster components are poorly

TABLE XXVII. Same as Table XXVI for cluster amplitudes relative to $|\Phi_2\rangle$.

α	Method	t_8	t_9	t_{10}	t_{11}	t_{12}	t_{13}	t_{14}	t_{15}	t_{16}
3.0	FCI	−0.026 335	−1.157 454	0.084 780	−0.484 518	−0.672 767	−0.006 699	−0.398 988	−0.452 019	0.348 497
	M-1	0.005 423	−1.018 278	0.088 590	−0.473 159	−0.714 515	−0.026 913	−0.436 891	−0.518 664	0.306 393
	M-2	0.005 652	−1.017 357	0.088 613	−0.473 187	−0.715 158	−0.025 601	−0.437 346	−0.518 935	0.306 560
	M-3	0.006 205	−1.014 004	0.089 052	−0.472 155	−0.714 983	−0.025 608	−0.437 302	−0.518 936	0.306 155
5.0	FCI	−0.018 618	−0.546 514	0.040 940	−0.229 161	−0.914 395	−0.000 475	−0.760 113	−0.828 145	0.490 187
	M-1	0.021 092	−0.280 509	0.033 475	−0.195 710	−0.960 162	−0.049 124	−0.812 926	−0.947 206	0.376 823
	M-2	0.021 375	−0.278 411	0.033 446	−0.195 160	−0.961 484	−0.046 634	−0.814 132	−0.948 113	0.376 976
	M-3	0.021 663	−0.277 368	0.033 696	−0.194 694	−0.961 539	−0.046 636	−0.814 185	−0.948 172	0.376 955
8.0	FCI	0.001 141	−0.026 715	0.001 600	−0.024 169	−0.995 202	−0.000 003	−0.981 209	−0.988 146	0.570 557
	M-1	0.008 458	0.007 713	0.007 185	0.003 368	−1.015 767	−0.067 087	−0.998 168	−1.104 432	0.396 070
	M-2	0.008 499	0.008 101	0.007 210	0.003 718	−1.017 064	−0.063 559	−0.999 407	−1.105 380	0.395 917
	M-3	0.008 501	0.008 101	0.007 209	0.003 720	−1.017 064	−0.063 559	−0.999 407	−1.105 380	0.395 917

TABLE XXVIII. Same as Table XXIV for the MBS P4 model with $a=2.0$ a.u. Only nonvanishing amplitudes are given. Four representative values of the parameter α are considered. They cover the region of orbital degeneracy ($\alpha=1.1428$ a.u.), configurational degeneracy ($\alpha=2.0$ a.u.), and the nondegenerate region ($\alpha=4$ and 10 a.u.).

α	Method	t_1	t_2	t_3	t_4	t_5	t_{12}	t_{13}	t_{14}	t_{15}	t_{16}
1.1428	FCI	−0.106 240	−0.169 365	−0.021 600	−0.164 031	−0.035 428	−0.074 129	−0.021 011	−0.054 818	−0.081 440	−0.018 648
	M-1	−0.105 905	−0.168 837	−0.021 690	−0.163 550	−0.035 326	−0.074 044	−0.021 693	−0.054 758	−0.081 487	−0.018 698
	M-2,3	−0.105 920	−0.168 862	−0.021 543	−0.163 542	−0.035 309	−0.074 096	−0.021 074	−0.054 798	−0.081 439	−0.018 661
2.0	FCI	−0.124 560	−0.151 323	−0.031 425	−0.169 155	−0.013 513	−0.151 323	−0.031 425	−0.124 560	−0.169 155	−0.013 513
	M-1	−0.124 381	−0.151 090	−0.032 474	−0.169 169	−0.013 646	−0.151 090	−0.032 474	−0.124 381	−0.169 169	−0.013 646
	M-2,3	−0.124 509	−0.151 257	−0.031 427	−0.169 092	−0.013 512	−0.151 257	−0.031 427	−0.124 509	−0.169 092	−0.013 512
4.0	FCI	−0.163 216	−0.163 569	−0.024 418	−0.177 830	0.058 906	−0.636 675	−0.013 864	−0.596 000	−0.637 160	0.311 420
	M-1	−0.164 514	−0.165 242	−0.044 215	−0.180 636	0.059 962	−0.685 523	−0.033 359	−0.638 167	−0.707 915	0.287 150
	M-2,3	−0.168 135	−0.169 280	−0.009 813	−0.176 538	0.063 318	−0.686 616	−0.031 741	−0.639 109	−0.708 529	0.287 658
10.0	FCI	−0.181 264	−0.181 180	−0.000 082	−0.181 263	0.102 580	−0.998 732	0.000 000	−0.999 055	−0.998 894	0.576 711
	M-1	−0.178 516	−0.178 494	−0.046 242	−0.184 881	0.100 943	−1.018 545	−0.068 953	−1.011 339	−1.115 930	0.397 717
	M-2,3	−0.184 181	−0.184 585	0.029 380	−0.172 407	0.104 506	−1.019 856	−0.065 310	−1.012 566	−1.116 903	0.397 538

described, since $|\Phi_2\rangle$ substantially contributes to it. Small discrepancies found for the $T_i^{(1)}$ components are of much smaller importance, since $|\Phi_1\rangle$ is almost absent from the first excited state of the D4 and P4 models when $\alpha\rightarrow\infty$ (see Secs. V B and V C). We must also remember that we always neglect tetraexcited components. FCI results indicate that this is acceptable for the $t_4^{(1)}$ amplitude, which is never large, but not for $t_4^{(2)}$ (Tables X and XII). It is simply impossible to obtain good results for the first excited state by keeping the dimension of the model space low and simultaneously assuming that $T_4^{(2)}=0$. In particular, we cannot obtain good $t_2^{(2)}$ amplitudes with MRCCSD methods employing a two-dimensional reference space.

Results for the P4 model with $\alpha=2$ a.u. (Table XXVIII) confirm our earlier observation that in the region of strong configurational quasidegeneracy involving $|\Phi_1\rangle$ and $|\Phi_2\rangle$, all two-reference CCSD formalisms employing the latter as model states provide a very accurate description of states $|\Psi_1\rangle$ and $|\Psi_2\rangle$. Interestingly enough, the same may be achieved for rectangular geometries with $\alpha<a$, in spite of the fact that both for $\alpha>a$ and $\alpha<a$ the model states $|\Phi_1\rangle$ and $|\Phi_2\rangle$ practically do not interact [cf. Fig. 9(c) and Table III]. We cannot, however, use the ground-state RHF MO's anymore. An example of such a situation is the P4 model with $\alpha=1.1428$ a.u. To obtain the MRCCSD-n results in this case ($\alpha<a$ in general) we employed MO's associated with configuration $(\phi_1)^2(\phi_2)^2$, although the ground-state RHF configuration for $\alpha<a$ is $(\phi_1)^2(\phi_3)^2$ (cf. Sec. IV). For $\alpha=1.1428$ a.u., active orbitals associated with the configuration $(\phi_1)^2(\phi_2)^2$ become exactly degenerate (cf. Fig. 2). As can be seen from Table XXVIII, this results in a very accurate description of pair clusters by all MRCCSD-n methods. The use of MO's associated with configuration $(\phi_1)^2(\phi_3)^2$ would never lead to quasidegeneracy of active orbitals. This would result in large values of $T_4^{(1)}$ components for $\alpha<a$ and, consequently, in a poor description of the first excited state in this region by all MRCCSD-n methods. The use of MO's associated with configuration $(\phi_1)^2(\phi_2)^2$ yields small values of both $T_4^{(1)}$ and $T_4^{(2)}$ (see Sec. V C), so that CCSD approximation performs well.

Cluster analysis of the two lowest-lying states of ${}^1A_g(D_{2h})$ symmetry for the MBS S4 model (see Table XXIX) clearly indicates that the CCSD approximation is adequate only in the region of small α's. For $\alpha\geq 4$ a.u., pair-cluster amplitudes are poorly represented by MRCCSD-n methods (in practically all cases, the corresponding errors relative to the FCI data exceed 15%; cf. Table XXIX), and the errors increase with α. Consequently, all MRCCSD-n methods fail for large α values. In fact (Sec. V D) all three MRCCSD-n approaches are plagued with singularities (most likely, algebraic branch points) in this region. The MRCCSD-1 approach becomes singular at $\alpha=6.4682$ a.u., while the singularity for the MRCCSD-2,3 method appears at $\alpha=4.9356$ a.u. Analytical continuation of the MRCCSD-n solutions beyond these critical points along the real axis α is not possible (see Fig. 7). This is related with the increasing role of $T_4^{(p)}$ clusters, since both $T_4^{(1)}$ and $T_4^{(2)}$ are large when $\alpha\rightarrow\infty$ (see Table XIV).

VIII. HIGHER EXCITED STATES

So far, our cluster analysis (see Appendix) was restricted to the lowest-energy states $|\Psi_1\rangle$ and $|\Psi_2\rangle$, although it applies to any pair of FCI eigenstates $|\Psi_\mu\rangle$ and $|\Psi_\nu\rangle$, provided that we use the SU cluster Ansatz and two-dimensional model space $\mathcal{M}_0=\text{span}\{|\Phi_1\rangle,|\Phi_2\rangle\}$. The resulting amplitudes may also be employed as a starting approximation in MRCCSD calculations to obtain various multiple solutions.

The question of whether or not the solutions obtained in this way describe the excited states arises. We must not forget that MRCCSD equations must possess a multitude of various solutions, some of which may not represent physically meaningful eigenstates (cf., Ref.

TABLE XXIX. Same as Tables XXIV–XXVIII for the MBS S4 model. We employed the fact that the pair-cluster coefficients for the MBS S4 model satisfy relations (111). See Appendix for the definition of cluster amplitudes t_i. For $\alpha=6$ a.u., MRCCSD-2,3 results are not available due to the appearance of a singularity at $\alpha=4.9356$ a.u.

α	Method	$t_1=t_{14}$	$t_2=t_{12}$	$t_3=t_{13}$	$t_4=t_{15}$	$t_5=t_{16}$
1.0	FCI	−0.037 961	−0.071 492	−0.012 833	−0.064 919	−0.028 822
	M-1	−0.037 945	−0.071 465	−0.012 883	−0.064 901	−0.028 815
	M-2,3	−0.037 947	−0.071 469	−0.012 833	−0.064 898	−0.028 813
2.0	FCI	−0.124 560	−0.151 323	−0.031 425	−0.169 155	−0.013 513
	M-1	−0.124 381	−0.151 090	−0.032 474	−0.169 169	−0.013 646
	M-2,3	−0.124 509	−0.151 257	−0.031 427	−0.169 092	−0.013 512
4.0	FCI	−0.614 498	−0.585 117	−0.013 932	−0.609 064	0.325 199
	M-1	−0.712 923	−0.690 927	−0.059 193	−0.726 379	0.356 756
	M-2,3	−0.736 591	−0.716 346	−0.007 029	−0.736 114	0.374 718
6.0	FCI	−0.907 132	−0.898 419	−0.000 262	−0.902 908	0.520 558
	M-1	−1.397 826	−1.405 627	−0.202 815	−1.391 948	0.748 160

[63]). The fact that MRCCSD equations possess multiple solutions is a consequence of their nonlinear character and in general it may be difficult to associate a given solution with one of the $\{|\Psi_\mu\rangle,|\Psi_\nu\rangle\}$ pairs. On the other hand, we have already found MRCCSD solutions matching the ground and the second excited states for H4 and D4 models. Actually, even the simplest L-MRCCSD method has the ability to approximate successively higher excited states (cf. Sec. V, especially Figs. 4–6). This suggests that nonlinear MRCCSD equations should also possess this capacity.

Using exact cluster amplitudes obtained by cluster analysis of FCI wave functions as an initial guess in MRCCSD calculations is the best way to verify whether a given pair of FCI eigenstates can be described by one of the MRCCSD solutions. If such a solution is found, we can employ our analytic continuation procedure to determine the region of its existence. Of course, the Newton-Raphson scheme may converge to a nonphysical solution or give a solution that matches some other pair of states than the one initially considered. Should this occur, or should no convergence be achieved, it is very likely that a given pair of FCI eigenstates cannot be described with reasonable accuracy by the two-reference MRCCSD formalism considered.

In the case of models considered in this study, and perhaps in general, it is rather unlikely that the MRCCSD formalism employing the two-dimensional model space span$\{|\Phi_1\rangle,|\Phi_2\rangle\}$, where $|\Phi_1\rangle$ or $|\Phi_2\rangle$ represents the ground-state RHF wave function, is capable of describing pairs of excited states, i.e., pairs other than those involving the ground-state wave function $|\Psi_1\rangle$. Participation of the model-space configurations $|\Phi_1\rangle$ and $|\Phi_2\rangle$ in FCI expansions of highly excited states is usually too small to assure the convergence of the Newton-Raphson scheme. It may happen, however, that a substantial participation of $|\Phi_1\rangle$ in the FCI expansion of the ground state is accompanied by a large participation of $|\Phi_2\rangle$ in the FCI expansion of one of the highly excited states. This is illustrated in Table XXX for the MBS D4 model with $a=2$ a.u. It is seen that for larger distances α, the weight of $|\Phi_2\rangle$ in the FCI expansion of the fifth excited state $|\Psi_6\rangle$ is substantial. In this region, the maximal value of the corresponding coefficient $d'_{2,6}$ is almost 0.7 and for $\alpha\geq 5$ a.u. the coefficient $d'_{2,6}$ is larger than 0.5. Contribution of $|\Phi_1\rangle$ is much smaller, but we must remember that $|\Phi_1\rangle$ is a dominant configuration in the FCI expansion of the ground-state wave function $|\Psi_1\rangle$. Cluster analysis of a pair $|\Psi_1\rangle$ and $|\Psi_6\rangle$ indicates a negligible role of $T_3^{(p)}$ clusters (except for $\alpha\approx 1$ a.u.). In fact, $T_4^{(p)}$ clusters are far more important (see Table XXX), particularly the $T_4^{(2)}$ component. Notice, however, that for $\alpha\approx 3-4$ a.u. and $\alpha>8$ a.u. the weight of pair clusters in the many-body expansion of $T^{(2)}$ (as measured by the sum of squares of cluster amplitudes $\langle\rho\sigma|t_2^{(2)}|\alpha\beta\rangle_i$) is visibly larger than that of $T_4^{(2)}$ clusters, even though the latter are not negligible. This suggests that our two-reference CCSD formalism should provide a reasonable description of the pair of states $|\Psi_1\rangle$ and $|\Psi_6\rangle$ for $\alpha\geq 3$ a.u. Slightly less reliable results may be expected for $\alpha\approx 5-8$ a.u., where $T_4^{(2)}$ clusters become large, but this should not lead to the total breakdown of the MRCCSD formalism (cf. the results for the first excited state of D4 and P4 models when $\alpha\rightarrow\infty$, where a similar situation occurs). We can expect, however, that this description cannot be continued into the $\alpha\leq 2$ a.u. region, where our model space is insufficient to describe a pair $\{|\Psi_1\rangle,|\Psi_6\rangle\}$. Indeed, the $T_3^{(p)}$ and $T_4^{(p)}$ components become very large, so that the simple CCSD approximation must fail.

This is precisely what we find when we perform MRCCSD-3 calculations using one- and two-body cluster components obtained by cluster analysis of the pair of

FCI functions $\{|\Psi_1\rangle,|\Psi_6\rangle\}$ for $\alpha=8$ a.u. The Newton-Raphson procedure converges to a solution that almost perfectly matches the ground and the fifth excited states. Carefully continuing this solution towards smaller α values, we obtain energies shown in Fig. 10. As expected, we are unable to proceed much beyond $\alpha\approx 3$ a.u. since at $\alpha=2.4623$ a.u. the Newton-Raphson procedure fails to converge. Even the use of very small steps $\Delta\alpha$ does not help, which indicates that the point $\alpha=2.4623$ a.u. represents a branch-point singularity, beyond which further continuation along the real α axis is impossible. Nonetheless, the MRCCSD-3 method provides us with a very good description of the pair of states $|\Psi_1\rangle$ and $|\Psi_6\rangle$. The second root of $\mathbf{H}^{\text{eff}}$ yields an excellent approximation to the energy of the fifth excited state of $^1\Sigma_g^+$ symmetry over a broad range of geometries. For $\alpha\approx 3$–4 a.u., the error is less than 2 mhartree (for $\alpha=3.3$ a.u. it equals about 0.4 mhartree). For $\alpha\approx 5$–8 a.u., the error is slightly larger (up to 12 mhartree), but overall agreement with FCI results is very good. Interestingly enough, the energy of the ground state is now better approximated by the

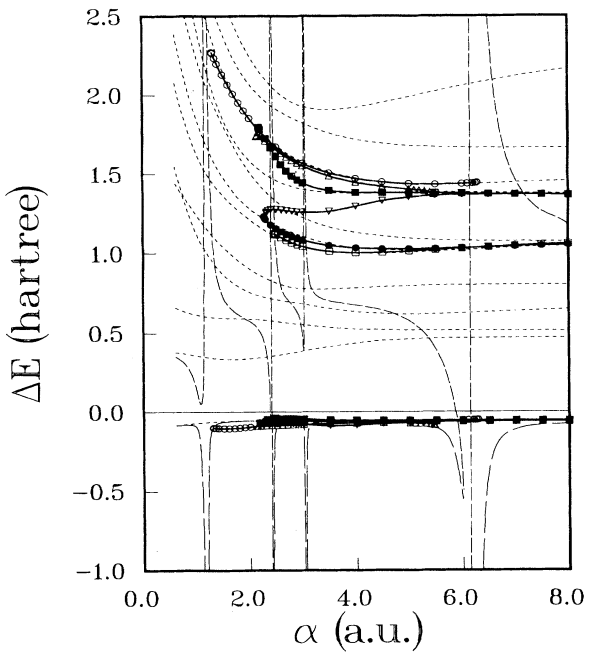

FIG. 10. Multiple solutions of MRCCSD-3 equations for MBS D4 model with $a=2.0$ a.u. Various MRCCSD-3 energies (thick solid lines) are compared with FCI energies (dotted lines) and results of L-MRCCSD calculations (long- and short-dashed lines). All energies (in hartrees) are calculated relative to the ground-state RHF energy. Five different solutions of the MRCCSD-3 system are displayed. Each solution describes the ground state and one of the excited states. Solution $\mathbf{t}_{1-6}(\alpha)$ describing $|\Psi_1\rangle$ and $|\Psi_6\rangle$ is represented by open squares (□), and $\mathbf{t}_{1-7}(\alpha)$ describing $|\Psi_1\rangle$ and $|\Psi_7\rangle$ by solid circles (●). Solid squares (■) and open triangles (▽) represent two different solutions [$\mathbf{t}_{1-9a}(\alpha)$ and $\mathbf{t}_{1-9b}(\alpha)$, respectively] describing the pair $\{|\Psi_1\rangle,|\Psi_9\rangle\}$. Two solutions describing $|\Psi_1\rangle$ and $|\Psi_{10}\rangle$ [$\mathbf{t}_{1-10a}(\alpha)$ and $\mathbf{t}_{1-10b}(\alpha)$, respectively] are represented by open circles (○) and open triangles (△).

TABLE XXX. The weights of reference configurations $|\Phi_1\rangle$ and $|\Phi_2\rangle$ in the FCI expansion of the fifth excited state $|\Psi_6\rangle$ and results of the cluster analysis (see Appendix) for a pair $|\Psi_1\rangle$ and $|\Psi_6\rangle$ for the MBS D4 model with $a=2.0$ a.u. and various values of the parameter α (in a.u.). We list the FCI expansion coefficients $d'_{1,6}$ and $d'_{2,6}$ and compare the triexcited and tetraexcited cluster amplitudes characterizing the pair $\{|\Psi_1\rangle,|\Psi_6\rangle\}$ with the total contribution of monoexcited and biexcited cluster components $T_1^{(p)}$ and $T_2^{(p)}$. The weight of $T_1^{(p)}$ and $T_2^{(p)}$ clusters is measured by the sum of squares of the corresponding amplitudes $\langle\rho|t_1^{(p)}|\alpha\rangle$ and $\langle\rho\sigma|t_2^{(p)}|\alpha\beta\rangle_i$ ($\sum_{i=1}^{7}t_1^2$ for the first reference and $\sum_{i=8}^{16}t_1^2$ for the second reference; cf. Table V).

α	1.0	2.0	3.0	4.0	5.0	6.0	7.0	8.0
$d'_{1,6}$	0.052	0.078	0.048	0.047	0.040	0.024	0.010	0.004
$d'_{2,6}$	−0.100	−0.170	−0.215	−0.381	−0.589	−0.691	−0.673	−0.633
$(\sum_{i=1}^{7}t_1^2)^{1/2}$	3.929 860	1.378 679	0.698 801	0.405 547	0.323 323	0.299 374	0.294 214	0.295 061
$(\sum_{i=8}^{16}t_1^2)^{1/2}$	12.206 876	6.271 063	4.506 075	2.204 529	0.953 918	0.381 650	0.505 720	0.730 027
t_{17}	3.054 614	−0.073 250	−0.004 521	−0.003 561	0.004 685	0.004 760	0.004 169	0.003 471
t_{18}	−0.565 844	0.088 439	−0.026 788	−0.013 029	−0.008 503	−0.006 206	−0.004 924	−0.004 080
t_{19}	−6.147 757	−0.540 185	0.042 655	0.020 942	0.010 471	0.008 568	0.009 133	0.010 218
t_{20}	−56.436 206	−16.268 972	−0.503 711	−0.631 691	−1.072 883	−1.050 929	−0.891 333	−0.730 131

lowest root of $\mathbf{H}^{\text{eff}}$ than in the case of a solution matching $|\Psi_1\rangle$ and $|\Psi_2\rangle$ (see Table IX; for $\alpha \geq 5$ a.u. the error does not exceed ~ 0.7 mhartree compared to 4.109 mhartree for $\alpha = 5$ a.u., 4.722 mhartree for $\alpha = 6$ a.u., or 5.257 mhartree for $\alpha = 8$ a.u. in the case of a solution matching the $\{|\Psi_1\rangle, |\Psi_2\rangle\}$ pair, see Sec. V B).

The possibility of obtaining the fifth excited state in simple two-reference CCSD calculations for the D4 model suggests that other solutions of nonlinear MRCCSD equations describe other pairs of FCI states. Because of our choice of model space, all these pairs should involve the ground state $|\Psi_1\rangle$. The knowledge of the FCI wave functions is certainly very helpful here, since we can simply employ the exact cluster amplitudes corresponding to a given pair $\{|\Psi_1\rangle, |\Psi_\mu\rangle\}$, $\mu \geq 2$, as an initial approximation in MRCCSD calculations. In the case of the D4 model, we were able to obtain five other solutions of MRCCSD-3 equations, describing $|\Psi_1\rangle$ and $|\Psi_7\rangle$, $|\Psi_9\rangle$ and $|\Psi_{10}\rangle$ (see Fig. 10). In the case of the solution $\mathbf{t}_{1-7}(\alpha)$ describing $|\Psi_1\rangle$ and $|\Psi_7\rangle$, and two solutions matching $|\Psi_1\rangle$ and $|\Psi_9\rangle$, which we designate as $\mathbf{t}_{1-9a}(\alpha)$ and $\mathbf{t}_{1-9b}(\alpha)$, we started from $\alpha = 8$ a.u. Then, we employed an analytic continuation procedure toward smaller values of α. In case of two solutions describing $|\Psi_1\rangle$ and $|\Psi_{10}\rangle$, labeled as $\mathbf{t}_{1-10a}(\alpha)$ and $\mathbf{t}_{1-10b}(\alpha)$, we started from $\alpha = 2$ and 4 a.u., respectively, and then employed an analytic continuation towards both $\alpha \rightarrow 0$ and $\alpha \rightarrow \infty$ limits. All five solutions exist over a broad range of geometries. Solutions $\mathbf{t}_{1-7}(\alpha)$, $\mathbf{t}_{1-9a}(\alpha)$, and $\mathbf{t}_{1-9b}(\alpha)$ seem to have branch-point singularities only in the short-range region (at $\alpha = 2.2697$, 2.1763, and 2.3148 a.u., respectively). Solutions $\mathbf{t}_{1-10a}(\alpha)$ and $\mathbf{t}_{1-10b}(\alpha)$ have branch-point singularities in short- and long-range regions. Solution $\mathbf{t}_{1-10a}(\alpha)$ is nonsingular for 1.3006 a.u. $\leq \alpha \leq$ 6.2835 a.u., whereas the solution $\mathbf{t}_{1-10b}(\alpha)$ is nonsingular for 2.1312 a.u. $\leq \alpha \leq$ 5.4715 a.u.

Description of the sixth excited state by the solution $\mathbf{t}_{1-7}(\alpha)$ and description of the ninth excited state by the solution $\mathbf{t}_{1-10a}(\alpha)$ is so good that it is hard to distinguish between the corresponding MRCCSD-3 and FCI energy curves in Fig. 10 [for $\alpha > 1.6$ a.u., i.e., over almost the entire range of existence $\mathbf{t}_{1-10a}(\alpha)$, the error in the energy of $|\Psi_{10}\rangle$ is smaller than 12 mhartree; for 4.3 a.u. $< \alpha <$ 5.9 a.u. it is smaller than 2 mhartree]. The same holds for the solution $\mathbf{t}_{1-9a}(\alpha)$, which almost perfectly describes the eighth excited state (for $\alpha > 3.5$ a.u., the error does not exceed 10 mhartree). Only solutions $\mathbf{t}_{1-9b}(\alpha)$ and $\mathbf{t}_{1-10b}(\alpha)$ provide poorer results.

Existence of solutions describing $|\Psi_7\rangle$, $|\Psi_9\rangle$, and $|\Psi_{10}\rangle$ (particularly $|\Psi_9\rangle$ and $|\Psi_{10}\rangle$), and good MRCCSD energies obtained for these states, are rather surprising. The weights of reference configurations $|\Phi_1\rangle$ and $|\Phi_2\rangle$ in the FCI expansions of these states are rather small, so that normally we would expect poor results or serious convergence problems. The corresponding solutions are, however, nonsingular over large regions of α values, indicating that the MRCCSD formalism has a much larger potential than one might expect solely on the basis of standard solutions.

We can thus conclude that, in principle, the nonlinear MRCCSD formalism may yield information about a significant part of the electronic energy spectrum even when a small reference space is employed. In case of the MBS D4 model, we were able to find as many as eight different solutions of the MRCCSD equations that describe seven different eigenstates of $^1\Sigma_g^+$ symmetry. Two solutions discussed in Sec. V B provided us with information about three lowest eigenstates $|\Psi_1\rangle$, $|\Psi_2\rangle$, and $|\Psi_3\rangle$, whereas the six solutions discussed in this section yielded the ground state $|\Psi_1\rangle$ and very good approximations for $|\Psi_6\rangle$, $|\Psi_7\rangle$, $|\Psi_9\rangle$, and $|\Psi_{10}\rangle$. Multiple solutions were also found for the H4 and P4 models. As in the case of the D4 model, each solution describes the ground and one of the excited states.

IX. SUMMARY AND DISCUSSION

In this paper we applied four different variants of the MRCCSD formalism to simple model systems consisting of four interacting hydrogen atoms in various geometrical arrangements. We focused our attention on four planar models in which the extent of quasidegeneracy of the ground state could be continuously varied from exact degeneracy to nondegenerate cases or cases of heavy mixing of orbital and configurational degeneracies. For all quasidegenerate systems that we examined, the ground-state electronic wave function is dominated by two closed-shell-type configurations involving two active orbitals of different spatial symmetry. We were thus able to exploit our orthogonally-spin-adapted formulation of the Hilbert-space MRCC theory that employs a two-dimensional model space spanned by closed-shell-type references [23,26,29].

One of the aims of the present study was to assess the importance of various nonlinear terms. We were particularly interested in the effect of the bilinear terms involving singly excited clusters and the role played by bilinear coupling terms. Thus, together with the linear approximation, in which all nonlinear terms are neglected, we examined three nonlinear MRCCSD theories, which represent different approximations to the fully quadratic MRCCSD-3 approach. Linear approximation was shown to be reliable only in quasidegenerate situations. In nondegenerate cases or cases of heavy mixing of orbital and configurational degeneracies, the linear MRCCSD formalism suffers from singular behavior. We showed that these singularities will appear whenever the energies of the low-lying excited configurations become close to energies of the reference configurations. Proximity of these energies results in a strong interaction of model states with states outside $\mathcal{M}_0$ and this leads to singular behavior of the L-MRCCSD coefficient matrix. We showed simple diagnostics for the occurrence of singularities based on the behavior of diagonal CI matrix elements. We also showed that in the region of singular behavior, the effective Hamiltonian matrix becomes strongly non-Hermitian, so that L-MRCCSD theory may even fail to yield real energies. This distinguishes the linear MR formalism from the SR one, which may become singular, but never yields complex energies.

As in the SR case, inclusion of nonlinear terms eliminates singular behavior of the L-MRCCSD approxima-

tion. Remarkably enough, it is sufficient to include the coupled-pair clusters $(T_2^{(p)})^2$ in the direct term to obtain a nonsingular and highly accurate formalism. Inclusion of these clusters in the coupling term, as well as inclusion of bilinear components involving singly excited clusters, usually further improves the results. In quasidegenerate situations, all nonlinear MRCCSD methods provide a very accurate description for both energies and wave functions. Surprisingly enough, the two-reference CCSD approach is capable of providing quite a realistic description of potential-energy surfaces even when dissociation of two chemical bonds is involved. As the nondegenerate limit is approached, nonlinear MRCCSD results deteriorate, but description of the ground-state electronic wave function remains satisfactory. Description of the first excited state is often quantitatively poor, but can still provide valuable information about the approximate shape of the corresponding potential-energy surface. In nondegenerate cases, or cases of heavy mixing of orbital and configurational degeneracies, the two-dimensional model space is too small to describe the low-lying states. When the model space is adequate for the ground state, but not rich enough to approximate the first excited state, only results for the latter become poor. This happens in nondegenerate cases, where the ground state is well described by the SRCC theory.

When a simultaneous breaking of several chemical bonds is examined, neither the ground nor the first excited state are adequately represented by the two-dimensional reference space. Consequently, the two-reference CCSD formalism yields equally poor results for the ground and the first excited states. We also found that despite its nonlinear and multireference character, it may suffer from singular behavior, which is similar in nature to the behavior of the SRCCD or SRCCSDT methods in highly degenerate situations [60–63]. Thus when the model space used cannot adequately describe the simultaneous breaking of several chemical bonds, algebraic branch points will occur beyond which the MRCCSD equations cease to possess real, physically meaningful, solutions. In all these cases, orbital and configurational degeneracies are heavily mixed and numerous configurations interact very strongly, so that we must either increase the dimension of the model space (an impractical solution) or go beyond the CCSD approximation. Cluster analysis of FCI wave functions indicates a rapid increase in the importance of the connected tetraexcited clusters. Thus if we wish to preserve a small dimension for the reference space, we have to include connected quadruply excited clusters in the MRCC equations. This seems to be the only method to obtain a highly accurate and nonsingular formalism in all regions of nuclear coordinate space. Inclusion of connected quadruply excited clusters (particularly those associated with the second reference) should essentially improve the MRCC results in nondegenerate situations. In particular, we should obtain a much better description of the potential-energy surface for the first excited state (other excited states should also be better represented). It is thus worthwhile to examine the possibility of extending the well-known approximate methods of accounting for connected quadruply excited clusters [ACPQ [77], ACP-D45 (approximate coupled pair method considering interaction diagrams that are separable over the hole lines, i.e., the fourth and fifth Brandow diagrams of Refs. [37,67,68,77]), also referred to as ACCD (approximate CCD [78])], or similar methods that proved to be useful in SR situations [e.g., ACP-D14 (ACP considering the first and fourth Brandow diagrams, see Ref. [71])], to the MR case. We also hope to address the role of semi-internal triexcited and tetraexcited configurations that are singly or doubly excited with respect to the other reference [23]. It would be instructive to account for them at least at the linear level of approximation [23]. Some of these studies are already in progress and the results will be presented elsewhere [80].

Another possibility is to employ different types of MO bases. We have seen that the use of the MO's associated with configuration $(\phi_1)^2(\phi_2)^2$ for the MBS P4 model with $\alpha < a$, where the ground-state RHF configuration is $(\phi_1)^2(\phi_3)^2$, leads to excellent results even when the ground-state electronic wave function possesses an evidently nondegenerate (single-reference) character. This is a consequence of the fact that this particular choice of the MO basis leads to quasidegeneracy of active orbitals and to very small values of the connected tetraexcited clusters in the nondegenerate region. This example shows that with appropriate orbital choice, the two-reference CCSD formalism may give a highly accurate result even in the region where it should give a poor description (at least for the first excited state). It would thus be instructive to examine other types of MO bases. This would correspond to the exploitation of various shifting techniques of one-electron levels in MR many-body perturbation-theory (MBPT) calculations, which extends the range of the applicability of the MR MBPT formalism for nondegenerate situations [42].

Finally, we have found that multiple solutions of nonlinear MRCCSD equations are capable of describing various pairs of states, as long as they contain a significant contribution from reference configurations. Actually, the weight of reference configurations in the FCI wave function of one of the two states can be relatively small and we can still obtain a convergent MRCC solution. This means that we can recover a large part of the electronic energy spectrum of a given molecular system without changing the model space. All the necessary information can be extracted from a single system of equations. Clearly, a great deal of numerical experience is needed to turn this observation into a practical method. The problem of a choice of an initial approximation, when highly accurate CI results are not available, is just an example of the potential difficulties.

Other problems, like examples of the Hamiltonian symmetry breaking by MRCC formalisms due to a wrong choice of the model space will be described in future work [36], where we shall examine three-dimensional models of the H_4 molecular cluster.

ACKNOWLEDGMENTS

Continued support by NSERC (J.P.) and by Grant No. BST 421/23 (B.J.) are gratefully acknowledged. One of

us (P.P) would like to express his sincere gratitude to Professor J. Paldus for his hospitality, thoughtfulness, and numerous helpful discussions during his stay in the Department of Applied Mathematics of the University of Waterloo.

APPENDIX: EXPLICIT EXPRESSIONS FOR CLUSTER ANALYSIS

Using the relations (126)–(131) together with Eqs. (121) and (122), we find the following explicit expressions for the monoexcited and biexcited cluster amplitudes

$$t_1 \equiv \langle 44|t_2^{(1)}|22\rangle_0 = d_{3,1} - \tfrac{1}{2}d_{9,1}^2 \ , \tag{A1}$$

$$t_2 \equiv \langle 33|t_2^{(1)}|11\rangle_0 = d_{4,1} - \tfrac{1}{2}d_{8,1}^2 \ , \tag{A2}$$

$$t_3 \equiv \langle 44|t_2^{(1)}|11\rangle_0 = d_{5,1} \ , \tag{A3}$$

$$t_4 \equiv \langle 34|t_2^{(1)}|12\rangle_0 = d_{6,1} - \tfrac{1}{2}d_{8,1}d_{9,1} \ , \tag{A4}$$

$$t_5 \equiv \langle 34|t_2^{(1)}|12\rangle_1 = d_{7,1} - \frac{\sqrt{3}}{2}d_{8,1}d_{9,1} \ , \tag{A5}$$

$$t_6 \equiv \langle 3|t_1^{(1)}|1\rangle = d_{8,1} \ , \tag{A6}$$

$$t_7 \equiv \langle 4|t_1^{(1)}|2\rangle = d_{9,1} \ , \tag{A7}$$

$$t_8 \equiv \langle 24|t_2^{(2)}|11\rangle_0 = d_{11,2} \ , \tag{A8}$$

$$t_9 \equiv \langle 22|t_2^{(2)}|13\rangle_0 = -d_{8,2} \ , \tag{A9}$$

$$t_{10} \equiv \langle 44|t_2^{(2)}|13\rangle_0 = -d_{10,2} \ , \tag{A10}$$

$$t_{11} \equiv \langle 24|t_2^{(2)}|33\rangle_0 = d_{9,2} \ , \tag{A11}$$

$$t_{12} \equiv \langle 22|t_2^{(2)}|11\rangle_0 = d_{4,2} \ , \tag{A12}$$

$$t_{13} \equiv \langle 44|t_2^{(2)}|11\rangle_0 = d_{12,2} \ , \tag{A13}$$

$$t_{14} \equiv \langle 44|t_2^{(2)}|33\rangle_0 = d_{3,2} \ , \tag{A14}$$

$$t_{15} \equiv \langle 24|t_2^{(2)}|13\rangle_0 = -\tfrac{1}{2}d_{6,2} - \frac{\sqrt{3}}{2}d_{7,2} \ , \tag{A15}$$

$$t_{16} \equiv \langle 24|t_2^{(2)}|13\rangle_1 = -\frac{\sqrt{3}}{2}d_{6,2} + \tfrac{1}{2}d_{7,2} \ . \tag{A16}$$

Here we employed the labeling of states given in Table IV [so that, for example, $d_{3,p}$ is the coefficient at $|\Phi_3\rangle = {}^{(1)}G_{22}^{44}(0)|\Phi_1\rangle$ in the FCI expansion of $|\tilde{\Psi}_p\rangle$, Eq. (120)], and the labeling of monoexcited and biexcited clusters introduced in Table V.

As explained in Sec. V B, the twofold symmetry, common to all our H_4 models, reduces the number of independent triexcited and tetraexcited cluster coefficients to four orthogonally-spin-adapted amplitudes

$$\langle 443|t_3^{(1)}|221\rangle_{0,0,1/2} \equiv \langle t_3^{(1)}\rangle_1 \ ,$$

$$\langle 334|t_3^{(1)}|112\rangle_{0,0,1/2} \equiv \langle t_3^{(1)}\rangle_2 \ ,$$

$$\langle 3344|t_4^{(1)}|1122\rangle_{0,0,0,0,0} \equiv \langle t_4^{(1)}\rangle \ ,$$

and

$$\langle 2244|t_4^{(2)}|1133\rangle_{0,0,0,0,0} \equiv \langle t_4^{(2)}\rangle \ .$$

After straightforward but lengthy manipulations, we find the following explicit expressions for these amplitudes in terms of the transformed FCI coefficients $d_{j,\mu}$:

$$t_{17} \equiv \langle t_3^{(1)}\rangle_1 = d_{10,1} - t_1t_6 - \tfrac{1}{2}t_4t_7 - \frac{\sqrt{3}}{2}t_5t_7 - \tfrac{1}{2}t_6t_7^2 \ , \tag{A17}$$

$$t_{18} \equiv \langle t_3^{(1)}\rangle_2 = d_{11,1} - t_2t_7 - \tfrac{1}{2}t_4t_6 - \frac{\sqrt{3}}{2}t_5t_6 - \tfrac{1}{2}t_6^2t_7 \ , \tag{A18}$$

$$\begin{aligned} t_{19} \equiv \langle t_4^{(1)}\rangle = {} & d_{12,1} - t_1t_2 - \tfrac{1}{2}(t_4^2 + t_5^2) - t_6t_{17} - t_7t_{18} \\ & - \tfrac{1}{2}t_1t_6^2 - \tfrac{1}{2}t_2t_7^2 - \tfrac{1}{2}t_4t_6t_7 \\ & - \frac{\sqrt{3}}{2}t_5t_6t_7 - \tfrac{1}{4}t_6^2t_7^2 \ , \end{aligned} \tag{A19}$$

$$t_{20} \equiv \langle t_4^{(2)}\rangle = d_{5,2} - t_{12}t_{14} - \tfrac{1}{2}(t_{15}^2 + t_{16}^2) + t_8t_{11} + t_9t_{10} \ , \tag{A20}$$

where t_I, $I = 1-16$, are given by Eqs. (A1)–(A16). General equations (A1)–(A20) simplify when we study the P4 and S4 models. In this case (cf. Tables IV and V),

$$d_{8,\mu} = d_{9,\mu} = d_{10,\mu} = d_{11,\mu} = 0 \ , \tag{A21}$$

so that

$$t_6 = t_7 = t_8 = t_9 = t_{10} = t_{11} = t_{17} = t_{18} = 0 \ . \tag{A22}$$

For the highly symmetric S4 model, pair and tetraexcited cluster amplitudes satisfy additional relations (111) and (112), which reduce the number of independent cluster coefficients to six (cf. Sec. V D for details).

[1] J. Čížek, J. Chem. Phys. **45**, 4256 (1966); Adv. Chem. Phys. **14**, 35 (1969); J. Čížek and J. Paldus, Int. J. Quantum Chem. **5**, 359 (1971).

[2] J. Paldus, J. Čížek, and I. Shavitt, Phys. Rev. A **5**, 50 (1972).

[3] J. Paldus, J. Chem. Phys. **67**, 303 (1977); B. G. Adams and J. Paldus, Phys. Rev. A **20**, 1 (1979).

[4] J. Paldus, J. Čížek, and B. Jeziorski, J. Chem. Phys. **90**, 4356 (1989).

[5] R. J. Bartlett, Ann. Rev. Phys. Chem. **32**, 359 (1981).

[6] J. Paldus, *Diagrammatic Methods for Many-Fermion Systems* (University of Nijmegen, Holland, 1981).

[7] J. Paldus, in *New Horizons of Quantum Chemistry*, edited by P.-O. Löwdin and B. Pullman (Reidel, Dordrecht, 1983), pp. 31–60.

[8] R. J. Bartlett, C. E. Dykstra, and J. Paldus, in *Advanced Theories and Computational Approaches to the Electronic Structure of Molecules*, edited by C. E. Dykstra (Reidel, Dordrecht, 1984), pp. 127–159.

[9] R. J. Bartlett, J. Phys. Chem. **93**, 1697 (1989).

[10] J. Paldus, in *Methods in Computational Molecular Physics*, Vol. 293 of *NATO Advanced Study Institute, Series B: Physics*, edited by S. Wilson and G. H. F. Diercksen (Plenum, New York, 1992), pp. 99–194.

[11] I. Lindgren and J. Morrison, *Atomic Many-Body Theory* (Springer, Berlin, 1982).
[12] D. Mukherjee and S. Pal, Adv. Quantum Chem. **20**, 292 (1989).
[13] F. Coester, in *Lectures in Theoretical Physics,* edited by K. T. Mahanthappa and W. E. Brittin (Gordon and Breach, New York, 1969), Vol. 11B, pp. 157–186.
[14] R. Offerman, W. Ey, and H. Kümmel, Nucl. Phys. A **273**, 349 (1976); R. Offerman, *ibid.* **273**, 368 (1976); W. Ey, *ibid.* **296**, 189 (1978).
[15] D. Mukherjee, R. K. Moitra, and A. Mukhopadhyay, Mol. Phys. **33**, 955 (1977); A. Haque and D. Mukherjee, J. Chem. Phys. **80**, 5058 (1984); S. Koch and D. Mukherjee, Chem. Phys. Lett. **145**, 321 (1988).
[16] I. Lindgren, Int. J. Quantum Chem. Symp. **12**, 33 (1978); J. Phys. B **24**, 1143 (1991); I. Lindgren and D. Mukherjee, Phys. Rep. **151**, 93 (1987).
[17] W. Kutzelnigg, J. Chem. Phys. **80**, 822 (1984); W. Kutzelnigg, D. Mukherjee, and S. Koch, Chem. Phys. **87**, 5902 (1987).
[18] L. Stolarczyk and H. J. Monkhorst, Phys. Rev. A **32**, 725 (1985); **32**, 743 (1985); **37**, 1908 (1988); **37**, 1926 (1988).
[19] A. Haque and U. Kaldor, Chem. Phys. Lett. **117**, 347 (1985); **120**, 261 (1985); Int. J. Quantum Chem. **29**, 425 (1986); U. Kaldor, J. Chem. Phys. **87**, 467 (1987); U. Kaldor, Theor. Chim. Acta **80**, 427 (1991), and references therein.
[20] B. Jeziorski and J. Paldus, J. Chem. Phys. **90**, 2714 (1989).
[21] B. Jeziorski and H. J. Monkhorst, Phys. Rev. A **24**, 1668 (1981).
[22] W. D. Laidig and R. J. Bartlett, Chem. Phys. Lett. **104**, 424 (1984); W. D. Laidig, P. Saxe, and R. J. Bartlett, J. Chem. Phys. **86**, 887 (1987).
[23] B. Jeziorski and J. Paldus, J. Chem. Phys. **88**, 5673 (1988).
[24] L. Meissner, Ph.D. thesis, Nicholas Copernicus University, Toruń, Poland, 1987 (in Polish); L. Meissner, K. Jankowski, and J. Wasilewski, Int. J. Quantum Chem. **34**, 535 (1988).
[25] L. Meissner, S. A. Kucharski, and R. J. Bartlett, J. Chem. Phys. **91**, 6187 (1989); S. A. Kucharski and R. J. Bartlett, *ibid.* **95**, 8227 (1991).
[26] J. Paldus, L. Pylypow, and B. Jeziorski, in *Many-Body Methods in Quantum Chemistry,* edited by U. Kaldor, Lecture Notes in Chemistry Vol. 52 (Springer, Berlin, 1989), pp. 151–170.
[27] A. Balková, S. A. Kucharski, L. Meissner, and R. J. Bartlett, Theor. Chim. Acta **80**, 335 (1991).
[28] A. Balková, S. A. Kucharski, and R. J. Bartlett, Chem. Phys. Lett. **182**, 511 (1991), A. Balková, S. A. Kucharski, L. Meissner, and R. J. Bartlett, J. Chem. Phys. **95**, 4311 (1991).
[29] P. Piecuch and J. Paldus, Theor. Chim. Acta **83**, 69 (1992).
[30] J. Paldus, P. Piecuch, B. Jeziorski, and L. Pylypow, in *Recent Progress in Many-Body Theories,* edited by T. L. Ainsworth, C. E. Campbell, B. E. Clements, and E. Krotscheck (Plenum, New York, 1992), Vol. 3, pp. 287–303.
[31] U. Kaldor, S. Roszak, P. C. Hariharan, and J. J. Kaufman, J. Chem. Phys. **90**, 6395 (1989).
[32] *Many-Body Methods in Quantum Chemistry* (Ref. [26]).
[33] For papers representing some most recent developments in CC theory, see Theor. Chim. Acta **80**, Nos. (2)–(6) (1991).
[34] K. Jankowski, J. Paldus, and J. Wasilewski, J. Chem. Phys. **95**, 3549 (1991).
[35] K. Jankowski, J. Paldus, I. Grabowski, and K. Kowalski, J. Chem. Phys. **97**, 7600 (1992).
[36] P. Piecuch and J. Paldus (unpublished).
[37] K. Jankowski and J. Paldus, Int. J. Quantum Chem. **18**, 1243 (1980).
[38] J. Paldus, P. E. S. Wormer, and M. Bénard, Collect. Czech. Chem. Commun. **53**, 1919 (1988).
[39] S. A. Kucharski, A. Balková, and R. J. Bartlett, Theor. Chim. Acta **80**, 321 (1991).
[40] S. Wilson, K. Jankowski, and J. Paldus, Int. J. Quantum Chem. **23**, 1781 (1983); **28**, 525 (1985).
[41] U. Kaldor, Int. J. Quantum Chem. **28**, 103 (1985).
[42] S. Zarrabian and J. Paldus, Int. J. Quantum Chem. **38**, 761 (1990).
[43] N. Iijima and A. Saika, Int. J. Quantum Chem. **27**, 481 (1985).
[44] J. Paldus and J. Čížek, Adv. Quantum Chem. **9**, 105 (1975).
[45] G. Hose and U. Kaldor, J. Phys. B **12**, 3827 (1979); Phys. Scr. **21**, 357 (1980); Chem. Phys. **62**, 469 (1981); J. Phys. Chem. **86**, 2133 (1982); Phys. Rev. A **30**, 2932 (1984); U. Kaldor, J. Chem. Phys. **81**, 2406 (1984).
[46] I. Lindgren, Phys. Scr. **32**, 291 (1985); **32**, 611 (1985); D. Mukherjee, Chem. Phys. Lett. **125**, 207 (1986); W. Kutzelnigg, D. Mukherjee, and D. Koch, J. Chem. Phys. **87**, 5902 (1987); D. Mukherjee, W. Kutzelnigg, and D. Koch, *ibid.* **87**, 5911 (1987).
[47] L. Meissner and R. J. Bartlett, J. Chem. Phys. **92**, 561 (1990).
[48] C. Bloch, Nucl. Phys. **6**, 329 (1958).
[49] T. Kato, *Perturbation Theory for Linear Operators* (Springer, Berlin, 1966).
[50] I. Lindgren, J. Phys. B **7**, 2441 (1974).
[51] V. Kvasnička, Czech. J. Phys. B **24**, 605 (1974); **27**, 599 (1977); Adv. Chem. Phys. **36**, 345 (1977).
[52] E. R. Davidson, in *The World of Quantum Chemistry,* edited by R. Daudel and B. Pullman (Reidel, Dordrecht, 1974), pp. 17–30.
[53] K. Jankowski, L. Meissner, and J. Wasilewski, Int. J. Quantum Chem. **28**, 931 (1985).
[54] J. Čížek, Theor. Chim. Acta **6**, 292 (1966).
[55] J. Paldus, B. G. Adams, and J. Čížek, Int. J. Quantum Chem. **11**, 813 (1977).
[56] The resulting orthogonally-spin-adapted two-reference CC formalism may be easily extended to an n-dimensional case provided that we limit ourselves to the CS-type reference configurations with doubly occupied and unoccupied valence orbitals (cf. Ref. [29]). However, the generalization to an arbitrary model space is far from being straightforward.
[57] P. Piecuch and J. Paldus, Int. J. Quantum Chem. **36**, 429 (1989).
[58] P. Piecuch and J. Paldus, Theor. Chim. Acta **78**, 65 (1990).
[59] J. Paldus and B. Jeziorski, Theor. Chim. Acta **73**, 81 (1988).
[60] J. Paldus, M. Takahashi, and B. W. H. Cho, Int. J. Quantum Chem. Symp. **18**, 237 (1984).
[61] J. Paldus, M. Takahashi, and R. W. H. Cho, Phys. Rev. B **30**, 4267 (1984).
[62] M. Takahashi and J. Paldus, Phys. Rev. B **31**, 5121 (1985).
[63] P. Piecuch, S. Zarrabian, J. Paldus, and J. Čížek, Phys. Rev. B **42**, 3351 (1990).
[64] S. Huzinaga, J. Chem. Phys. **42**, 1293 (1965).
[65] H. Fukutome, Prog. Theor. Phys. **47**, 1156 (1972).

[66] H. Fukutome, M. Takahashi, and T. Takabe, Prog. Theor. Phys. **53**, 1580 (1975).
[67] B. G. Adams, K. Jankowski, and J. Paldus, Chem. Phys. Lett. **67**, 144 (1979).
[68] (a) B. G. Adams, K. Jankowski, and J. Paldus, Phys. Rev. A **24**, 2316 (1981); (b) **24**, 2330 (1981).
[69] J. Paldus, P. E. S. Wormer, F. Visser, and A. van der Avoird, J. Chem. Phys. **76**, 2458 (1982).
[70] J. Paldus and M. J. Boyle, Int. J. Quantum Chem. **22**, 1281 (1982).
[71] P. Piecuch and J. Paldus, Int. J. Quantum Chem. Symp. **25**, 9 (1991).
[72] J. Paldus and P. Piecuch, Int. J. Quantum Chem. **42**, 135 (1992); P. Piecuch, J. Čížek, and J. Paldus, *ibid.* **42**, 165 (1992).
[73] M. Takahashi and J. Paldus, Int. J. Quantum Chem. **28**, 459 (1985).
[74] The GAMESS system of computer programs by M. Dupuis, D. Spangler, and J. J. Wendoloski, National Resource for Computations in Chemistry, Software Catalog, University of California, Berkeley, CA (1980), Program No. QG01; M. W. Schmidt, K. K. Baldridge, J. A. Boatz, J. H. Jensen, S. Koseki, M. S. Gordon, K. A. Nguyen, T. L. Windus, S. T. Elbert, QCPE Bull. **10**, 52 (1990).
[75] Y. S. Lee and R. J. Bartlett, J. Chem. Phys. **80**, 4371 (1984); Y. S. Lee, S. A. Kucharski, and R. J. Bartlett, *ibid.* **81**, 5906 (1984); **82**, 5761(E) (1985).
[76] M. Urban, J. Noga, S. J. Cole, and R. J. Bartlett, J. Chem. Phys. **83**, 4041 (1985).
[77] J. Paldus, J. Čížek, and M. Takahashi, Phys. Rev. A **30**, 2193 (1984).
[78] R. A. Chiles and C. E. Dykstra, Chem. Phys. Lett. **80**, 69 (1981); S. M. Bachrach, R. A. Chiles, and C. E. Dykstra, J. Chem. Phys. **75**, 2270 (1981).
[79] J. Paldus and J. Pylypow (unpublished).
[80] P. Piecuch, R. Tobola, and J. Paldus (unpublished).